6-30-2016

Quantum Dot Metrics for Preparative Chemistry and Fluorescence Applications

Yi Shen
University of South Carolina

QUANTUM DOT METRICS FOR PREPARATIVE CHEMISTRY AND FLUORESCENCE APPLICATIONS

by

Yi Shen

Bachelor of Science
Nanjing University, 2010

Submitted in Partial Fulfillment of the Requirements

For the Degree of Doctor of Philosophy in

Chemistry

College of Arts and Sciences

University of South Carolina

2016

Accepted by:

Andrew B. Greytak, Major Professor

Richard D. Adams, Committee Member

Brian C. Benicewicz, Committee Member

Christopher T. Williams, Committee Member

Lacy Ford, Senior Vice Provost and Dean of Graduate Studies

DEDICATION

This work is dedicated to:

My parents, Jin Shen & Xiaomei Song

and

My wife, Ying Zheng

I love you all

ACKNOWLEDGEMENTS

I always dreamed of this moment. When you have almost finished your study, you can sit down and spend some time to look back through the entire five years. It has been a great part of my life. I have learned a lot about knowledge, partnership and leadership. I have been supported by a lot of people from this big Carolina Family and I truly want to thank all of them.

First and foremost, I want to express my greatest appreciation to my advisor Dr. Andrew B. Greytak. He is absolutely an ideal professor for a young ambitious chemist. He taught me not only what to do, but also how to think. I believe the hardest time of my PhD study was at the end of my second year when I decided to change my research focus from the electronic application of quantum dots to nanomaterials' surface chemistry study. Andrew showed great patience during that period of time, and guided me to get started into a new area. I still remembered the first party we had in his house, he asked me "Have you seen Star Wars yet?"; I said "No."; and then he said "Oh, come on, you should definitely watch it. This is America!" To be honest, I still have not finished watching the whole series yet, but I think I have found my Master Yoda.

I want to acknowledge my committee group: Dr. Richard Adams, Dr. Brian Benicewicz and Dr. Christopher Williams. Dr. Adams is a great professor in class and role model for all the young chemists. The light from his office is always one of the biggest motivations for me to finish experiments at night. Dr. Benicewicz is a great collaborator

and an extremely knowledgeable professor. The bioimaging work shown here would never have been possible without his insightful suggestions. Dr. Williams gave me a lot of advice during my proposal defense. It is a great honor to have these three professors as my committee members. I also want to give thanks to my collaborators Dr. Anand Viswanath, Warren Steckle from Dr. Benicewicz's group and Dr. Xia Zhao from Dr. Qian Wang's group. I learned a lot of polymer chemistry / biochemistry knowledge while working with them.

I would like to appreciate the Greytak group members, who has provided tremendous help in the past five years. Dr. Rui Tan is an inorganic synthetic chemist / Matlab genius and he helped me a lot on the nanocrystal fabrication / Matlab coding. Megan Gee started to collaborate with me since the first day she joined the lab and has always been a great support in the past three years. I will always cherish the memory when we worked together to get reproducible results on the ITC machine. Stephen Roberts and Adam Roberge are two talented hardworking young graduate students. I really enjoyed working with both of them. Pravin Paudel, Bobby Barker and Preecha Kittikhunnatham worked on a different area in our group, but have provided a lot of suggestions during my PhD study. Christopher Pinion, Colin Johnson and Abigail Loszko are the undergraduates in our group, who have also contributed to the projects described below.

As Andrew said, "Graduate school without a solid set of friends would be tough," I want to give thanks and my great gratitude to my friends during my time at USC for all their help and friendship. To Haorui Wu, Jiuyang Zhang, Yu Feng, Weiwei Xu, Xueyang Li, Ping Li, Lanlan Meng, Li Wang, Bing Gu, Qingfeng Zhang, Lichao Sun, Kangming Xie, Guangfang Li, Tian Zhang and Sahan Salpage. It is your unlimited help and

encouragement that have supported me to overcome a lot of difficulties. To Dr. Soumitra Ghoshroy and Dr. Jibin Zhao, I gained a lot under your kind guidance when I worked at the Electron Microscopy Center. I also want to express my appreciation to Ryan Chen, Helen Wang and Yijia Zhao. They are my friends from Business School and they showed me another direction to look at the world.

Finally, I would like to thank my parents, Jin Shen and Xiaomei Song. They are the best parents in the world. My father shared a lot of extremely valuable suggestions he gained during his PhD study and I believe I will be benefitting from his words for my entire life. My mother has a unique way to guide me with her wisdom to experience my own road since I was a child, and the method is still functioning well. Without their unconditional love and support, none of this would be possible.

My wife, Ying Zheng, is the most amazing person that I have ever known. She is always my best friend and my cheer leader. Her support and encouragement are undeniably the building block for my PhD study. Our marriage is the greatest happiness and accomplishment I have ever had.

ABSTRACT

Colloidal semiconductor quantum dots (QDs) are considered to be a promising candidate for bio-imaging and solar cells because of their extraordinary photo-physical properties. The ultimate goal of this dissertation is to design a reliable matrix and a reproducible method to prepare QDs-based biocompatible probe for fluorescence applications. Synthesis of quantum dots requires a large amount of ligands to improve the stability at high temperature. However, for further application and surface modification of QDs, excess ligands must be removed. In this dissertation, I will first describe using gel permeation chromatography (GPC) as a media to purify different types of QDs. A more systematic study of the tolerance of the GPC purification method against other nanocrystal materials will also be addressed. I will further demonstrate that GPC can be used as a reactor to perform solvent change and ligand exchange reactions with QDs. With the help of GPC purification technique, well-isolated and characterized nanomaterials are prepared to study the sequential chemistry of QDs. I specifically study the effect of neutral ligands on the photo-physical properties of the QDs and their influence on the inorganic surface overcoating (shell growth) reaction. This information is essential in preparing bio-compatible QDs with high brightness and long term stability. The GPC purified QDs have also been used to perform surface modification reactions with a range of polymeric imidazole ligands (PILs). The PIL capped QDs display colloidal stability, low toxicity and non-specific binding, and high brightness in aqueous solution. Measles virus, a model

envelope virus, has been labeled by these bio-compatible QDs and retained its infectious ability against host cells.

TABLE OF CONTENTS

LIST OF TABLES

LIST OF FIGURES

CHAPTER 1

INTRODUCTION TO SEMICONDUCTOR QUANTUM DOTS

1.1. Introduction

Semiconductor nanocrystals, known as quantum dots (QDs), are roughly spherical pieces of direct band-gap semiconductors with diameters on the order of 1-10 nm. The most well-known examples are the II-VI, III-V and IV-VI binary and their alloyed materials such as CdS, CdSe, InP and PbS. Compared with organic dyes, the QDs display a number of better characteristics for fluorescence applications, namely (1) narrower emission coupled with greater excitation cross-sections, (2) better photo-stability and high quantum yield, (3) most importantly rationally tunable emission wavelengths[1,2]. The electronic characteristics of quantum dots are determined by their size and shape. This means we can control the color of the emission light given off by a quantum dot just by changing its size[3].

The application of quantum dots can be grouped into two areas. When a photon is absorbed, the QD will be excited and generate an electron-hole pair. If we allow the electron and hole pair to recombine and emit a photon, we can use QDs in the labeling techniques [2,4] or in the light emitting technology[5,6]. For example, QD Vision, a company focusing on advancing the application of QDs, has commercialized the QD-embedded Color IQ™ optical component, which can provide more natural viewing experience through saturated color in display applications, such as TVs and monitors. On the other hand, if we separate the electron and hole pair, we can apply the QDs in the solar cell[1,7,8] or photo catalysis area[9,10]. Sargent's group from University of Toronto is one of the leading

group in studying QDs-based solar cells. According to their most recent study, they have promoted the power conversion efficiency to 9.9%, which is the new record for QD-based solar cells[8].

1.2. Synthesis of quantum dots

The most widely used procedure to prepare the binary QDs is the hot-injection method[11]. In order to produce quantum dots with well-defined shapes (typically spherical) with narrow size distribution, the reaction is kinetically controlled by running the system at high temperature and quenching the reaction before the Ostwald ripening. As shown in **Figure 1.1**, once the two precursors are mixed at high temperature, the concentration of the monomers will rapidly increase. At the very beginning, the nucleation rate is much faster than the growth rate, thus nuclei are formed during this process. Following nucleation, when the monomer concentration has decreased lower than the nucleation threshold where the reaction rate is slower than the growth rate, homogeneous growth of particles is enforced. When the monomers are nearly consumed, the small particles may start to dissolve, and redeposit onto larger particles. This process is known as the Ostwald ripening, which significantly increases the size distribution of the mixture. Therefore, the reaction should be quenched before the Ostwald ripening begins, for example by lowering the reaction temperature.

A vast number of studies have been focused on developing the precursor chemistry for hot-injection method over the past 20 years. In 1993, Bawendi's lab first developed the hot-injection method by using organometallics (such as dimethylcadmium) and trioctylphosphine chalcogenide[11]. In 2001, Peng's group advanced this technique by using salts prepared by mixing metal oxide with organic acid as the metal precursor to replace

the toxic and unstable organometallics[12]. Then Cao's group[13] and Hens' group[14] changed the chalcogenide precursor into chalcogen powders or chalcogen oxide, which shows better control during the reaction. Most recently, Owen's group has shown thioureas as another alternative chalcogenide precursor to prepare QDs with high monodispersity[15]. Researchers have also tried to reduce the reaction temperature by extending the reaction time. Manna's group[16] and Owen's group[17] have shown that CdSe QDs can be prepared from magic size clusters at 80 ℃ in 40 hours, but even now, the quality of the QDs prepared at lower temperature is still not comparable with the samples prepared by hot-injection method.

However, the quantum yield (QY) of the as-synthesized QDs is relatively low due to the trap states generated by the dangling bonds present on the surface. In order to optimize photo-physical properties of quantum dots, core/shell heterostructures have been introduced and widely explored. The inorganic shell on the surface can eliminate the dangling bonds and passivate both anionic and cationic surface sites simultaneously[18]. The representatives for core/shell stucture samples are CdSe/CdS QDs[19,20], CdSe/CdZnS QDs [21]and InP/CdS QDs[22].

In order to perform a successful shell growth experiment, the lattice mismatch between the core and shell materials needs to be minimized. For example, since CdSe and CdS have similar crystal structure, a giant CdS shell can be grown onto the CdSe core sample[23]. While the lattice mismatch between CdSe and ZnS is relative large, people normally grow an alloy $Cd_xZn_{1-x}S$ (note: in this dissertation, CdZnS represents the $Cd_xZn_{1-x}S$ formula) shell onto the CdSe core surface instead of growing ZnS shell directly[21].

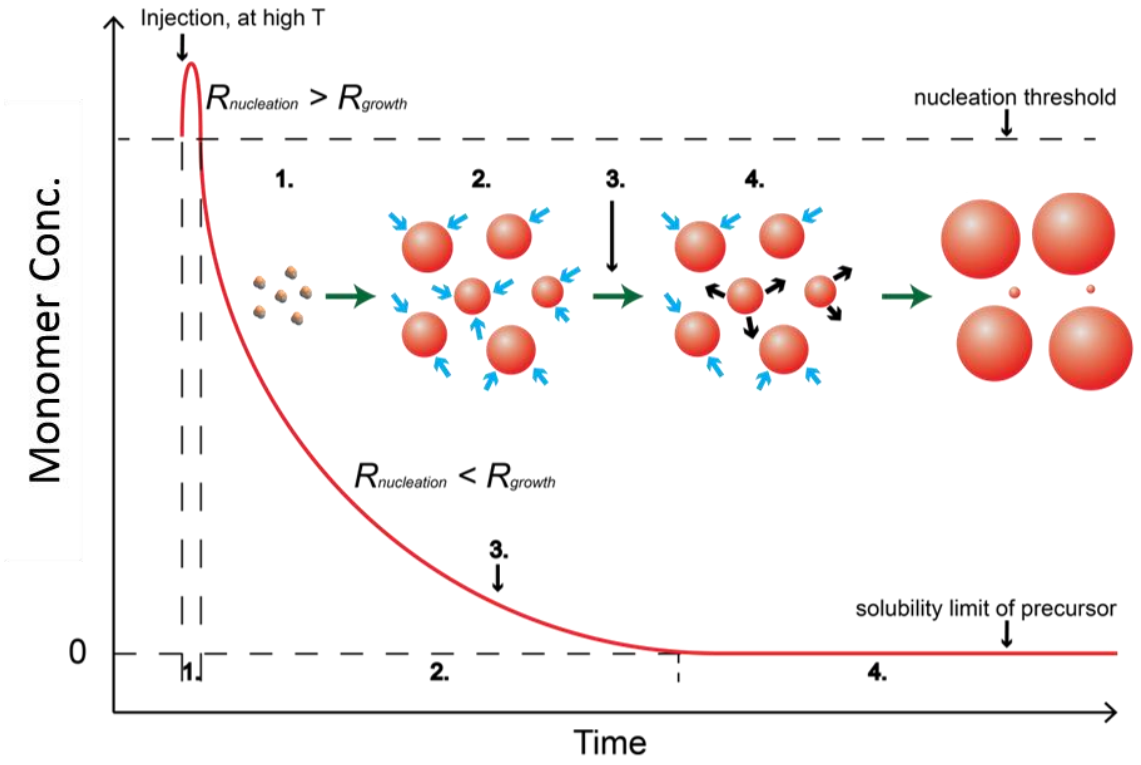

Figure 1.1 Reaction scheme for preparation of monodispersed colloidal QDs. Stage 1. Nucleation reaction; stage 2. Nanocrystal growth reaction; stage 3. Reaction quenching; stage 4. Ostwald ripening.

There are two strategies to perform shell growth over the QD core samples. The first method is the simultaneous addition of the two precursors. For example, Bawendi's lab has shown by using cadmium oleate and octanethiol as the precursor, high quality monodispersed round shape CdSe/CdS core/shell QDs are obtained[24]. Simultaneous addition method has also been used to achieve anisotropic shell growth. Alivisato's group[25] and Manna's group[26] have shown that by changing the surfactants during the growth process, CdSe/CdS nanorods and tetrapods can be prepared by addition of cadmium and sulfur precursors at the same time.

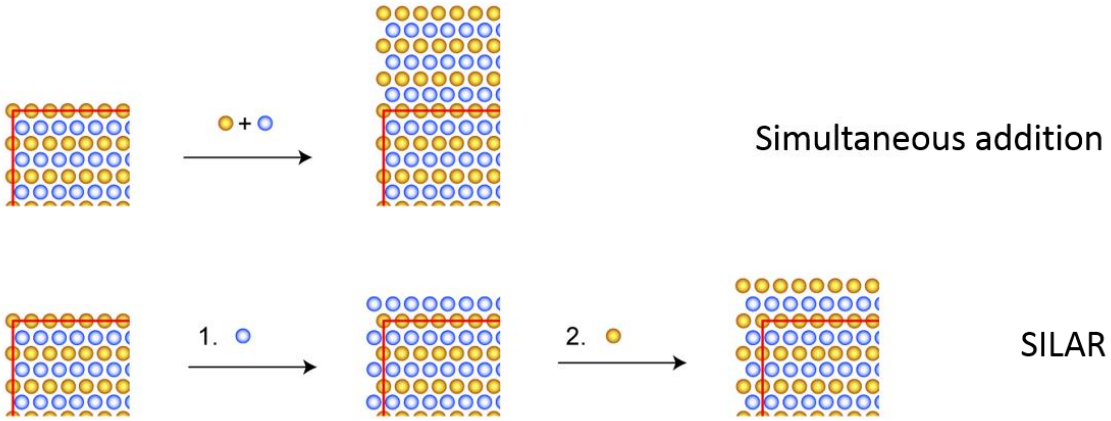

Figure 1.2 Scheme for growth of core/shell quantum dots via simultaneous addition and SILAR methods

The second method for shell growth is called Selective Ionic Layer Adhesion and Reaction (SILAR). As shown in **Figure 1.2**, the idea is instead of injecting two precursors at the same time, for each monolayer growth only one precursor is introduced at a time and all available surface sites are saturated in each half cycle. This method was first proposed by Peng's group[27] and has become widely used in preparation of binary structures in solution. The advantage of this method is that (1) the isotropic growth is enforced and the homogenous nucleation side reaction of the shell material is minimized; (2) the sample shell thickness can be easily controlled by changing the amount of addition cycles during SILAR shell growth process[19]. Additionally, as shown in a recent study from our group, using a sub-monolayer equivalent in each cycle can increase the yield of the shell growth reaction and reduce the influence of the nucleation side reaction[20]. Therefore, the majority of the core/shell materials described in the dissertation are prepared by a SILAR method with 0.8 monolayers equivalent precursor addition in each cycle.

1.3. Surface modification of quantum dots

The as-synthesized core only or core/shell QDs are capped with long hydrocarbon ligands such as oleic acid. These capping ligands separate the particles from each other and are crucial in maintaining the colloidal stability of the particles under synthetic conditions. However, for both electronic application and bioimaging applications, the original ligands are not ideal since they behave as an insulting layer and are not water-soluble. Therefore, surface modification of the QDs is normally required for any QDs-based device / probes.

For electronic applications of QDs, the biggest requirement for surface modification is to replace original surfactants with shorter ligands. Waston's group has shown that by shortening the distance between particles, the charge transfer efficiency is dramatically improved[28]. In order to improve the stability of the QDs after the ligand exchange, the binding affinity between the new ligands and QD surface must be high. Therefore, new ligands bearing a strong nucleophilic anchoring group such as thiol and amine are commonly used for the surface modification reactions. Representative ligands in this group are pyridine[29], mercaptopropionic acid[30] and ethanediol[31]. Recently, Talapin's group has proposed to use inorganic ligands such as metal chalcogenide complex (MCC) as an alternative surfactant to completely replace the insulating hydrocarbon chain[32]. They further demonstrated that single atoms (like halide[33] or chalcogenide[34]) can also be used to passivate the surface sites and maintain the QDs colloidal stability.

To use QDs as a probe or sensor in a biological system, the QDs need to be water-soluble. Besides, desirable QD properties such as high QY and small size are hoped to be maintained. The most common ligands people have used for this purpose are mono-thiol based ligands, such as mercaptopropionic acid[35] and cysteine[21]. However, the binding

strength between mono-thiol ligands and the QD surface is not that strong and thiol ligands are known to be photo unstable. In order to improve the stability of the exchanged sample in aqueous solution, ligands with multiply binding groups / non-thiol based anchoring groups have also been studied and this part will be further discussed in Chapter 4.

1.4. Quantum dots in bioimaging applications

As mentioned previously, the photo-physical properties of QDs make them particularly attractive for use as luminescent biological probes. The emission wavelength of lead chalcogenide based QDs is within the near-infrared (NIR) region, which makes them exceedingly interesting for in vivo biological imaging[36]. In addition, the large two-photon absorption cross section of QDs makes them attractive for multi-photon microscopy application as well[37].

In order to use QDs for selective labeling in bio-imaging applications, the linker needs to have at least three different functional groups: one group to stabilize QDs in water; one group providing binding ability with the QDs surface; and the last group for attachment onto the biological target. So far, there are four common strategies to link QDs with specific biological targets through different interactions / reactions. They are (1) avidin-biotin bridging[38]; (2) coupling between carboxyl and amine groups;[39] (3) metal affinity between polyhistidine-appended biomolecules and metal-rich QDs;[40] (4) azide-alkyne "click" reactions[41]. With these specific functionalization onto the nanocrystal surface and biomaterials, QDs have been used to label proteins[42], cells[2] and viruses[41].

Some demonstrations of the conjugation of QDs with specific ligands targeting biomolecular imaging applications are provided in the following examples. In an early work from Bruchez's group, they employed CdS/ZnS QDs encapsulated within an amine-modified copolymer and coupled to streptavidin tospecifically label the cancer marker Her2, actin filaments, and nuclear antigens[4]. Around the same time, Simon's group demonstrated the use of QD bioconjugates for long-term multicolor imaging of living cells.[43] Later, Nie's group prepared water-soluble QDs encapsulated by a polymer bearing the tumor-targeting ligands, and performed in vivo cancer targeting and imaging.[43] Ting's group has shown that QDs can be tagged onto mammalian cell surface proteins.[42] Cai's group has labeled the enveloped baculovirus with polymeric imidazole ligands (PILs) capped QDs through a copper-free click reaction and maintained the virus infectivity[41].

1.5. Thesis overview

The ultimate goal of this dissertation is to design a reliable matrix and a reproducible method to prepare QDs-based biocompatible probe for fluorescence applications. The first body of work, described in Chapter 2, demonstrates that gel permeation chromatography (GPC) can be used as a media to purify a large variety of nanomaterials with better efficiency and reproducibility. This is an essential step for further surface modification since the impurities and excess ligands have negative impact on the reactions. I further use GPC as a reactor to perform solvent change and ligand exchange reactions with QDs, which shows better control and efficiency though the reaction process.

Chapter 3 is a study of the influence of neutral ligands effect on the photo-physical properties of the QDs and their influence on the inorganic surface overcoating (shell

growth) reaction. The ensemble quantum yield (QY) and lifetime components will be changed upon introduction of ligands to purified QD surface. Strong binding ligands such as trioctylphosphine tend to significantly restore the brightness in a reversible manner. The neutral ligands are also involved in the shell growth reaction. Three different amines are used to grow core/shell QDs by the SILAR method. Compared to strong binding primary amine ligands, weakly associated tertiary amine can increase the yield of the reaction and improve the quality of the synthesized particles. This information is essential in preparing high quality core/shell QDs and designing new hydrophilic ligands to prepare high quality QDs as biocompatible probes in fluorescence applications.

In Chapter 4, GPC purified QDs are used to perform surface modification reactions for biological applications: a range of methacrylate backbone polymeric imidazole ligands (MA-PILs) prepared by RAFT polymerization and post-modification were synthesized and associated to the QD surface. These MA-PIL capped QDs provide water solubility, colloidal stability, low toxicity and non-specific binding, and high brightness. These bio-compatible QD samples are further used to label Measles virus, a model envelope virus. The labeled virus retains its infectious ability against host cells, which demonstrates that MA-PIL capped QDs have a potential to be widely used in areas of biolabeling and bioimaging.

CHAPTER 2

ADVANCES IN THE USE OF GEL PERMEATION CHROMATOGRAPHY (GPC) TO NANOCRYSTALS: PURIFICATION, SOLVENT CHANGE AND SURFACE MODIFICATION

2.1 Introduction

Quantum dots (QDs) are coated with a layer of surfactant molecules (ligands) that provides charge balance and colloidal stability. As-synthesized samples also contain unreacted precursors as well as reaction byproducts, high boiling point solvent(s), and/or an excess of ancillary ligands added to control growth and improve stability[44–46]. Applications almost universally require purification and/or surface modification of the as-synthesized QDs: (1) for optical applications, the as-synthesized QDs are not very bright, which requires the formation of an inorganic shell to increase the quantum yield (QY);[19,24,47,48] (2) for bioimaging applications, surface modification by encapsulation or ligand exchange is essential for water solubility;[2,21,49] and (3) for electronic applications, excess ligands adsorbed on the surface hinder the charge transfer between the QDs and receiving substrates.[50–52] Effective means for the isolation of QDs with well-defined surface properties is essential to the applications of QDs in solution or assembled into matrices, and is also a necessary condition for the development of sequential preparative chemistry for QD-based nanostructures.

The traditional method for purification of QDs is a sequential precipitation and redissolution (PR) process[52,53]. For the frequent case of QDs sterically stabilized by ligands with long hydrocarbon tails in nonpolar phase (e.g., hexane, toluene, chloroform, or tetrahydrofuran), flocculation of QDs is achieved by introducing anti-solvents (e.g., acetone, methanol, isopropanol) to increase the polarity of the solvent mixture. Impurities that remain soluble can then be decanted away, and the QDs redissolved in a suitable solvent.

While the PR method is convenient and scalable, it carries several limitations. Fundamentally, the separation is based on solubility; for differently prepared batches of QDs the necessary precipitation conditions are not identical since the intermolecular forces governing the solubility of the as-synthesized QDs are not inherently controlled properties. Some impurities may have solubility properties similar to the QDs, such that multiple PR cycles are necessary for complete removal. From a practical perspective, in some cases, the amounts of polar anti-solvents that are used are not tightly controlled, but even if these procedures are performed systematically, the turbidity that is considered to represent adequate precipitation of the QDs is often a subjectively determined parameter; this can lead to run-to-run variability and present difficulties in adequately describing procedures in literature. An important consideration for any QD purification method is the effect not only on the amounts of unbound species remaining in the sample but also the effect on the number and type of bound ligands that terminate the QD surface[53]. In the case of the PR method, the introduction of a foreign solvent can perturb the QD surface by displacing native ligands, as has recently been reported for the case of QDs purified by PR with methanol as the anti-solvent.[54]

The strong dependence of the photo-physical properties[55,56] and chemical reactivity of QDs on the surface ligand population has helped to motivate increasing interest in alternative nanoparticle purification methods[57]. One alternative to PR methods is the use of biphasic extraction processes[58]; however, separation is still based on differences in polarity. Other methods include ultracentrifugation of non-flocculated samples[59,60], electrophoretic deposition[61,62], and chromatographic techniques[38,63–65]. The relatively large size of QDs compared to small molecule impurities makes size-exclusion chromatography (SEC) an attractive technique.

In the work described below, we have introduced a highly precise and effective gel permeation chromatography (GPC) purification technique for QDs and other nanocrystals. GPC is a type of SEC that operates with an organic mobile phase and is widely used in characterization of macromolecules such as polymers. As with any SEC technique, GPC employs a mobile phase that is a solvent for the mixture to be separated; the mixture passes through a stationary phase and subsequently fractionates, with elution volumes that directly correlate with the hydrodynamic size of the analytes. Colvin's group[63] and Roman's group[65] have studied the application of SEC to reduce the size distribution of Cd-based QDs in the organic and aqueous phases, respectively. Winnik's group[64,66] and Kanelidis et al.[67] have used SEC to separate QDs from excess polymers after surface modification. Bawendi and co-workers have demonstrated the use of size-exclusion gel filtration chromatography (GFC) to isolate QDs from dye molecules in the aqueous phase[38,68], and Biesta et al. have used GPC to separate Si nanoparticles from dye molecules in acetonitrile[69]. Until now, however, chromatography has not been described as a method to

isolate natively capped nanocrystals as the basis for further manipulations, nor has its efficacy as a purification technique been compared directly to precipitation-based methods.

Initially I used GPC with a polystyrene stationary phase as a technique to purify two types of as-synthesized nanoparticles: CdSe QDs and CdSe/$Cd_xZn_{1-x}S$ core/shell QDs. Compared with the PR purified samples, the GPC purified QDs exhibited significantly smaller ligand/QD ratios, similar stability at room temperature, and even better stability at high temperature (toward precipitation and/or ripening). Then the tolerance of this technique has been studied by testing a variety of nanoparticles with different shapes and capping ligands. Furthermore, we demonstrate CdS shell growth on the same CdSe QDs with different purification methods and cysteine ligand exchange on CdSe/$Cd_xZn_{1-x}S$ QDs to reveal how impurities and excess ligands can alter the surface chemical reactions of the QDs. Finally, GPC has been used as a reactor to perform solvent change and ligand exchange reactions with different QD samples.

2.2 Purification of CdSe and CdSe/CdZnS QDs

2.2.1 Feasibility of QDs purification by GPC

We elected to use a polystyrene gel medium to study the purification of hydrophobically-capped QDs. Previous authors have reported successful GPC of QDs using such media.[64] According to studies of GPC in the polymer area,[70] strong ionic interactions with the stationary phase tend to prevent metal containing polymers from successfully travelling through the column. Therefore, before attempting to purify the QDs by GPC, we first tested whether the QDs would irreversibly adsorb in the column due to

particle-column interaction. The QD samples we used to test the efficacy of the column were **CdSe1** and **CdSe/CdZnS1** as described in the Materials Section. Due to the difficulty in visualizing the concentration of impurities and excess ligands separated from the QDs solution, the dye alizarin was initially chosen to represent "small" molecules and we compared its chromatogram to that of the QDs. As shown in **Figure 2.1A-C**, the QDs exit the column when the elution volume equals approximately 1/3 of the total volume of the column (the expected void volume). Because the molecular weight operating range of the SX-1 GPC medium is described by the manufacturer as 600 to 14000 and both CdSe QDs and CdSe/$Cd_xZn_{1-x}S$ QDs are larger than that, the QDs do not spend any time in the pores and elute quickly from the column. However, small molecules (such as impurities, excess ligands or alizarin) should enter the pores more easily, which is expected to increase their retention time relative to that of the QDs. Alizarin was eluted at a volume close to the total volume of the column, thus indicating highly precise resolution from the QD samples.

The yield of the GPC column purification is always around 100% (CdSe1 QDs, 100.2%; CdSe/CdZnS1 QDs, 98.3%; alizarin, 101.4%), which avoids sample loss associated with biphasic or PR purification processes. Additionally, the QDs elute in a tight band (95% of the QDs sample flows out in 2 mL), which maintains the high concentration of the QDs solution and improves the column separation resolution against the later eluting impurities and excess ligands. After being rinsed with toluene following each purification process, the column can be used more than 10 times and provide very comparable purification results.

We also tested the stability of the QDs after GPC purification. According to absorption spectra shown in **Figure 2,1E and 2.1F**, both CdSe QDs and CdSe/$Cd_xZn_{1-x}S$

QDs maintain their absorption features after the GPC purification (there is a decrease in relative absorbance in the UV range, which may be associated with the absorption spectrum of impurities prior to purification). Since the absorption of the QDs is determined by their size and size distribution, this confirms that QDs do not aggregate or etch during the GPC purification process. At room temperature the **1GPC** CdSe QDs are stable for more than 2 weeks when stored in toluene on the bench (we only continuously measured the absorption spectrum for 2 weeks, the actual lifetime of the CdSe QDs may be much longer than this), while the CdSe/$Cd_xZn_{1-x}S$ QDs began to slowly precipitate out from the solution after 1 day.

At high temperature, the **CdSe1_1GPC** sample demonstrated even better stability than **2PR** samples. In particular, purified samples were injected to a simulated shell growth solvent of 1:2 oleylamine:ODE (v/v, 9 mL total) and heated up to high temperature. As shown in **Figure 2.1F**, the first absorption peak position is almost fixed (or blueshifted ~1nm) when the temperature reaches 180 ℃, and then slowly redshifts after extended heating at 200 ℃. This phenomenon is unlike the relatively larger blueshift (around 3-4nm) that is frequently observed in PR purified QDs under similar conditions[71], which might be explained by the etching of QDs' surface in the presence of excess ligands. The redshift observed in **Figure 2.1F** upon extended heating may be a signature of Ostwald ripening.

2.2.2 Analysis of the GPC purified QDs: CdSe samples

The GPC purified **CdSe1** QDs samples were characterized by ^{1}H NMR to measure the amount of organic solvents and ligands that remained. The **1PR** and **2PR** samples were also characterized for comparison. Both ODE and oleic acid have resonances from their olefin protons with distinctive chemical shifts in the range of 5 ppm to 6 ppm, which makes

them convenient as representative impurities and ligands whose presence and concentration can be determined by NMR[72–74].

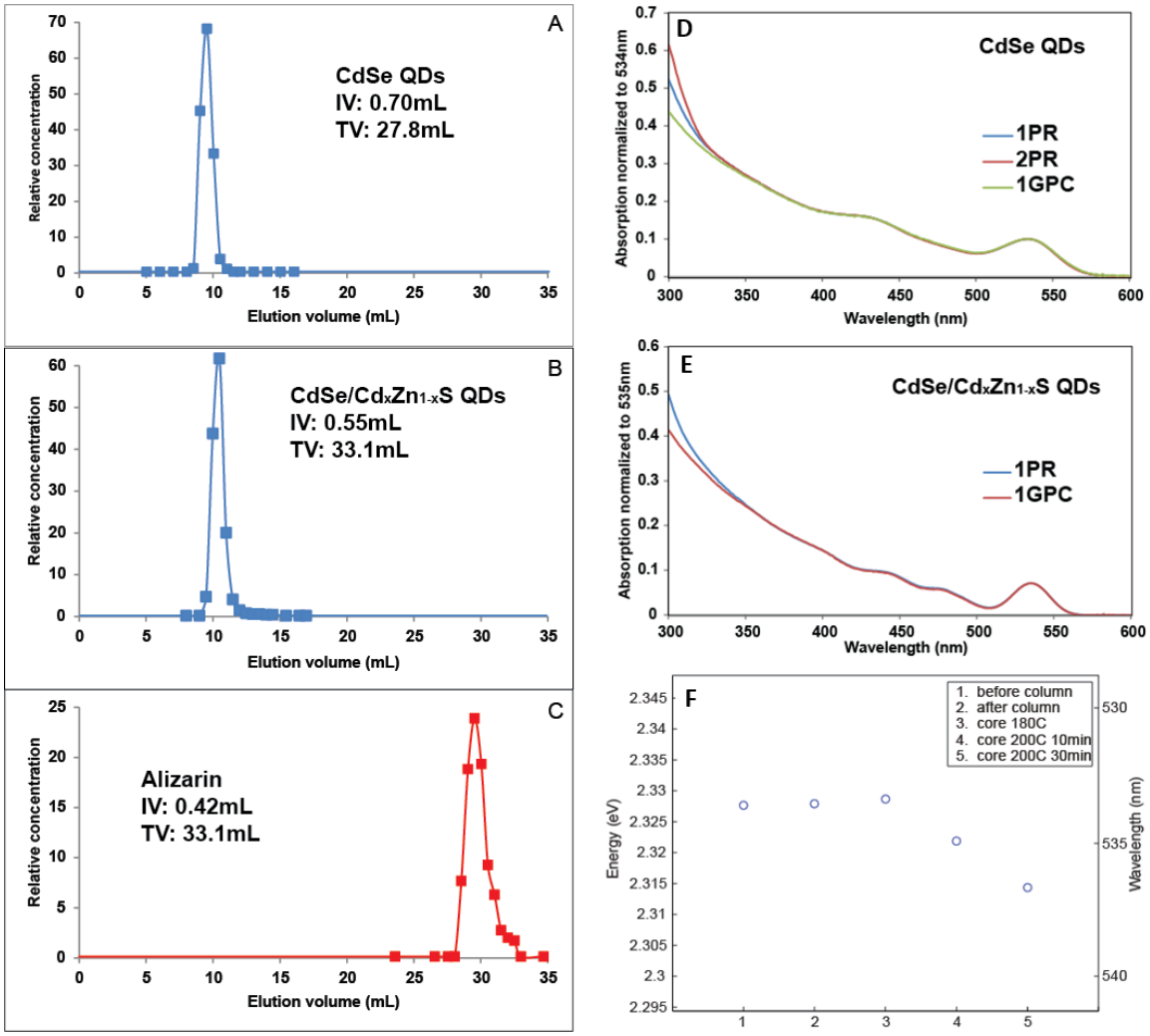

Figure 2.1 (A-C) GPC traces of QDs and small molecule representative dye. The sample concentrations (shown by the square points) are measured by UV-Vis and normalized to the concentration of the injection solution (considered as 100). IV = injection volume. TV = total volume of column. (A) CdSe1 QD sample; (B) CdSe/CdZnS1 QD sample; (C) Elution of alizarin in toluene. (D-F) Stability verification of core and core/shell QDs purified by GPC based on absorption spectra. (D) Absorption spectra of CdSe1 (normalized to the 1st absorption peak at ~534nm) purified by 1PR, 2PR, and 1GPC; (E) Absorption spectra of CdSe/CdZnS1 (normalized to the 1st absorption peak at ~535nm) purified by 1PR and 1GPC; (F) Lowest energy extinction peak position shift of GPC purified CdSe1 at high temperature. Copyright 2013 American Chemical Society.

The ^{1}H NMR results shown in **Figure 2.2** reveal two types of olefin features: sharp peaks characteristic of the molecules in free solution, and a broadened peak that we associate with molecules bound to (or in dynamic exchange with) the QD surface. The spectrum in **Figure 2.2A** indicates that the **1PR** sample still had a significant amount of ODE. After one additional PR purification, the amount of ODE is shown to have been reduced but not completely removed. The **1GPC** sample, on the other hand, shows a clean spectrum with only a broadened (~50 Hz) olefin resonance in the 5 ppm to 6 ppm range. We attribute this resonance to oleate species that are strongly interacting with the QD surface; in what follows we will use "OA" to refer to oleate-based constituents of all types.

In order to have a better understanding of the ligand/QD ratio for samples with different purification processes, THF was used as an internal standard in subsequent quantitative ^{1}H NMR measurements. The total concentration of the ligands can be calculated based on the ^{1}H NMR peak integrals; dividing by the QD concentration, as determined by the absorption spectrum, gives the ligand/QD ratio in each sample. Taking into account the uncertainty associated with the integration of the NMR peaks, we are able to specify average ligand/QD ratios with a precision of ±5 ligands per QD (any inaccuracy in the molar extinction coefficient of the QD batch would affect all samples by a constant factor). The **2PR** sample had an average 172 OA and 56 ODE per QD, while the **1GPC** sample had only 135 OA on the QD surface. We did not observe any sharp peaks in the ^{1}H NMR spectrum at the olefin region of OA, which suggests that there was no free OA in either system. Consequently, the ligand density difference is more likely due to weakly bound OA or OA-bearing impurities (i.e. $Cd(oleate)_2$ or $Cd_xSe_y(oleate)_z$)[33,75]. We also measured the ligand density for a sequential **6PR** sample, which shows a comparable, but

still larger result than the **1GPC** sample (147 OA per QD). As shown in **Figure 2.2D**, we also used GPC to purify the same QDs sample twice, which yields a similar ligand density on the QDs. For the **2GPC** samples, the extra column purification did not decrease the ligand density on the QDs' surface, which suggests that all the weakly adsorbed ligands can be effectively removed during **1GPC** process. ^{31}P NMR spectra were also measured to confirm the complete removal of phosphorus containing species (i.e. TOPSe, TOP, TOPO appearing as byproducts of QD synthesis) by GPC (**Figure 2.2E-F**). Excess ODE and OA species could be detected by ^{1}H NMR in GPC solvent fractions eluted at later times (**Figure 2.3**). To test the dependence of the GPC purification technique on the initial sample concentration, we purified a series of three aliquots of the same CdSe QD sample with different initial concentrations (58 μM, 115 μM and 175 μM) by GPC and observed <1% variation in the number of ligands/QD in the eluted products.

These results demonstrate that GPC purification is an efficient method to isolate QDs with reproducible ligand ratios. Because GPC operates on the basis of the hydrodynamic size difference and not polarity or a specific affinity interaction, the (entropic) driving force that contributes to the separation is fixed and we can get highly reproducible results from this purification method. The fact that the samples prepared by multiple PR cycles contained larger numbers of ligands raised the question of whether the "excess" OA ligands in such samples represented higher surface coverage, or the presence of soluble OA-containing species.

Diffusion ordered NMR spectroscopy (DOSY) can be used to characterize the association of molecules with nanoparticles[74,76,77] and was used here to determine the extent to which oleate in each sample is associated with the QDs' surface. Here, relative

diffusion constants were used to measure the hydrodynamic radius to accommodate some run to run instrument variability in the absolute diffusion constant measurements.

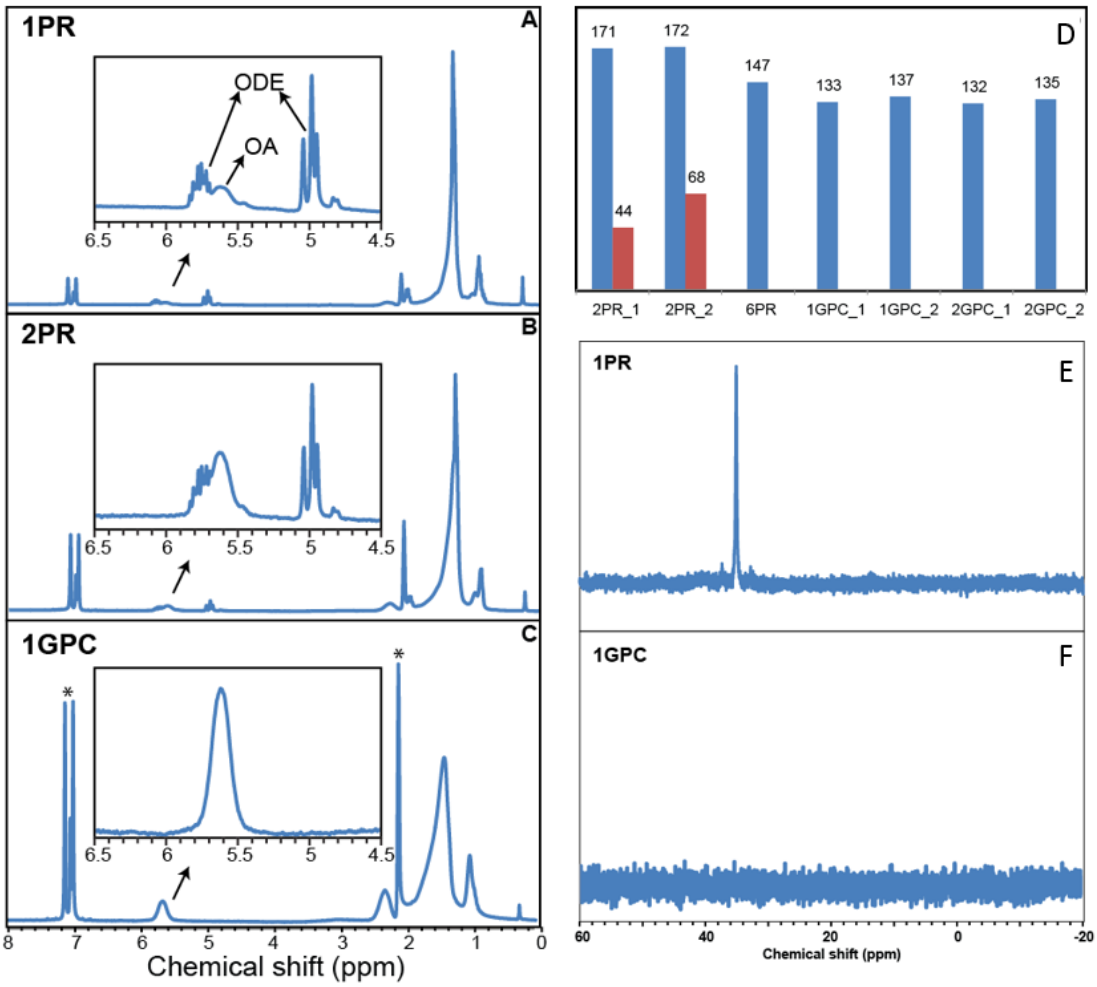

Figure 2.2 (A-C) Qualitative ^{1}H NMR spectra of the **CdSe1** QD sample purified by different methods. The insets are the expanded views of the spectra in the range 4.5-6.5 ppm for the olefin protons of OA and ODE. (A)**CdSe1_1PR**; (B)**CdSe1_2PR**; (C)**CdSe1_1GPC**. Asterisks in (C) indicate peaks associated with the toluene solvent that are present in each sample. (D) Ligand/impurities-to-QDs ratio for **CdSe1** QDs purified by different methods; the ratio is calculated based on the quantitative ^{1}H NMR and UV-Vis spectra. (E-F) The ^{31}P NMR spectra of **CdSe1 1PR** (E) **and 1GPC** (F) QD samples, demonstrating the removal of phosphorus containing species (such as TOPO) by the column purification. Copyright 2013 American Chemical Society.

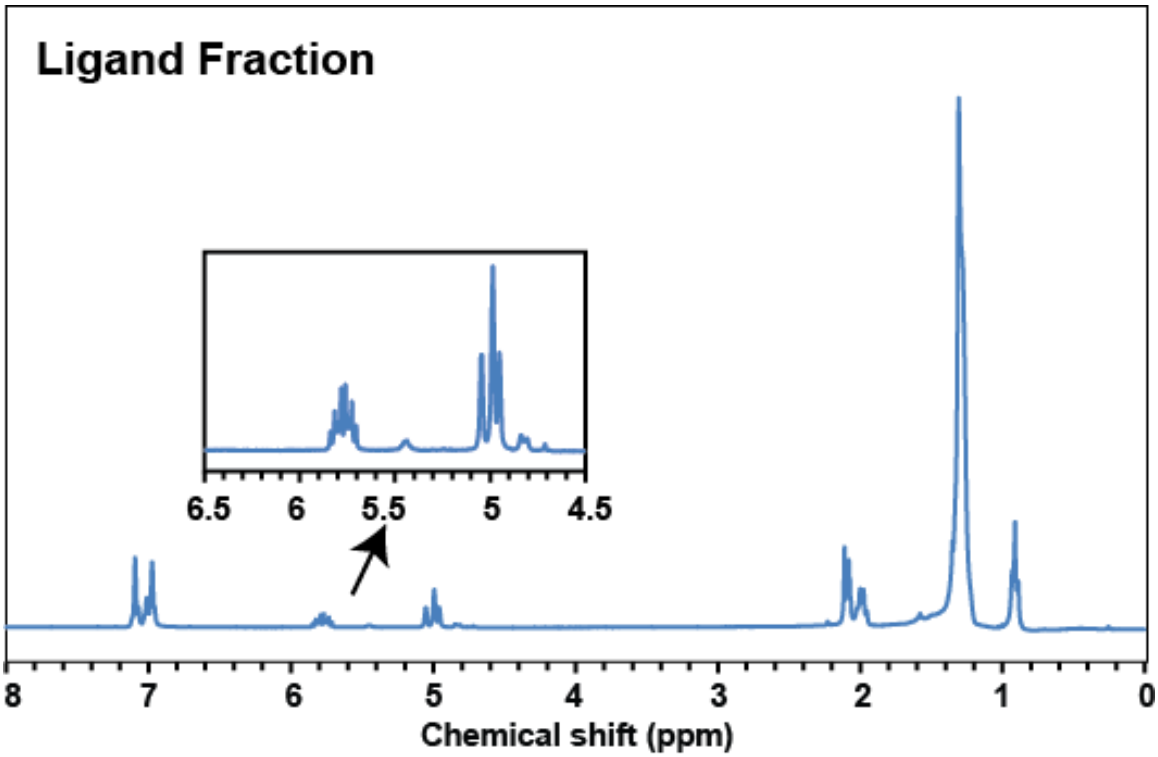

Figure 2.3 The ^{1}H NMR spectrum of material separated from the **CdSe1** QD sample after the GPC purification, revealing the presence of ODE and OA.

In order to obtain the characteristic diffusion constant for OA, we relied upon the olefin peaks because their chemical shift is well separated from those of THF protons. Based on the measured diffusion coefficients of the OA and THF in each run (shown in **Figure 2.4**), the characteristic hydrodynamic diameter (D_H) of the OA in different samples can be calculated using the Stokes-Einstein equation by assuming the D_H of THF is fixed at 0.63 nm (as reported by Dyadin *et al.*[78]). The average D_H of the OA from the **CdSe1_1GPC** sample was 4.42 nm, which is very close to the core diameter (3.5 nm) and an OA shell with thickness of 1~2 nm. However, the average D_H of the **2PR** sample was 1.85 nm, which suggests an average among OA bound to the QD surface and faster diffusing OA associated with small molecule impurities. If we assume all the OA from the

CdSe1_1GPC QD sample is bound to the surface and consider molecular oleic acid as representative of the unbound oleate species in QD samples (D_H = 0.88 nm), then 66% of the OA in **CdSe1_2PR** sample were attached to the QD surface, while 34% remained unbound.

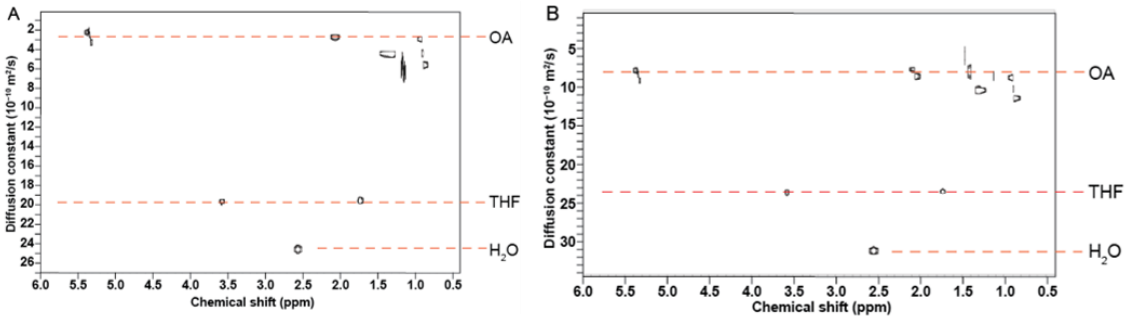

Figure 2.4 DOSY spectra of **CdSe1** samples in THF-d_8. The measurements were done with 100ms diffusion delay and 2ms diffusion gradient length. (A)**CdSe1_1GPC** QDs; (B)**CdSe1_2PR** QDs. Copyright 2013 American Chemical Society.

The **1PR**, **2PR** and **1GPC CdSe1** QDs samples were also characterized by TGA to corroborate the NMR results of ligand/QDs ratio differences from the different purification processes. As **Figure 2.5** shows, the TGA curves can be separated into 3 regions[79]. Below 120 ℃, mass loss primarily signifies the evaporation of the solvent (toluene); between 120 ℃ and 300 ℃, mass loss is attributed to the disappearance of neutral molecules; between 300 ℃ and 500 ℃, the ionically bonded ligands break down. We assume the remaining mass after heating to 500 ℃ was attributed to the inorganic core. As listed in **Table 2.1**, the **CdSe1_1GPC** sample did not show any significant weight difference until the temperature reached 300 ℃; while both **CdSe1_1PR** and **CdSe1_2PR** QDs demonstrated neutral molecule removal over 120-300 ℃, which is in agreement with the NMR results. Based on the observed mass losses, the ionic-ligands/QDs mass ratio of **CdSe1_2PR** sample was 1.35, whereas **CdSe1_1GPC** sample was only 0.73. This

difference can be explained by previously mentioned possible impurities in the **2PR** sample, such as $Cd(oleate)_2$ or $Cd_xSe_y(oleate)_z$. The mass loss from 120-500 ℃ can be attributed to the removal of all the organic molecules from the system (except for the solvent) and the organic/inorganic ratios of **CdSe1_2PR** and **CdSe1_1GPC** samples were 1.83 and 0.78 respectively.

According to the absorption spectrum of CdSe QDs before and after the GPC purification, the size and size distribution of the samples did not change. However, we also considered the possibility that there could be some Cd and/or Se containing impurities remaining in the **2PR** sample that are removed by GPC purification. In order to understand how the more stringent removal of impurities by GPC altered the Cd/Se ratios in the samples, the inorganic core portions of the **CdSe1_2PR** and **CdSe1_1GPC** were characterized by ICP_MS[75,80]. As shown in the **Figure 2.6**, the Cd/Se ratio is similar between the two samples, but the **2PR** sample has a slight, but statistically significant, increase in Cd that can be attributed to the residual Cd rich impurities (e.g. $Cd(oleate)_2$).

2.2.3 Analysis of the GPC purified QDs: CdSe/CdZnS core/shell samples

$CdSe/Cd_xZn_{1-x}S$ QDs were prepared by a selective ionic layer adhesion and reaction (SILAR) process with CdSe QDs as the core and $(TMS)_2S$, $Zn(oleate)_2$ and $Cd(oleate)_2$ as the shell precursors. Since the shell generation process involves the highly reactive reagent $(TMS)_2S$ and a more complicated reaction mixture than the synthesis of CdSe QDs, there are likely more impurities in the core/shell samples than in the core-only ones. Additionally, core/shell samples frequently encounter solubility problems after multiple

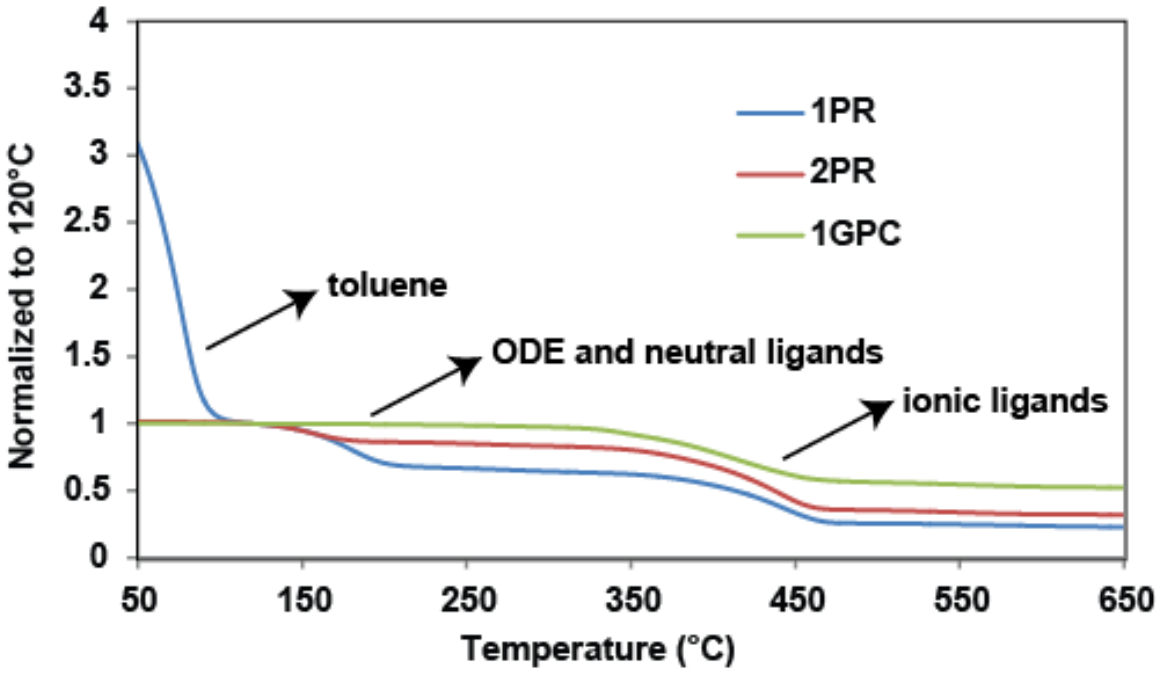

Figure 2.5. TGA curves of CdSe1 QDs purified by different methods with the arrows indicating regions assigned to the loss of the specified solvent or ligand. Copyright 2013 American Chemical Society.

Table 2.1. Summary of the mass remaining at different temperatures from TGA trace[a]

CdSe1 QD samples		**1PR**	**2PR**	**1GPC**
Mass remaining at different temperatures	120 ℃	1.000	1.000	1.000
	300 ℃ [b]	0.644	0.832	0.975
	500 ℃ [c]	0.256	0.354	0.562

[a] Results are normalized to the mass at 120 ℃, at which point the solvent (toluene) is presumed to have been removed. [b] Weakly binding ligands are removed before 300 ℃. [c] Ionically binding ligands are presumed to disappear in the region of 300-500 ℃. Copyright 2013 American Chemical Society.

PR cycles[81,82], and published ligand exchange procedures for core/shell QDs often describe only a single precipitation step[83]. Therefore, it is imperative to find an alternative way to purify the core/shell QDs other than the PR method. In order to prove the efficacy of the

GPC purification process, both **1PR** and **1GPC CdSe/CdZnS2** QDs were characterized by ^{1}H NMR and TGA.

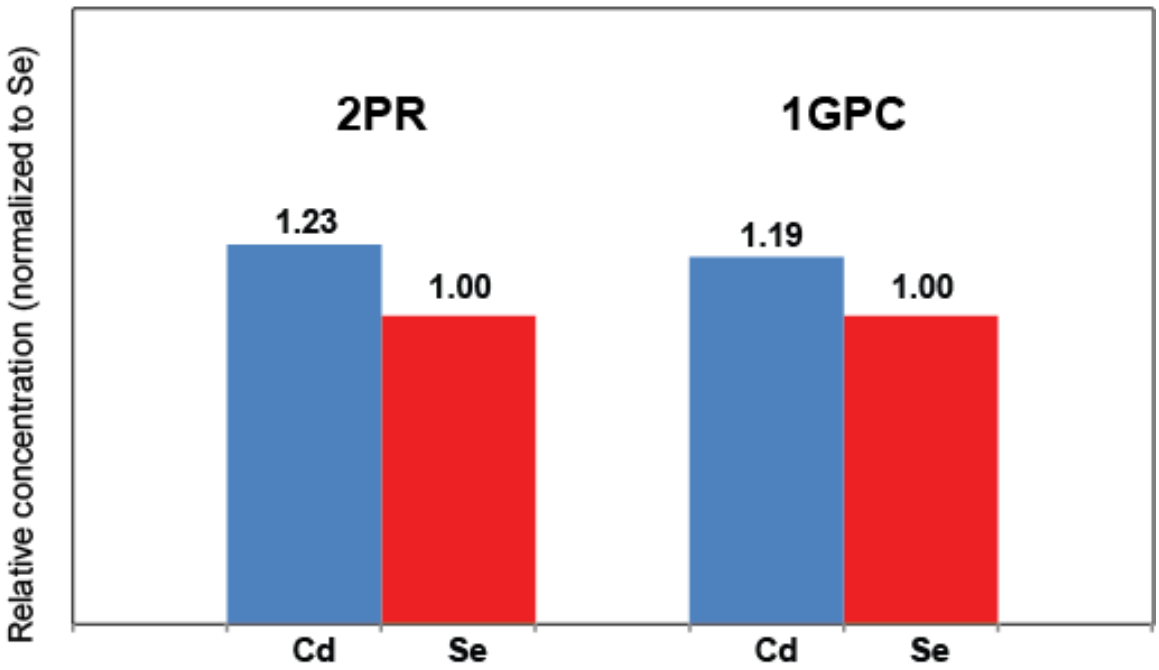

Figure 2.6 Inductively-coupled plasma mass spectrometry (ICP-MS) analysis of the Cd and Se content in **CdSe1_2PR** and **CdSe1_1GPC** QD samples. The concentrations are normalized to that of Se to find the Cd-to-Se ratio in each sample.

As shown in **Figure 2.7**, the large difference in the organic/QD ratio between the two samples was confirmed by the TGA results. In the **CdSe/CdZnS2_1PR** sample, more than 72% of the mass was lost in the organic molecule breakdown region (from 100 ℃ to 500 ℃), whereas the amount was less than 23% in the **1GPC** sample. In the ^{1}H NMR measurements, both OA and ODE can be observed in the spectrum of **CdSe/CdZnS2_1PR** sample, whereas the **1GPC** sample displays a much cleaner spectrum with only OA appearing on the QD's surface. Therefore, GPC purification can also be used for CdSe/$Cd_xZn_{1-x}S$ QDs with high efficiency.

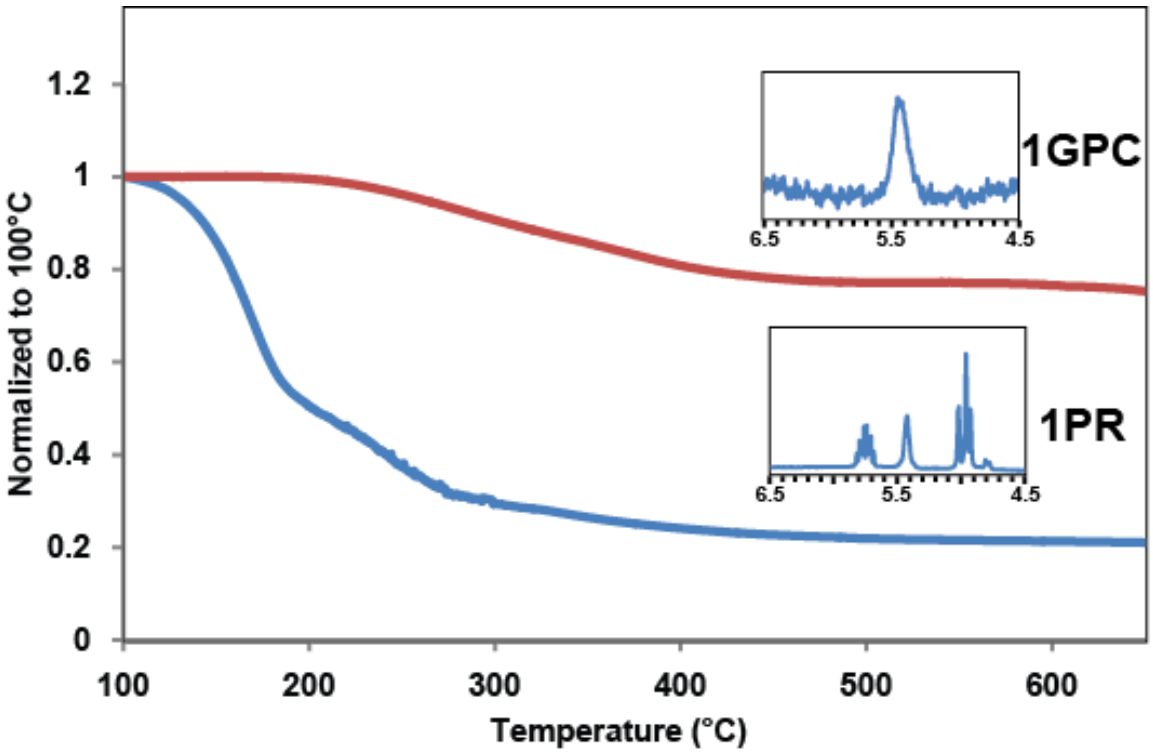

Figure 2.7. TGA curves of **CdSe/CdZnS2 1PR (blue)** and **1GPC (red)** QDs, normalized to 100 ℃, where the solvent (toluene) has been completely removed. The insets highlight the region of olefin protons from OA and ODE (4.5-6.5ppm) in the ^{1}H NMR spectra. Copyright 2013 American Chemical Society.

2.3 Purification of other nanomaterials in different shapes and with different capping ligands

In order to study the tolerance of the GPC purification technique, a variety of nanomaterials have been prepared and purified by the column. We first studied the purification efficiency of three different nanomaterials with different capping ligands to confirm this technique is not limited to oleate capped II-VI materials. The three samples we used were organic phosphonate capped CdSe QDs[12], carboxylate capped InP QDs[84] (prepared by Brandi Cossairt's group at the University of Washington) and thiol capped Au nanoparticles[85]. The tetradecylphosphonate (TDPA) capped CdSe QD samples were prepared with organic phosphonate capping in trioctylphosphine (TOP) and

trioctylphosphine oxide (TOPO) solvents. Therefore, all the ligands and impurities prepared by this method should be phosphorus-containing molecules, which makes ^{31}P NMR a sensitive technique to characterize the impurities / surface ligands in the sample solution. As shown in **Figure 2.8A-C**, after two times PR cycles, there were still a significant amount of free TDPA, TOP and TOPO remaining in the system, while the only remaining phosphorus-containing molecules in the GPC purified sample are the ionic binding phosphonate ligands. For the other two samples, we did not have a good handle (like olefin proton or phosphorus) for the NMR measurements. Therefore, TGA was used to compare the ligands-to-nanocrystal-ratio directly before and after the GPC purification. As shown in **Figure 2.8D-E**, a significantly smaller mass loss was observed after GPC purification for both samples, which indicates that this method can also be used for a large variety of materials with different capping ligands.

Another concern is the influence of the nanocrystal shape on the GPC purification results. Therefore, four CdSe/CdS core/shell heterogeneous structure nanocrystals with different shapes were prepared[19,26]. As shown in **Figure 2.9**, Sample A is a typical core/shell spherical CdSe/CdS QDs made by SILAR method; samples B to D are CdSe/CdS nanorods prepared following a published experimental procedure, and the shapes were controlled by changing the ligand ratio and seed concentration. From sample A to sample D, these nanomaterials have different sizes and aspect ratios, which provides a good model to study the nanoparticle shape effect on the GPC purification technique.

As shown in **Figure 2.10A-B**, similar to the CdSe/$Cd_xZn_{1-x}S$ samples, after GPC purification, the only remaining surfactant on the OA capped CdSe/CdS QDs were the strongly associating oleate ligands. All the other olefin containing or phosphorus

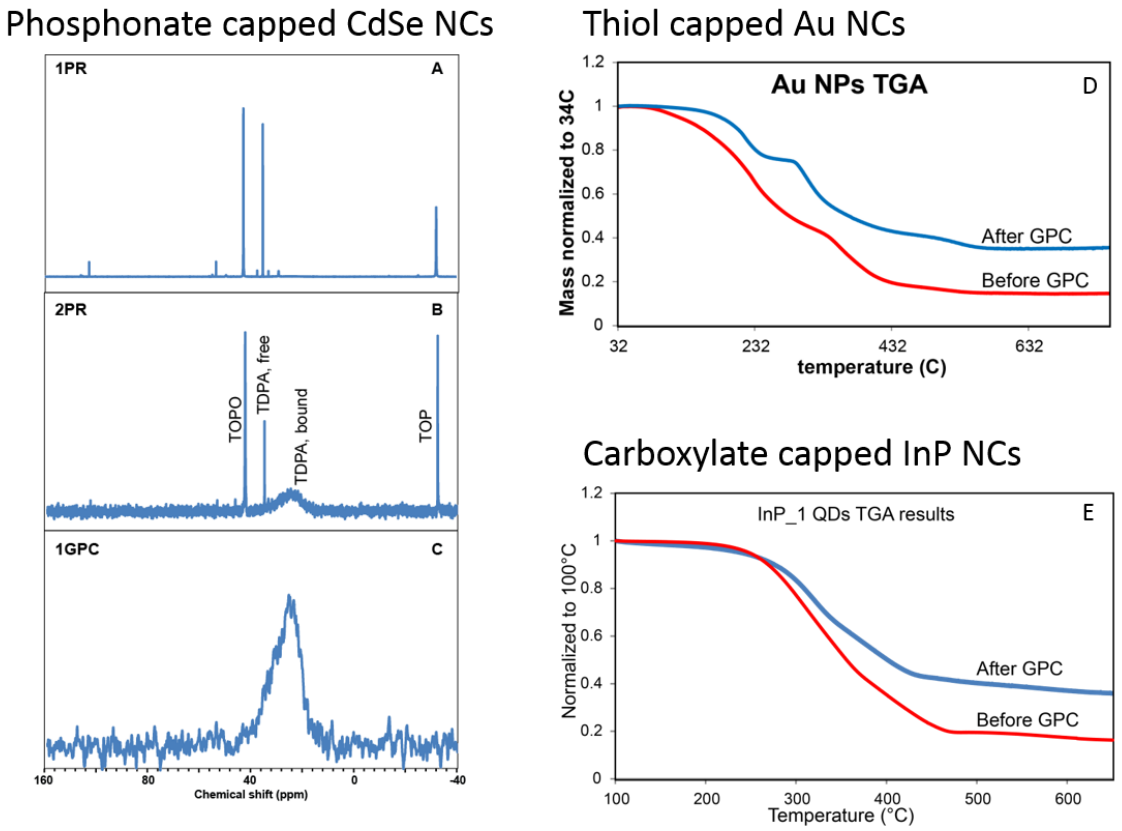

Figure 2.8 (A)-(C) The ^{31}P NMR spectra of phosphonate capped CdSe QD samples purified by different methods, demonstrating the removal of phosphorus containing species (such as free TDPA, TOP and TOPO) by the column purification. (D)-(E) normalized TGA curves of thiol capped Au nanoparticles (D) and carboxylate capped InP QDs before (red) and after (blue) GPC purification.

containing impurities and excess ligands have been successfully removed. The CdSe/CdS nanorod samples behaved similarly to the phosphonate capped CdSe QD samples. As shown by the ^{31}P NMR spectra before and after the GPC purification (**Figure 2.10C-D**), we can clearly see that after GPC, the only remaining phosphorus containing molecules are the ionic binding ligands, which have a broad signal in the spectrum. All the other free phosphorus containing ligands were effectively removed. These results confirm that the GPC purification technique is not limited by the shape/size of the nanomaterials.

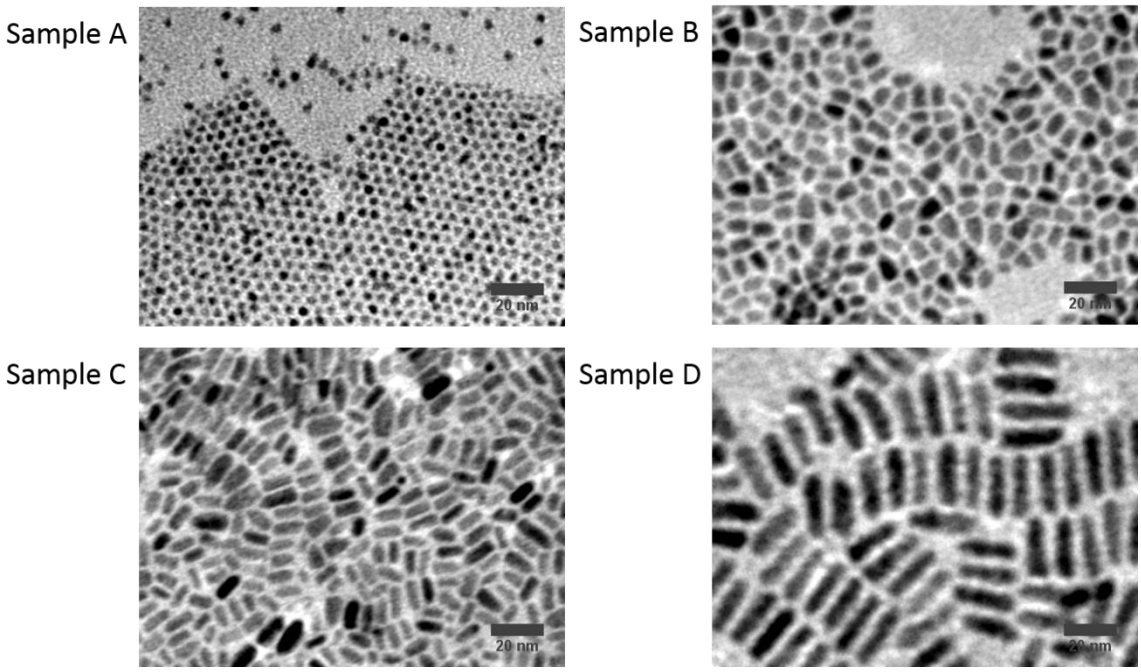

Figure 2.9 The TEM images of CdSe/CdS nanocrystals with different shapes and sizes

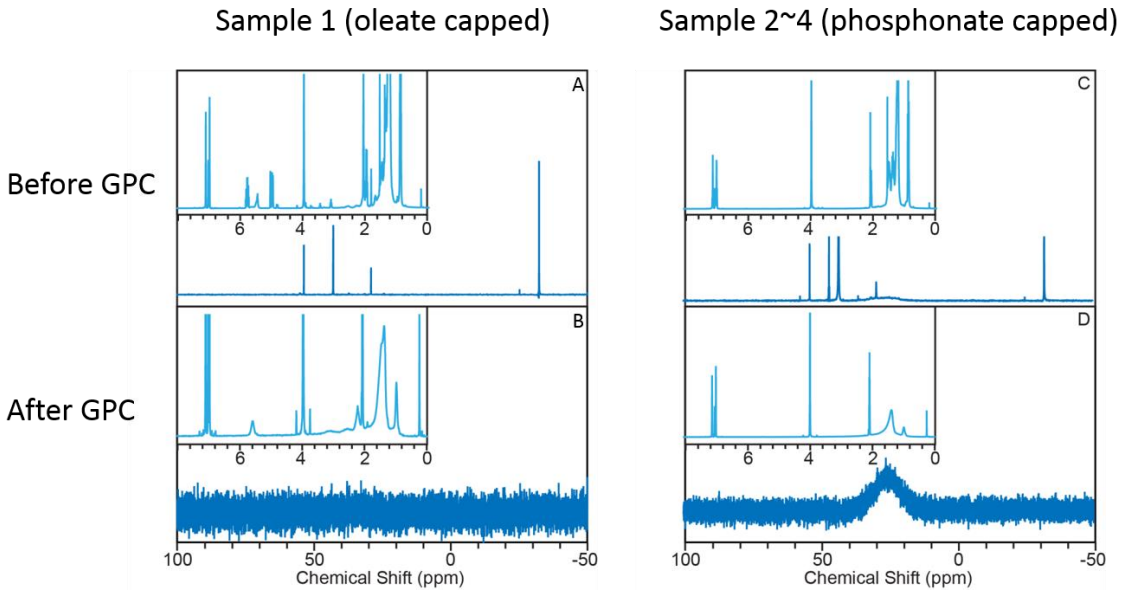

Figure 2.10 ^{31}P NMR spectra, with ^{1}H NMR spectra inset, of the CdSe/CdS nanocrystals with different shapes before and after GPC

2.4 The excess ligands' impact on further surface modification of QDs

On the basis of the results presented above, GPC has been proven to be a highly effective method for the nanocrystal purification. The achievement of an efficient method for the preparation of clean QD samples allows us to test whether impurities that reside in samples prepared by standard purification methods have a significant effect on further surface modification reactions. In the discussion shown below we employed a CdS shell growth titration experiment on CdSe QDs, and cysteine ligand exchange on CdSe/$Cd_xZn_{1-x}S$ QDs to study the effect of excess ligands and impurities on the surface reactivity of QDs.

2.4.1 Titration of CdS Shell Growth on CdSe QDs.

CdSe/CdS core/shell QDs are known for high QY[19,86] and asymmetric charge separation[87]. Some of the most widely practiced preparation procedures utilize the SILAR method to grow a CdS shell on the CdSe core[18,19,23]. The shell growth process requires that initial organic ligands be displaced so that material can be added to the crystal surface; as a result, we expect that shell growth could depend strongly on the surface environment[80,88], including the presence of excess ligands and/or impurities. Here, we employed a set of titration experiments to test whether the differences observed in analyses of GPC and PR purified QDs lead to different synthetic outcomes in the initial stages of core/shell growth by SILAR. A quantity of Cd and S precursors equivalent to 1.0 monolayer of CdS shell growth was added to **CdSe1** core samples purified by GPC or by PR only. In **Figure 2.11A-B**, 1.0 monolayer equivalent of $Cd(oleate)_2$ was added first, followed by 1.0 monolayer equivalent of $(TMS)_2S$. In **Figure 2.11C-D**, the order of addition was reversed so that S was added first. In all cases, the additions were conducted stepwise in doses of 0.1 monolayer, and time was allowed following each step for the reaction to near

completion prior to the withdrawal of a small aliquot for spectroscopic analysis. The progress of the shell growth is characterized based on the bathochromic shift of the absorption spectrum (**Figure 2.11E-H**) versus effective shell thickness applied.

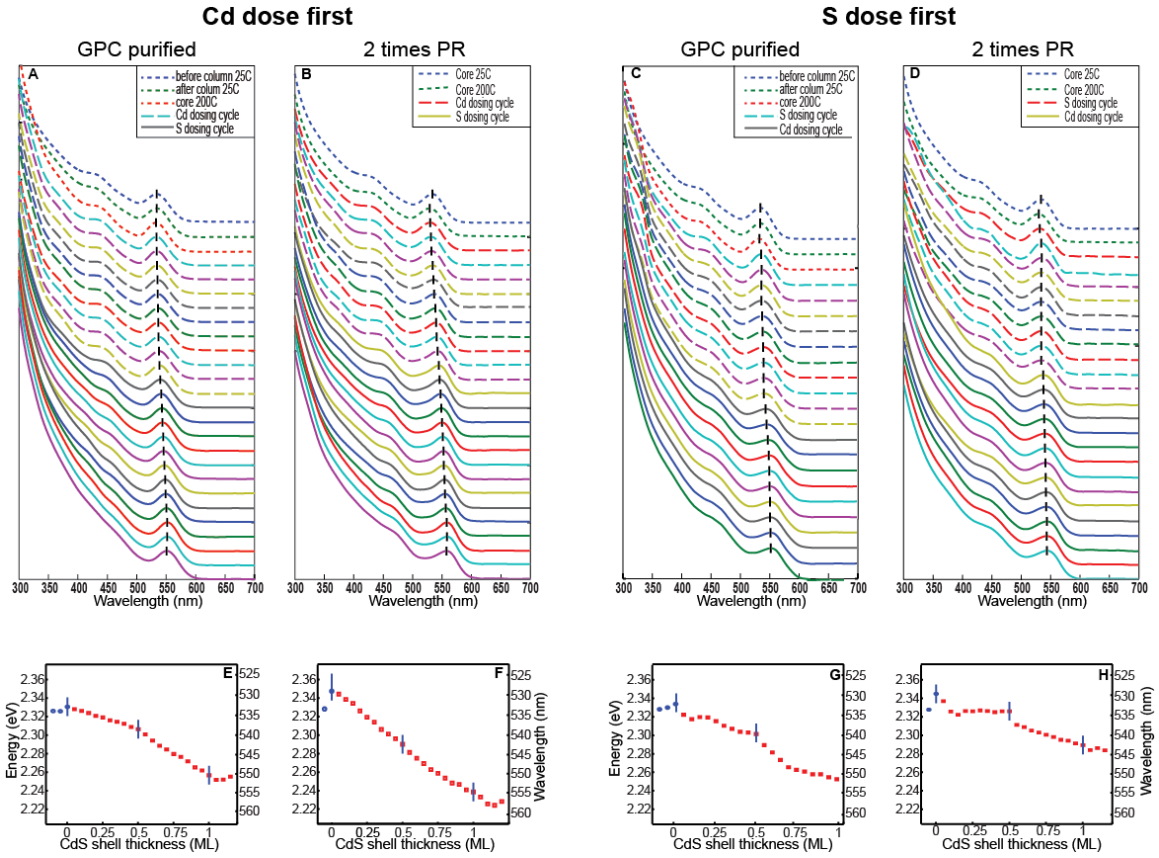

Figure 2.11 Absorption spectra and the lowest energy extinction peak position shift of the aliquots taken during the CdS shell growth titration experiment on **CdSe1** QDs purified by either **2PR** or **1GPC**. Waterfall absorption spectrum (A) **1GPC**, Cd dosing first; (B) **2PR**, Cd dosing first; (C) **1GPC**, S dosing first; (D) **2PR**, S dosing first. The interval between aliquots was 10 min. (E,F,G,H) Plots of lowest energy exciton absorption as a function of targeted CdS shell thickness for (E) **1GPC**, Cd dosing first; (F) **2PR**, S dosing first; (G) **1GPC**, S dosing first; (H) **2PR**, S dosing first. Copyright 2013 American Chemical Society.

As shown in **Figure 2.11**, the **1GPC** purified QDs experienced a lower rate of red-shifting than did the **2PR** purified sample when Cd was introduced first in the SILAR process. After the Cd cycle, both of these samples exhibited a similar growth rate in the S

cycle. We interpret the smaller redshift as an indication of a lower growth rate for Cd in the **1GPC** sample. Experiments in which the S precursor was added first also show a difference in the initial reactivity of **1GPC** and **2PR** samples. The **2PR** sample (**Figure 2.11D**) displayed little change in effective bandgap upon the addition of $(TMS)_2S$, suggesting little reaction with the QD surface given the large redshift associated with S addition following Cd (**Figure 2.11B**). In the subsequent Cd dosing cycle, we saw a relatively large redshift in the first Cd injection followed by a continuous redshifting at a slower rate. In contrast, the **1GPC** sample (**Figure 2.11C**) experienced a continuous redshift during the entire S dosing process followed by a large shift in the first four Cd injections and smaller shifts for the later ones. The FWHM of the emission peak (**Figure 2.12**) was measured to characterize the size distribution during the titration process and is helpful in explaining the difference in reactivity towards added $(TMS)_2S$ between the **1GPC** and **2PR** samples. Compared to the results when Cd is introduced first, the size distribution increases significantly during the S dosing titration cycle, with a larger increase for the **1GPC** sample.

We believe that the difference in reactivity of the initial QD surface towards the addition of $Cd(oleate)_2$ can be explained by the presence of a Cd-bearing impurity in the **2PR** sample. For the **1GPC** sample, once the $Cd(oleate)_2$ was introduced as the Cd precursor, part of it was diverted to saturate the solution instead of reacting on the QDs' surface. However, for the **2PR** sample, due to the possible presence of $Cd(oleate)_2$ as an impurity and surface etching by the excess amount of weakly bonded oleic acid, the equilibrium solubility limit for $Cd(oleate)_2$ above the QD surface had already been reached.

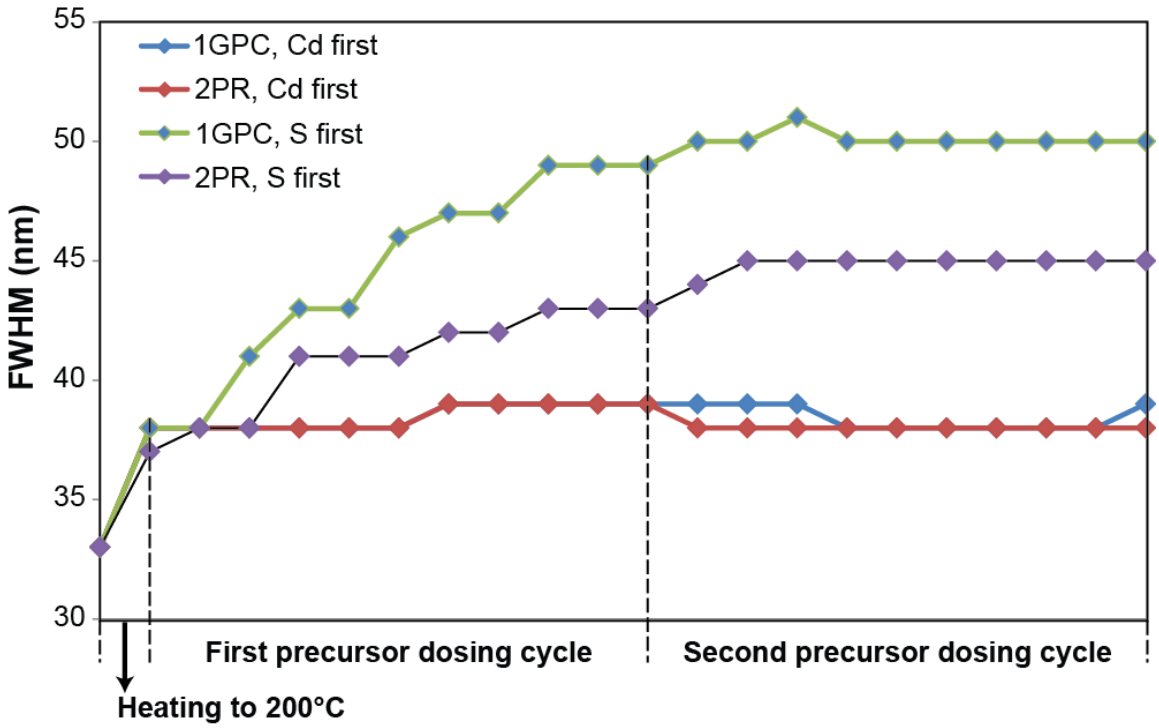

Figure 2.12 Full width at half maximum (fwhm) of the emission peaks during the titration experiment described in **Figure 2.11** of the narrative. A larger peak width is representative of a broader size distribution, though the intrinsic linewidth of QD emitters at room temperature also contributes.

Hence, in the **2PR** sample more of the added $Cd(oleate)_2$ could be used for the shell growth, which resulted in a faster growth rate and larger redshift than was observed in the **1GPC** sample.

Our observations suggest that etching and/or ripening processes are competing with shell growth when $(TMS)_2S$ is added first in both the **1GPC** and **2PR** samples. Ligand exchange experiments have shown that TMS reagents can facilitate removal of oxyacid ligands through the formation of O-TMS byproducts[89,90]. In the present case, the total amount of $(TMS)_2S$ for 1.0 monolayer shell growth, 319 per QD, is much larger than the total OA ligand density on the QD surface in either sample. The relatively larger size

distribution change observed on $(TMS)_2S$ addition in the **1GPC** titrations could be an indication that effective removal of excess ligands and impurities decreases the colloidal stability of the QDs towards the addition of excess $(TMS)_2S$.

Based on our observations, impurities and/or excess ligands present in PR purified samples influence the reactivity of the CdSe QD surface towards the addition of shell precursors in both Cd-first and S-first cases. For both PR and GPC purified samples, initiating the SILAR process with Cd produced larger redshifts and better maintained the emission linewidth; this result is in keeping with much SILAR literature in which Cd is added first[19,20]. Despite the slower initial redshift under Cd addition seen in the GPC purified sample, we stress that we have obtained core/shell QDs with good optical properties from these starting materials after multiple SILAR cycles. The availability of highly purified QD samples via GPC should allow the possible roles of various intrinsic and purposely-added minor constituents in shell growth reactions to be investigated more thoroughly in future work.

2.4.2 Cysteine ligand exchange reaction of $CdSe/Cd_xZn_{1-x}S$ QDs.

Ligand exchange reactions are essential to prepare water-soluble QDs with minimal hydrodynamic diameters; cysteine is a convenient monothiol ligand that presents a zwitterionic nanoparticle surface and has been shown to enable renal clearance of QDs[21]. In order to achieve better ligand exchange efficiency, the amount of original ligands should be reduced as much as possible. Based on the ^1H NMR and TGA results described above, the **CdSe/CdZnS2_1GPC** sample had a much smaller amount of OA than the

CdSe/CdZnS2_1PR sample. We investigated the influence of this difference in purity on a biphasic (toluene/water) cysteine ligand exchange reaction.

Before mixing the aqueous and the organic solutions, both phases are clear in each of the two samples (photographs available in **Figure 2.13A-E**). After stirring the mixtures for 15 min, material began to precipitate in the aqueous phase of the **1PR** sample and this appeared to impede the ligand exchange reaction. After 30 minutes, we observed that the aqueous phase became colorful in the **1GPC** sample; this change in solubility is evidence that the ligand exchange reaction is proceeding successfully. After 1 hour, almost all of the color had transferred in the **1GPC** sample, while the **1PR** sample still had not recovered. This result demonstrates that a clean surface of the original QDs aids in promoting a successful ligand exchange reaction, and that CdSe/$Cd_xZn_{1-x}S$ core/shell QDs with such a clean surface can be achieved by GPC. The cysteine capped **1GPC** QDs were stored in a refrigerator and slowly precipitated out after 2 days (such limited stability is characteristic of cysteine-capped QDs). The QY of these water-soluble QDs is 46.6%, which is suitable for bioimaging applications. We have achieved a successful cysteine ligand exchange with **1PR** QDs previously, but due to the limited reproducibility of the PR purification method, the reaction rarely proceeded. In contrast, the GPC purified sample consistently showed efficient exchange with the new cysteine ligand and transfer to the aqueous phase.

2.5 In situ solvent change with QDs on GPC

Applications of QDs sometime requires solvent change in order to optimize surface modification / device fabrication process. The traditional method to change the solvent of

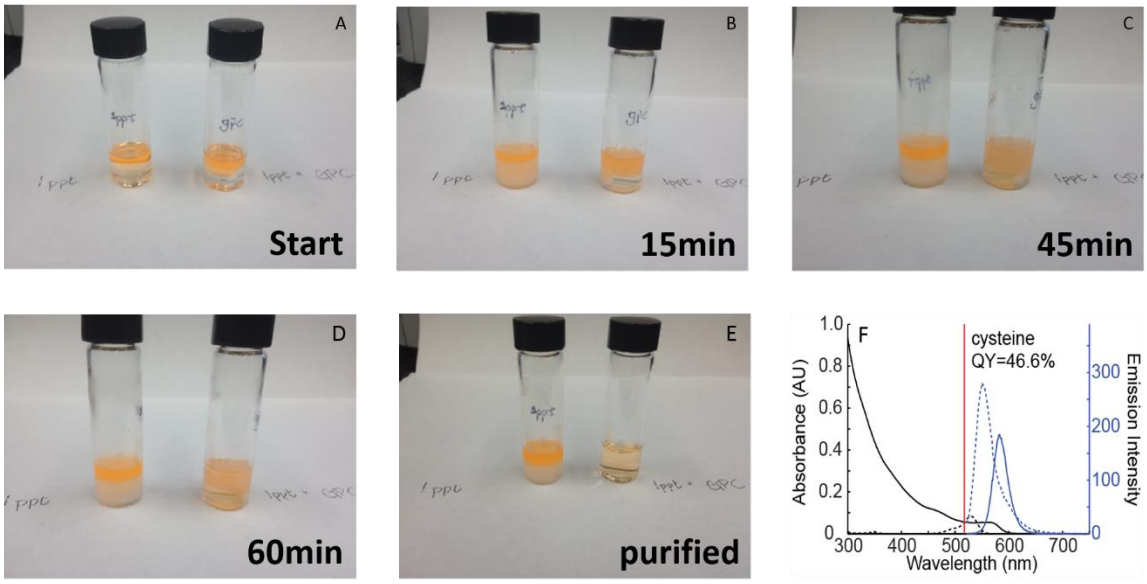

Figure 2.13 (A)-(E) Photographs of the QDs and cysteine mixtures during the ligand exchange. **CdSe/CdZnS2 1PR** sample is on the left and **1GPC** sample is on the right. The purification process includes one-time precipitation by ethanol and hexane, QDs redissolution in pH=8 buffer and filtration by polyethersulfone membrane (pore size: 0.2 μm). (F) QY of the cysteine capped QD sample. The excitation wavelengths used for each measurement are marked by the red line. Absorption spectra (black) and emission spectra (blue) of QDs are shown as solid lines, while dashed lines indicate rhodamine 590 in ethanol. Copyright 2013 American Chemical Society.

nanocrystal solution is by pumping the old solvent out by vacuum and redispersing the sample in the new solvent. However, since the sample has to be pumped dry to remove the old solvent, it is likely to cause irreversible aggregation of the particles, especially for the purified ones[55]. It would be ideal if we could change the solvent in solution phase while simultaneously doing the purification. The size of the solvent molecules is also much smaller than the nanoparticles, which made GPC probable media to perform the solvent change process. By injecting the nanocrystal sample in old solvent directly to the GPC column swallowed in the new solvent, I was able to test this hypothesis. Since in GPC the

larger molecule elutes out faster than the small ones, the nanocrystals should flow out in new solvent while the old solvent molecules are trapped by the gel porous sites.

Two solvents that have been used frequently for QD purification and single phase surface modification experiments in this lab have been tetrahydrofuran (THF) and toluene, and so they were chosen for initial tests on the GPC solvent change. There are two concerns while using GPC to change the solvent of the nanocrystals solution. One is that if the diffusion rate between two solvents is faster than the size selection process, the solvent change would not completely proceed; the other issue is that the gel could collapse while mixing with two solvents and lose its size selectivity. Therefore, I first flowed pure THF through the toluene GPC column. Based on NMR results, THF flowed out when the elution volume was close to the total volume of the column and we observed a very sharp switch between the old solvent (toluene) and the new solvent (THF). This demo experiment confirmed that the mixing between two solvents does not influence the size selective behavior of the GPC column.

In order to further confirm that the gel would not collapse when mixing with two solvents, an un-purified sample was used to test the solvent change process. If we could effectively switch the solvent of the nanocrystal sample solution and purify the nanocrystals at the same time, it would demonstrate that the mixing of two solvents does not change the overall structure of the gel in the column. Besides, it is also convenient to combine these two processes into one sequence. As shown in **Figure 2.14**, organic phosphonate capped CdSe QDs in toluene were used to study this in situ solvent change on a THF GPC column. According to the ^{31}P NMR, the sample was purified after traveling through the column. Moreover, the solvent of the sample solution completely changed from

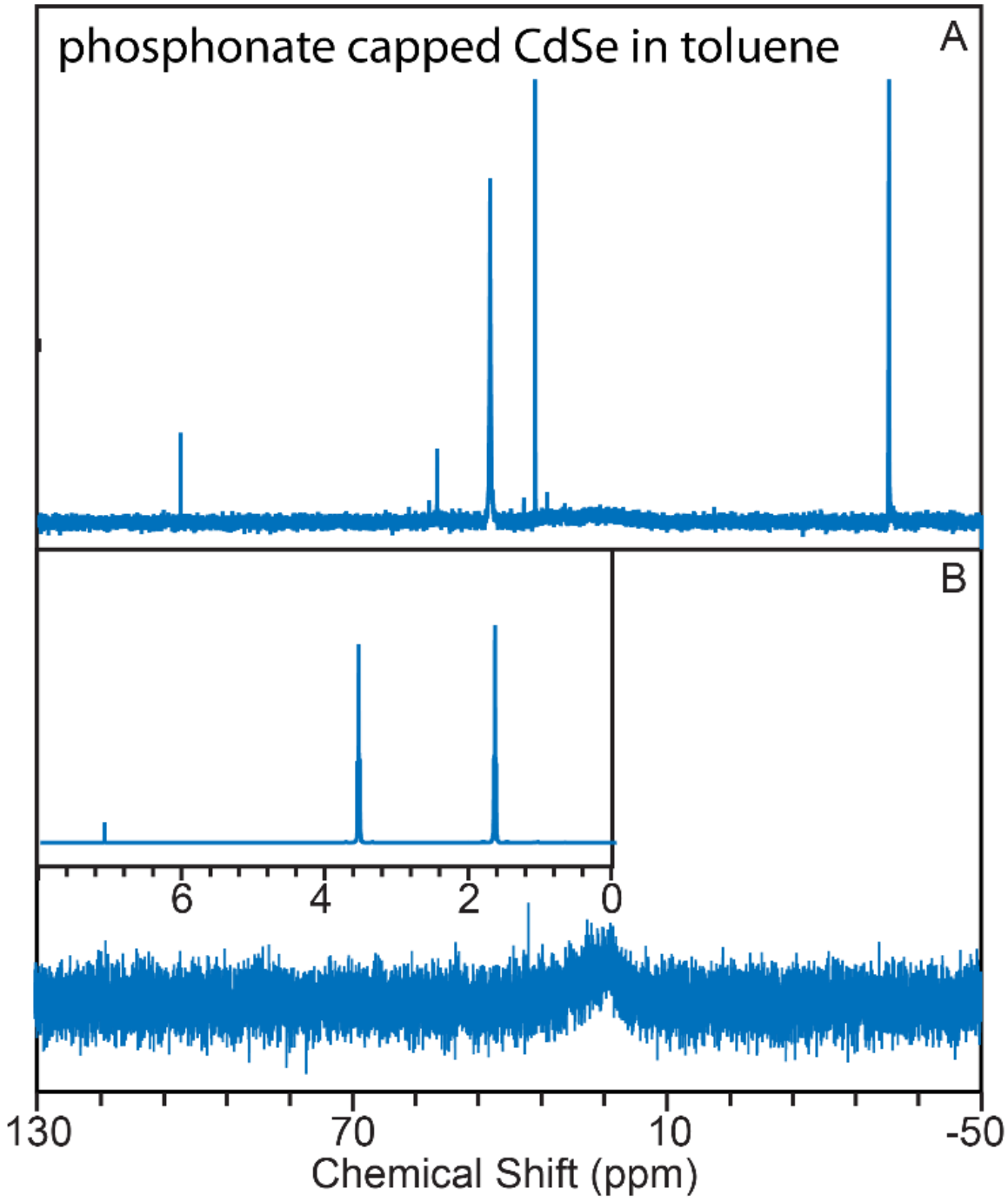

Figure 2.14 ^{31}P NMR of the sample before (A) and after (B) the GPC solvent change process. The inset in B was the ^{1}H NMR of the solvent after GPC, which confirms that the solvent is completely switched into THF.

toluene to THF after this process. We also performed a similar process, but flipped the old/new solvents (old solvent: THF, new solvent: toluene), and obtained similar results. These data confirmed that solvent change can be achieved by the GPC.

2.6 In situ ligand exchange reaction with QDs on GPC

Traditional method for ligand exchange reaction with QDs employ a huge excess of new ligands[21]. One reason is that there has not been a convenient method to separate the exchanged sample and old ligands during the exchange reaction, and the only way to drive the equilibrium to the forward direction is by increasing the amount of reagent, which is the new ligand. The old ligands on the nanocrystal surface are typically metal carboxylate or phosphonate, which are much smaller than the nanocrystals in size. If we used GPC as the ligand exchange reactor and perform the reaction on the column, we should be able to effectively separate the old ligands from the exchanged nanocrystals and improve the reaction efficiency. Additionally, the reaction time can be easily tuned by adjusting flow rate. Moreover, as we demonstrated previously, GPC can be used as a media to effectively purify the nanocrystals. That means we could potentially combine purification of as synthesized QDs, ligand exchange reaction and purification of exchanged QDs into one step. The ligand exchange reaction can be grouped into two categories based on the size of the new ligands relative to the operating range of the column. With this in mind, two model reactions have been studied: octanethiol (small new ligands) exchanging oleate-capped CdSe QDs and polymeric imidazole ligands (PILs, big new ligands) exchanging oleate-capped CdSe/CdZnS QDs.

2.6.1 Oleate-capped CdSe QDs modified by octanethiol

We first loaded the new ligands (octanethiol) into the column, and then rinsed with a small volume of the pure solvent (toluene), and then injected the unpurified QD samples. As shown in the cartoon in **Figure 2.15**, the QDs will first be purified by going through a certain volume of the GPC column without reacting with the new ligands. And then the purified QDs will contact the new ligands and perform ligand exchange reaction. The excess new ligands will be removed since the exchanged QDs will travel through another blank part of GPC before eluting out from the column. Since the GPC can assist in separating the old ligands from the exchanged QD samples, this in-situ GPC exchange should be more effective than the traditional benchtop experiment. As shown in **Figure 2.15 C-D**, the remaining oleate species of the GPC exchanged sample was only one third of the ones on the normal exchanged samples (both exchanges were close to complete, which makes it difficult to get exact ligand-to-QD-ratio according to quantitative NMR measurements). Additionally, the starting material of the GPC exchange reaction was the unpurified sample (**Figure 2.15A**) while the QD sample for the benchtop experiment is the GPC purified one (**Figure 2.15B**), which further addressed the efficiency of the GPC in-situ exchange technique.

One more advantage of the GPC in situ exchange with small molecules is that it could remove the excess new ligands after the exchange reaction. The thiol capped QDs are known to be photo unstable, and normally people put more ligands into the exchange sample to slow down this process[21,91,92]. On the other hand, if the excess new thiol ligands are removed, the sample should be more likely to precipitate. As shown in **Figure 2.16 A-B**, after storing the sample in the fridge for 12 hours, the GPC exchanged sample started to

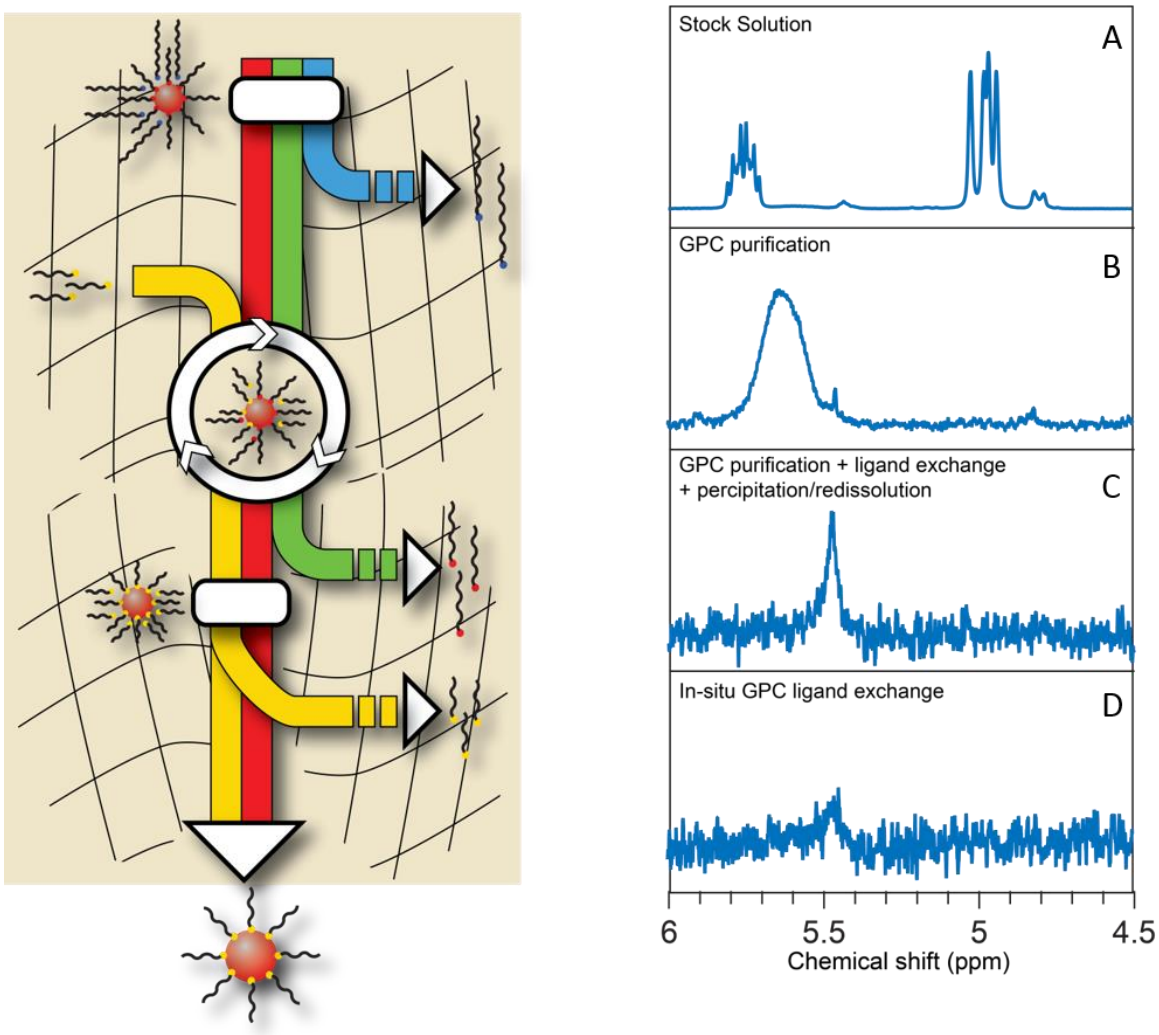

Figure 2.15 Left: Cartoon of reaction scheme for in-situ GPC exchange reaction with small molecules. Right (A-D): the expanded views of the ^{1}H NMR spectra in the range 4.5-6.0 ppm for (A) unpurified stock solution, (B) GPC purified sample, (C) benchtop exchanged sample and (D) in-situ GPC exchanged sample.

precipitate while the benchtop exchanged one remain stable in solution, which indicates that there were much less amount of free thiol remaining in the GPC exchanged solution than the benchtop one. TGA was also used to confirm the removal of the excess ligands. Since the thiol exchange reaction were close to complete in both experiments, smaller mass

loss from GPC exchanged sample suggest that excess new thiol ligands have been effectively removed from the system.

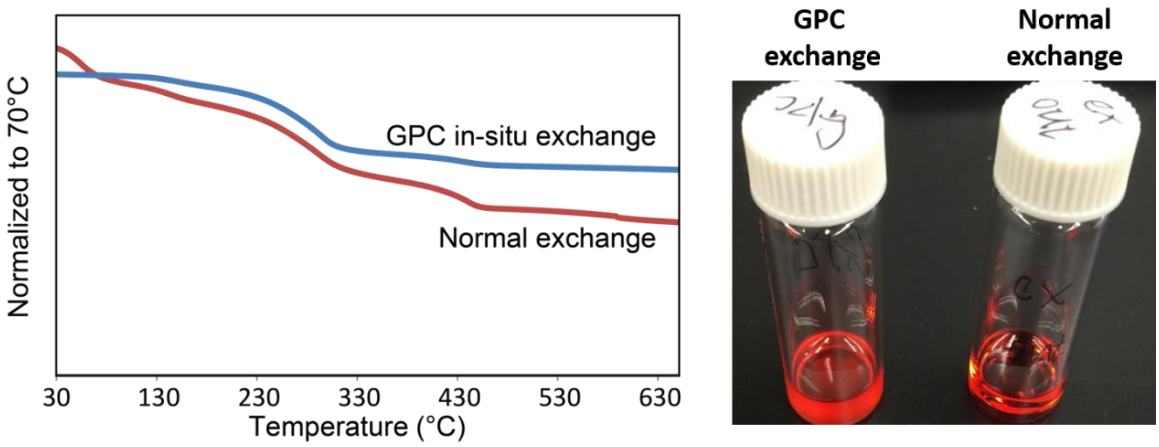

Figure 2.16 Left: normalized TGA curves of GPC in-situ exchange sample (blue) and normal exchange sample (red). Right: Pictures of the thiol capped GPC in-situ exchange sample and normal exchange sample after 12 hour storage in fridge.

2.6.2 Oleate-capped CdSe/CdZnS QDs modified by polymeric ligands

Polymeric imidazole ligands (PILs) have been considered as a promising candidate in preparation of bio-compatible QDs and they will be further addressed in Chapter 4. Here, we used PILs as a representative of the macromolecule to study the in-situ GPC ligand exchange. As shown in the cartoon in **Figure 2.17**, for the macromolecule, the elution rate is the same as the nanoparticles while traveling inside the column. Therefore, a mixture of the PILs and unpurified CdSe/CdZnS QDs were injected together through the GPC column swallowed in chloroform. Since the flow rate of this column is faster than the toluene column (1mL/min compared to 0.4mL/min), within 10 minutes, the ligand exchange reaction was finished. As shown in **Figure 2.17C**, the original ligands oleate were almost

completely replaced by the new PILs and the PIL capped QD samples prepared by in-situ GPC exchange can be easily dispersed in water for biological labeling and imaging.

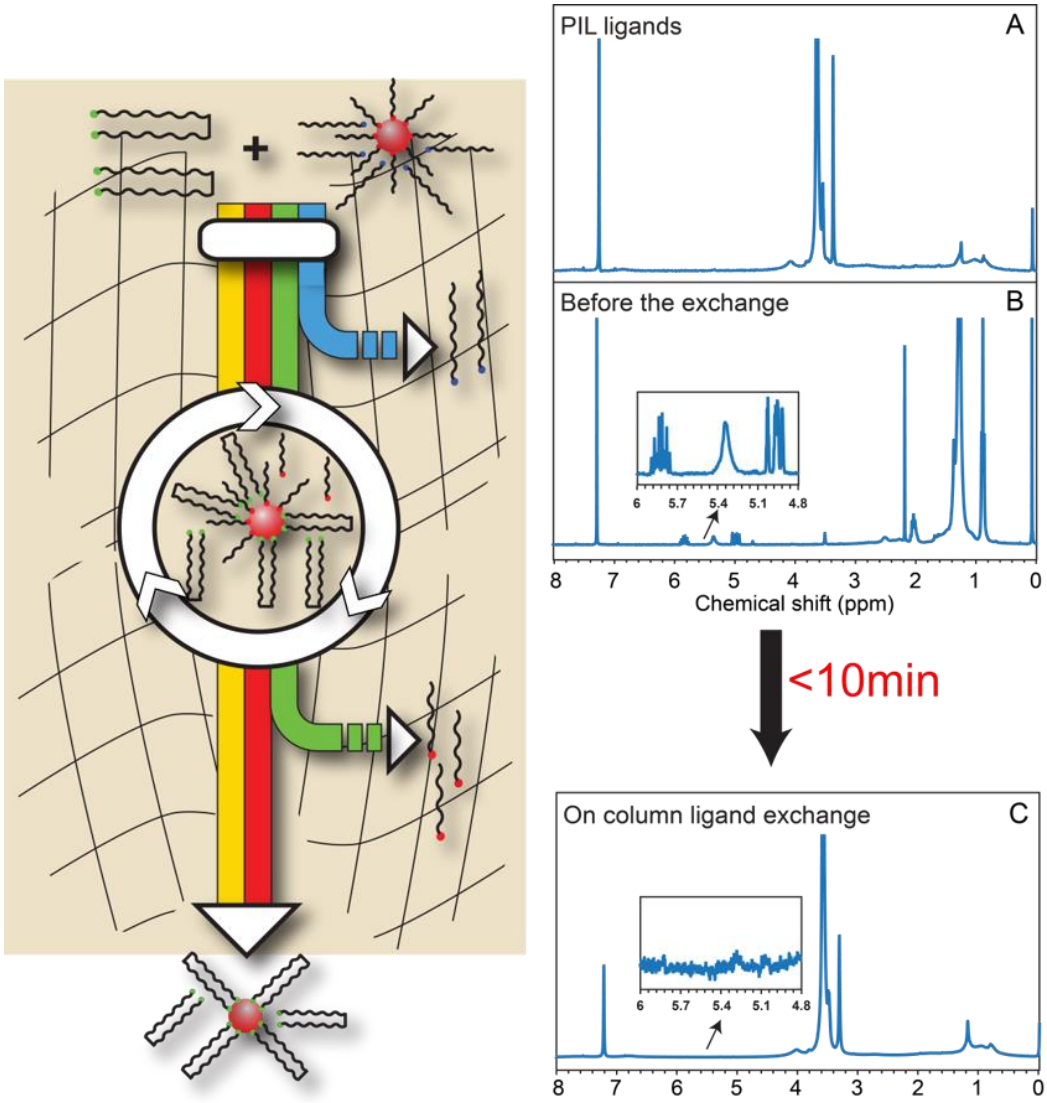

Figure 2.17 Left: Cartoon of reaction scheme for in-situ GPC exchange reaction with macromolecules. Right (A-C): ^{1}H NMR spectra of the (A) pure PILs (B) unpurified CdSe/CdZnS QDs (C) PIL capped QDs prepared by in-situ GPC exchange. Insets are the expanded views of the ^{1}H NMR spectra in the range 4.5-6.0 ppm.

2.7 Conclusion

We have demonstrated that gel permeation chromatography can be used as a simple and highly effective technique to purify monodisperse nanocrystal samples from their

inevitable by-product and excess ligand impurities. This method provides more confidence and better reproducibility than the traditional precipitation/redissolution purification processes. As stated previously, GPC purifies the nanocrystals of their synthetic impurities and excess ligands on the basis of hydrodynamic size by a fixed separation driving force with high resolution. The mobile phase for this chromatographic technique is an organic solvent in which the nanocrystals remain miscible, and therefore affords a single phase purification that does not risk perturbing the original binding environment. Polarity is an essential factor in the precipitation of nanocrystals; however, due to its variance among different batches and uncertainty as to the solubility characteristics of undesired impurities and/or excess ligands, it is an unreliable property on which to base the isolation of nanocrystals. Furthermore, core/shell QDs can present solubility limitations after multiple precipitations, which are amply circumvented by the GPC purification technique.

A variety of spectroscopic methods (including NMR, DOSY and electronic absorption), elemental analysis, thermogravimetric analysis and surface modification techniques have been combined in order to present a systematic analysis of the GPC purification of the nanocrystals. These combined analyses provide qualitative and quantitative information about the nanocrystals surface, and validate both the feasibility and efficiency of the GPC purification.

The surface modification experiments that we performed on the core and core/shell QDs, coupled with the analyses above, demonstrated that constituents of crude QD samples that may remain following precipitation/redissolution purification, but can be effectively removed by GPC, can have a profound effect on subsequent surface modification reactions. It is clear that studies of the mechanistic details of such reactions, which are of primary

concern for proposed fluorescence and optoelectronic applications of QDs, must be conducted in view of the possible roles of impurities and excess ligands.

I have also described how we have demonstrated that GPC can be used as a reactor to perform solvent change and ligand exchange reaction with higher efficiency and better control. Combined with purification, GPC can be used as a multi-step processor for the surface modification of nanocrystals.

In providing a relatively clean and highly stable QD surface, GPC purification has the potential to contribute significant value in investigations of ligand exchange, ligand-mediated growth of inorganic layers, and other nanoparticle/ligand interactions. For example, it is our hope that future applications of this purification method can enable measurement of surface ligand exchange reactions of QDs with well-defined mass action relationships, address the role of weakly and/or neutrally-binding ligands in controlling non-radiative recombination, and perhaps most importantly, contribute to the development of quantifiable metrics of sample quality that allow QDs batches prepared in different settings to be used interchangeably in applications or as the basis for further synthetic work.

2.8 Materials

The following chemicals were used as received. Cadmium oxide (CdO; 99.999%), Zinc oxide (ZnO; 99.999%), Trioctylphosphine (TOP; 97%) and Trioctylphosphine oxide (TOPO; 99%) were purchased from STREM Chemicals. Oleic Acid (99%), 1- Octadecene (ODE; 90% technical grade), 1-Tetradecylphosphonic Acid (TDPA; 98%), Selenium (Se; 99.999%) and L-Cysteine (98^{+} %) were purchased from Alfa Aesar. Bio-Beads S-X1 GPC

medium was obtained from Bio-Rad Laboratories, Inc. Toluene-d_8 (D, 99.5%) and Tetrahydrofuran-d_8 (THF; D, 99.5%) were obtained from Cambridge Isotope Laboratories, Inc. Decylamine (95%) was purchased from Sigma Aldrich. Oleylamine (80-90%) and Bis(trimethylsilyl) sulfide ($(TMS)_2S$; 95%) were purchased from Acros Organics. Rhodamine Chloride 590 (R590, MW 464.98) was obtained from Exciton. Toluene (99.5% ACS analysis grade) was purchased from Mallinckrodt Chemicals. 200 Proof Ethyl Alcohol (Ethanol) was obtained from Decon Laboratories, Inc. Acetone (99.9%) was purchased from VWR. Methanol (99.9%) was purchased from Fisher Scientific. Synthetic or analytical procedures either under nitrogen (N_2) or vacuum environment were carried out using Schlenk line techniques, or a glovebox.

Synthesis of CdSe QDs. 60 mg CdO and 330 mg oleic acid were introduced into a three-neck flask with 6 mL ODE as the noncoordinating solvent. The flask was heated to 100 ℃ and vacuum was applied to remove air and water from the system. The flask was continuously heated to 270 ℃ under N_2 environment to produce a colorless and clear mixture. Afterward, the reaction mixture was cooled to 130 ℃ and vacuum was applied again to remove evolved water. The mixture was reheated to 270 ℃ under N_2 and 0.64 mL TOPSe solution (prepared by dissolving Se in TOP in a glove box, with concentration 2.2M) was quickly injected. The reaction flask was allowed to cool down in ambient air to room temperature (the temperature decreasing trajectory is available in the Supporting Information, Figure S1). The ratio between Cd:Se:oleic acid is 1:3:2.5 and the lowest energy extinction peak is at 534 nm.

Synthesis of core/shell QDs. A selective ionic layer adhesion and reaction (SILAR) approach was used to grow both CdSe/CdS and CdSe/$Cd_xZn_{1-x}S$ core/shell QDs.

A portion of as-synthesized CdSe core was diluted with hexane and flocculated by methanol and acetone. After decanting the supernatant, the QDs were redissolved into hexane and stored in the fridge (4 ℃) for more than 12 hours. All the undissolved materials were removed by centrifugation and the sample was precipitated again by an addition of methanol and acetone. Afterward, the QDs were brought into a measured volume of hexane. The UV-Vis absorption spectrum was recorded at a known dilution of the sample to determine the size and quantity of QDs[45].

The solution of QDs in hexane was transferred to a solvent of 1:2 oleylamine:ODE (v/v, 9mL total) and degassed at 100 ℃ to remove hexane. Before the addition of the reagent via syringe pump, the system was heated to 190 ℃ under nitrogen. The metal precursor metal oleate with a concentration of 0.1M. The S precursor was a 0.1M solution of $(TMS)_2S$ in TOP. The volume increase associated with 1 monolayer coverage of CdS ($Cd_xZn_{1-x}S$) is calculated based on the radius increase of 3.37 Å (3.2 Å), which is half of the wurtzite *c*-axis unit cell dimensions. Alternating injections of metal precursor and sulfur precursor were performed, adding the metal precursor solution first, with injections starting every 15 minutes. The flow rate was adjusted to complete each injection over the course of 3 minutes. The volume of each injection was calculated to apply 0.8 monolayers coverage each cycle (a cycle is defined as one metal precursor injection and one sulfur precursor injection) and 5 cycles total were performed. After the reaction, the mixture was cooled down to the room temperature and the molar extinction coefficient was estimated based on the amount of the core introduced at the beginning and the total volume of the solution after the synthesis.

Synthesis of TDPA capped CdSe cores. The synthetic solvent is a mixture of 3g TOPO and 3mL TOP. The Cd precursor was prepared by heating 60mg CdO and 285mg TDPA at 300 ℃ under nitrogen flow until the solution became colorless and clear (Cd:Se:TDPA ratio of 1:3:2.2). Afterward, the reaction mixture was cooled to 130 ℃ and vacuum was applied to remove evolved water. The mixture was heated back to 360 ℃ and quickly mixed a solution of TOPSe in TOP (2.2M). The flask was cooled down under a stream of air to room temperature.

Synthesis of thiol capped Au particles. The thiolate-capped Au nanoparticles (NPs) were prepared by a modified two phase liquid-liquid synthesis method designed by Mathias Brust and co-workers[85]. Briefly, tetrachloroaurate ($AuCl_4^-$) was transferred from aqueous solution to toluene by tetrabutylammonium bromide and then the $AuCl_4^-$ was reduced in the presence of dodecanethiol by stirring the toluene solution with aqueous sodium borohydride; the dodecanethiol functions as the ligand for the resulting reddish or black solution of Au nanoparticles.

Synthesis of CdSe/CdS nanorods. The nanorods were synthesized based on a published work.[26] The Cd precursor for Sample 2 was a mixture of Cd phosphonate in TOPO (92mg CdO, 291mg octadecylphosphonic acid (ODPA) and 80mg hexylphosphonic acid (HPA) dissolved in 3g TOPO). After heating the Cd precursor solution to 370 ℃, a mixture of 100nmol phosphonate capped CdSe QDs in TOP and S precursor (60mg S dissolved in 1.5g TOP) was injected into the solution. The temperature was kept at above 350 ℃ for 10 minutes and then cooled down to the room temperature. Sample C was prepared in the same method with higher amount of HPA (101mg). Sample D was prepared with less amount of CdSe seeds (60nmol)

GPC column packing. To pack the preparative column, 4~5 g of Bio-Beads were first swollen in toluene overnight. 5 mL clean toluene was placed in the glass column (inner diameter ~1 cm) with a filter (0.2 μm pore size filter and glass wool) and a Teflon valve. All of the swollen beads were transferred to the column. After the gel settled down and formed the column with a height of approximately 31~38 cm, toluene was used to rinse the column until no free polystyrene was present in the eluent (tested by UV-Vis absorption).

QD purification: Precipitation/redissolution process. A portion of the as-synthesized QD batch was centrifuged to remove any undissolved material. Acetone and methanol were used as the anti-solvent to precipitate the QDs (for CdSe QDs, both acetone and methanol were used; for CdSe/$Cd_xZn_{1-x}S$ QDs, acetone alone can flocculate the solution). After centrifuging for 5 minutes, the QDs can be separated from the mixture. For CdSe QDs, the spin speed is 8000 rpm (8228 × *g*), while it is 5000 rpm (3214 × *g*) for the CdSe/$Cd_xZn_{1-x}S$ QDs. The QDs were redissolved in toluene and labeled as 1 time precipitation/redissolution purified sample (**1PR**). By repeating the above process, we obtained 2 times PR purified samples (**2PR**) and also a 6 times PR purified sample (**6PR**).

QD purification: GPC purification process. In order to remove most of the synthetic solvent and concentrate the QD sample in toluene, we always carried out a single PR cycle before the GPC purification. **1PR** QDs (concentration ranges from 5~150 μM with 0.5~1 mL injection volumes) were added to the GPC column with toluene as the eluent . The sample was collected when the elution volume equaled ~1/3 of the total volume of the column (the expected void volume for irregularly spaced spherical beads); this volume corresponds to the fraction at which the purified QDs eluted. The total volume we collected after GPC purification is approximately 2 mL (more than 95% of the QDs will

come out in this range) and the solution was labeled GPC purified sample (**1GPC**). We also obtained 2 times GPC purified samples (**2GPC**) by reusing the column to purify the **1GPC** samples a second time.

CdS shell growth on CdSe core titration experiment. After having been purified by different methods, the solution of QDs in toluene was transferred to a growth flask with an added solvent of 1:2 oleylamine:ODE (v/v, 9 mL total) and degassed at 100 ℃ to remove the toluene. Before addition of the reagent via syringe pump (J-KEM Scientific Dual Syringe Pump, Model 2250), the flask was heated to 200 ℃ under nitrogen. The Cd precursor is prepared by diluting 0.2M $Cd(oleate)_2$ in ODE with 2 equivalents of decylamine and a volume of TOP to yield a Cd concentration of 0.1M. The S precursor is a 0.1M solution of $(TMS)_2S$ in TOP. The CdSe core radius was estimated by a calibration curve for its radius as a function of the position of the lowest energy absorption peak. The volume increase associated with 1 monolayer coverage of CdS is calculated based on the radius increase of 0.337 nm, which is half of the wurtzite *c*-axis unit cell dimension for CdS. We chose to apply dosage equivalents to approximately 0.1 monolayer incremental shell thickness in each injection in order to observe the shell growth progression. Each injection started every 10 minutes with 3 minutes dosing and 7 minutes delay to ensure the completion of the reaction. After dosing 1monolayer (10 injections) of one precursor, the other precursor was introduced until the lowest energy absorption peak stopped redshifting.

Cysteine ligand exchange reaction for CdSe/$Cd_xZn_{1-x}S$ QDs The ligand exchange reaction was performed by a modification of a published method. Purified QDs samples were mixed with 1 mL L-Cysteine solution (prepared by dissolving 40 mg L-cysteine in 1 mL pH=7.4 phosphate buffer solution). The biphasic mixture was stirred

vigorously at room temperature for 1 hour, by which time we observed the color transfer to the aqueous phase. The QDs were precipitated once by ethanol/hexane, redissolved in pH=8 buffer solution and filtered by polyethersulfone membrane (pore size: 0.2 μm) for further analysis.

In-situ ligand exchange reaction. For the reaction between oleate capped CdSe QDs and octanethiol, 30nmols of dots were used to react with 0.1g thoil ligands. The total volumn of the toluene GPC column is close to 40mL. First the thiol ligands were dissolved in 10mL toluene and then loaded onto the column. After that, 6mL pure toluene was introduced and then 30nmols unpurified QDs in 0.7mL toluene was injected. The sample was rinsed out by toluene. The flow rate for this reaction is 0.4mL/min. A similar experiment was performed on the bench with GPC purified QDs mixing with the same amount of octanethiol ligands (0.1g). The reaction was quenched by precipitation of acetone and methanol.

For the reaction between oleate capped CdSe/CdZnS QDs and PILs, 10nmols of unpurified dots were used to react with 500nmols of 26k MA-PILs described in Chapter 4. The mixture of the polymer and QDs were injected into a chloroform GPC (flow rate is 1 mL/min and total volume is 28mL) and eluted out within 10 min.

Optical Spectroscopy. The formation of CdSe QDs and CdS or $Cd_xZn_{1-x}S$ shell on the surface was monitored by the absorption spectrum from UV-Vis spectroscopy. The optical absorption spectrum was recorded using a Thermo Scientific Evolution Array UV-Visible Spectrophotometer with toluene as the solvent as well as the blank in a 1cm path quartz cuvette. The fluorescence spectra were also used to monitor the growth and size

distribution of the QDs. Emission spectra were recorded by an Ocean Optics USB 4000 spectrometer under ~365 nm excitation.

NMR Analysis of QDs. Routine NMR samples of the QDs were prepared in toluene-d_8. The QDs' concentration is set at approximately 60~100 μM for CdSe QDs and 5~10 μM for CdSe/$Cd_xZn_{1-x}S$ QDs; the exact value in each case was measured by UV-Vis using the calculated molar extinction coefficient. The qualitative ^{1}H NMR spectra were recorded on a Varian Mercury/VX 300 NMR. The quantitative ^{1}H NMR spectra were recorded on a Varian Mercury/VX 400 NMR with THF as the internal standard. The relaxation delay used is 26s and the acquisition time is 3s, which in total is equal to $5 \times T_1$ of the THF peak at around 3.5ppm (T_1=5.8s) and much greater than the $5 \times T_1$ of the olefin peak of the oleic acid (T_1=0.8s), allowing the system to reach a reliable equilibrium. The T_1 experiments were performed by using the standard inversion-recovery pulse sequences (180 °pulse --- delay --- 90 °pulse). Diffusion measurements were performed on a Varian Mercury/VX 400 using the vendor-supplied Doneshot pulse sequence. QDs were dissolved in THF-d_8 and spectra were recorded with 100ms diffusion delay and 2ms diffusion gradient length. Diffusion ordered spectroscopy (DOSY) analysis was done using the routines incorporated in the VnmrJ 2.2D software. The spectra of oleic acid and ODE in toluene-d_8 were recorded on a Varian Mercury/VX 400. The ^{31}P NMR spectra of **CdSe1** (concentration around 100 μM) samples were measured by a Bruker Avance III HD 400 with 512 scans.

Thermogravimetric Analysis (TGA). Samples were prepared by concentrating them under vacuum, and then transferring them to the platinum pan in liquid form (colloidal QDs are difficult to transfer in solid form). TGA was conducted on a TA

Instruments Q5000 with a heating rate of 10 ℃/min from 40 ℃ to 650 ℃ under constant nitrogen flow.

Inductively Coupled Plasma-Mass Spectrometry Analysis. Inductively coupled plasma-mass spectrometer (ICP-MS) samples were prepared by drying the CdSe QDs solution via vacuum and digesting the samples in 2 mL aqua regia. The concentrations of both Cd and Se were detected by a Thermo-Finnigan Element XR ICP-MS.

Quantum Yield Measurements. The quantum yield (QY) of the CdSe/$Cd_xZn_{1-x}S$ QD samples was measured relative to rhodamine 590 (R590, QY=99% in ethanol).[2] The excitation wavelength was chosen based on the optical isosbestic point of the QDs-toluene solution and R590 in ethanol. Fluorescence spectra of QD and R590 dye were taken under identical spectrometer conditions on Varian fluorescence spectrometer in triplicate and averaged. The optical density was kept below 0.1 between 500 and 800nm to avoid internal filtering effects. The QY was calculated based on the integrated intensities of the emission spectra, the absorption at the excitation wavelength and the refraction index of the solvent using the equation:

$$QY_{QDs} = QY_{dye} * \frac{Absorbance_{dye}}{Absorbance_{QDs}} * \frac{Emission\ integral_{QDs}}{Emission\ integral_{dye}} * \frac{Refraction\ index^2_{toluene}}{Refraction\ index^2_{ethanol}}$$

The precision of this measurement in our case is limited by the precision of the absorbance measurement (~1%) while the accuracy among samples in different solvents will be limited by the accuracy of the refractive index correction term.

CHAPTER 3

EFFECT OF NEUTRAL LIGANDS ON THE PHOTO-PHYSICAL PROPERTIES AND SHELL FORMATION OF THE QUANTUM DOTS

3.1 Introduction

The surfactants on the quantum dots (QDs) surface not only maintain the particle colloidal stability, but also influence QDs' electronic structure and optical properties[55,93,94]. As described previously, according to the covalent bond classification, the ligands on QDs can be grouped into three different groups, namely X-type ligands (ionic bond), L-type ligands (neutral electron donor) and Z-type ligands (neutral electron acceptor).[95] Compared to bulk atoms, the surface atoms have lower coordination and the binding strength between the nanocrystal (NC) surface and L-type ligands is typically weak. As shown in Chapter 2, these weakly associated ligands can be easily removed by standard purification steps. However, the remaining unpassivated sites can create electronic states within the semiconductor bandgap and trap the photo generated carriers before they recombine, which significantly influences the photoluminescence properties of the QDs. Therefore, a better understanding of the ligand coordination chemistry is essential for QDs' application in lighting and bio-imaging. Besides, during the shell growth process, the precursors need to associate to the NC surface and it is possible that such ligand coordination is competing with the precursor conversion. In this chapter, we will focus on studying how the neutral

ligands, especially the L-type ligand, affect the growth and the photo-physical properties of the core/shell QD structure.

The first project described here is an experiment designed to identify the role of specific molecular ligands in maintaining the high photoluminescence (PL) quantum yield (QY) observed in as-synthesized CdSe/CdZnS and CdSe/CdS QDs. Although it has been possible for many years to prepare core/shell quantum dots with near-unity quantum yield through high-temperature colloidal synthesis, purification of such colloidal particles is frequently accompanied by a reduction in quantum yield. Here, the previously described gel permeation chromatography (GPC) technique is used to remove weakly associated ligands without a change in solvent: a decrease in ensemble QY and average PL lifetime are observed. Minor components of the initial mixture that were removed by GPC are then added separately to purified QD samples to determine whether re-introduction of these components can restore the photo-physical properties of the initial sample. We show that among these putative ligands, trioctylphosphine and cadmium oleate can regenerate the initial high QY of all samples; but only the "L-type" ligands (trioctyphosphine and oleylamine) can restore the QY without changing the shapes of the optical spectra. Based on the PL decay analysis, we confirm that quenching in GPC-purified samples and regeneration in ligand-introduced samples are associated chiefly with changes in the relative population fraction of QDs with different decay rates. The reversibility of the QY regeneration process has also been studied; the introduction and removal of trioctylphosphine and oleylamine tend to be reversible while cadmium oleate is not. Finally, isothermal titration calorimetry (ITC) has been used to study the relationship

between the binding strength of the neutral ligands to the surface and photo-physical property changes in QD samples to which they are added.

In the second project, we monitored precursor conversion and shell growth on CdSe QDs in the presence of three different amine solvents in an effort to increase the synthetic yield of the shell growth. UV-vis absorption and photoluminescence spectroscopy are applied to monitor shell growth. Photoluminescence excitation spectroscopy was applied to confirm the presence/absence of precursor nucleation. The binding affinities of the amine molecules to the QD surface are also studied to understand the influence of such interactions on shell growth. We find that a tertiary amine solvent is effective in increasing precursor conversion and suppressing nucleation of side products when compared to primary and secondary amines at a similar solvent mole fraction. The difference appears to be associated with competition for surface sites between the metal carboxylate precursor and the primary amine.

3.2 Quantum Yield Regeneration: Influence of Neutral Ligand Binding on Photo-physical Properties in Colloidal Core/Shell Quantum Dots

3.2.1 Introduction

As a result of their size-tunable narrow emission with high quantum yield and remarkable photo-stability, quantum dots are of particular interest for bio-imaging applications and display applications. However, a limitation in many of these cases is the nonradiative decay rate, which competes with light emission or charge transfer[96]. Nonradiative decay is manifested in less-than-unity quantum yields in ensemble samples and in fluorescence intermittency (blinking) in single-particle measurements.[23,97–100]

Whereas the radiative rate is largely controlled by the delocalized band-edge electronic states,[101–103] nonradiative decay rates can depend sensitively on the interfacial structure.[104,105] In particular, the surfaces are typically populated by exchangeable ligand layers, and numerous studies have examined the ability of ligand exchange to enhance or quench QD photoluminescence (PL). [23,33,56,106–108]

As described previously core/shell nanostructures, in which a material with a larger bulk band gap encapsulates the core, are a highly effective way to create QDs with lower nonradiative decay rates and achieve near-unity quantum yield (QY)[19,109]. It is notable that even in samples with shells only a few monolayers thick, in which the excited states are clearly not isolated from the surface, very high QY can be achieved (for example the samples we will describe in this chapter). This demonstrates that molecular surface termination can be achieved in which almost no intergap states or resonant excitations are present. As-synthesized colloidal QD samples typically or inherently contain large concentrations of molecules that could coordinate the surface.[110] However, applications almost universally require purification and/or surface modification of as-synthesized QDs. Purification methods have frequently been seen to decrease QY[38,111], and also to decrease ligand populations[53,54,111]. It is essential to understand whether the changes in QY are reversible, how ensemble QY and decay profiles depend on ligand occupation, and the conditions under which surface structures that support high QY can be maintained or restored.[112]

Photo-physical studies involving the effect of ligands on QDs have recently been reviewed.[108] Previous reports have largely focused on intraband relaxation[113–115], on molecules that act as quenchers[87,107,116,117], on core-only QDs[95,118–121], or have not been

accompanied by the analytical tools to assess the extent of binding as an independent variable controlling decay rates[122]. Mulvaney's group has studied the effects of Lewis bases and other ligands on radiative recombination in CdSe core-only QDs.[106] Ginger's group has studied PL quenching in CdSe-based core and core/shell QDs upon introduction of ligands,[107] while PL enhancement in QDs has been observed with thiol-bearing ligands[123,124] and amine-bearing ligands[125–127] that are not present in the synthetic mixture. Until now, however, the effect of putative ligands present in as-synthesized core/shell QDs that display high QYs has not been studied.

As described in Chapter 2, the use of gel permeation chromatography (GPC) to separate natively capped colloidal QDs from small molecules in organic solvents has been proven to be an effective way to purify the QDs[111]. This has the effect of removing impurities and weakly bound ligands, including phosphines, phosphine oxides, and primary amines; enabling the preparation of QDs with surfaces bearing a low and consistent number of metal carboxylate equivalents.

In the study described below, we take advantage of GPC purification of core/shell QDs to explore the role of neutral ligands in maintaining high QY. In particular, we measured the ensemble QY and PL decay profile of oleate-capped core/shell QDs before and after GPC, and then upon re-introduction of putative ligands that were present in the growth solution. Historically, PL decays of QDs recorded at low excitation densities have frequently displayed multiexponential behavior, which has been interpreted as a consequence of a distribution of trapping rates inhabited by different QDs in the ensemble.[128–130] Through lifetime analysis, it may be possible to distinguish between different modes of QY reduction and regeneration in QDs with different densities of

unoccupied ligand binding sites. For example, a given reduction in the ensemble QY could be brought about by a reduction in QY among all QDs in the sample, leading to a reduction in lifetime among all decay components. Another possible mechanism would be the selective quenching of a portion of the QDs, leading to an increase in the relative amplitudes of short-lifetime decay components. The former case might be expected if non-radiative recombination in purified QDs occurs *via* a large number of traps associated with vacant surface sites, while the latter case might be expected if ligand occupation modulates stochastic quenching processes such as those responsible for fluorescence intermittency in single QDs.[97,107,131]

In analyzing the response of QDs to the introduction of neutral ligands, it is essential to know whether changes in ligand concentration lead to irreversible structural changes in the QDs. Therefore, we have also studied the reversibility of the QY regeneration process. Additionally, it is valuable to be able to evaluate the actual extent of ligand coverage on the QD surface: in other words, what fraction of the added ligand is interacting with the QD surface at one time. Changes in the NMR line shape between bound and free ligands may not be resolvable in the case of rapidly exchanging ligands, and changes in the effective diffusion constant as measured by diffusion-ordered NMR spectroscopy (DOSY)[74,111] may be difficult to detect for low bound-ligand mole fractions. Here, we used isothermal titration calorimetry (ITC)[132–136] to differentiate the extent of ligand binding in QD samples exposed to phosphine, primary amine, and phosphine oxide ligands in an organic solvent.

3.2.2 Quantum yield decrease upon purification

We chose four types of CdSe based core/shell QD materials that we synthesized by a selective ionic layer adhesion and reaction (SILAR) method[19]. The effect of ligand occupation on QY in QDs with either pure CdS or CdZnS alloy shells, and with different shell thicknesses were studied. **CdSe/CdS_1** and **CdSe/CdZnS_1** are the thin shell samples (1.6 monolayer equivalent shell thickness), and **CdSe/CdS_2** and **CdSe/CdZnS_2** represent thicker shells (4 monolayer equivalent shell thickness). The formation of the shell was monitored by withdrawing a small aliquot and diluting into toluene; the aliquots were characterized by UV-Vis absorption spectroscopy and fluorescence emission spectroscopy (**Figure 3.1**).

The QYs of these samples were recorded after isolation of the particles by one cycle of precipitation with acetone and redissolution in toluene. As shown in **Figure 3.2**, the high QY indicates a complete formation of the shell onto the CdSe core materials. The detailed information of the samples has been summarized in **Table 3.1.**

As shown in Chapter 2, NMR has been demonstrated as a useful technique for the determination of the presence and interactions between ligands and nanocrystals, especially for ligands with a distinctive signal[74]. As a result, some of the best studied ligands on the QDs fall into two groups, namely, the phosphorus-containing group and the olefin-proton-containing group, which both can be distinguished easily in ^{31}P NMR or ^{1}H NMR spectra. In the present study, the phosphorus-containing group includes trioctylphosphine (TOP) and trioctylphosphine oxide (TOPO), which are among the solvents used in core synthesis and shell growth, and tetradecylphosphonic acid (TDPA) and its cadmium salt (CdTDPA), which were used as the Cd precursor during CdSe core

preparation. The olefin-proton-containing species are frequently introduced in the shell growth process: for example, cadmium oleate (CdOA) and oleic acid (OA) as the Cd precursor, and oleylamine (OAm) and octadecene (ODE) as solvents[27]. Here, we used ^{31}P NMR and quantitative ^{1}H NMR to characterize the QD samples before and after the

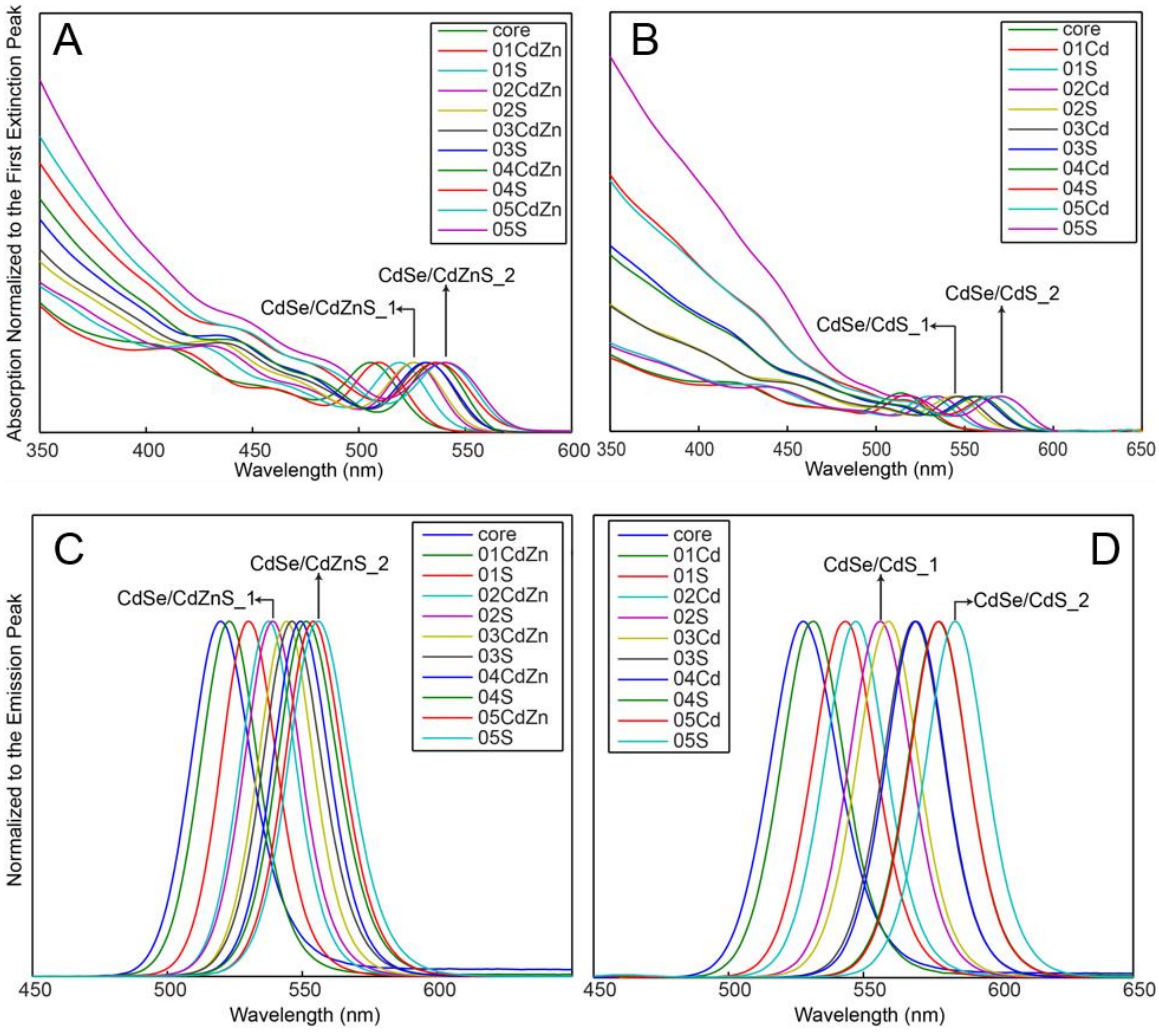

Figure 3.1 Absorption and fluorescence emission spectra of aliquots taken during the CdZnS (A, C) and CdS (B,D) overcoating processes. Aliquots were taken prior to the shell synthesis at reaction temperature and after each injection of the SILAR process (14 minutes after the start of the precursor addition). The spectra were normalized to the position of the lowest energy extinction peaks. The marks show the points where the desired thickness for thin shell (**CdSe/CdZnS_1** and **CdSe/CdS_**1) and thick shell (**CdSe/CdZnS_2** and **CdSe/CdS_2**) samples are achieved.

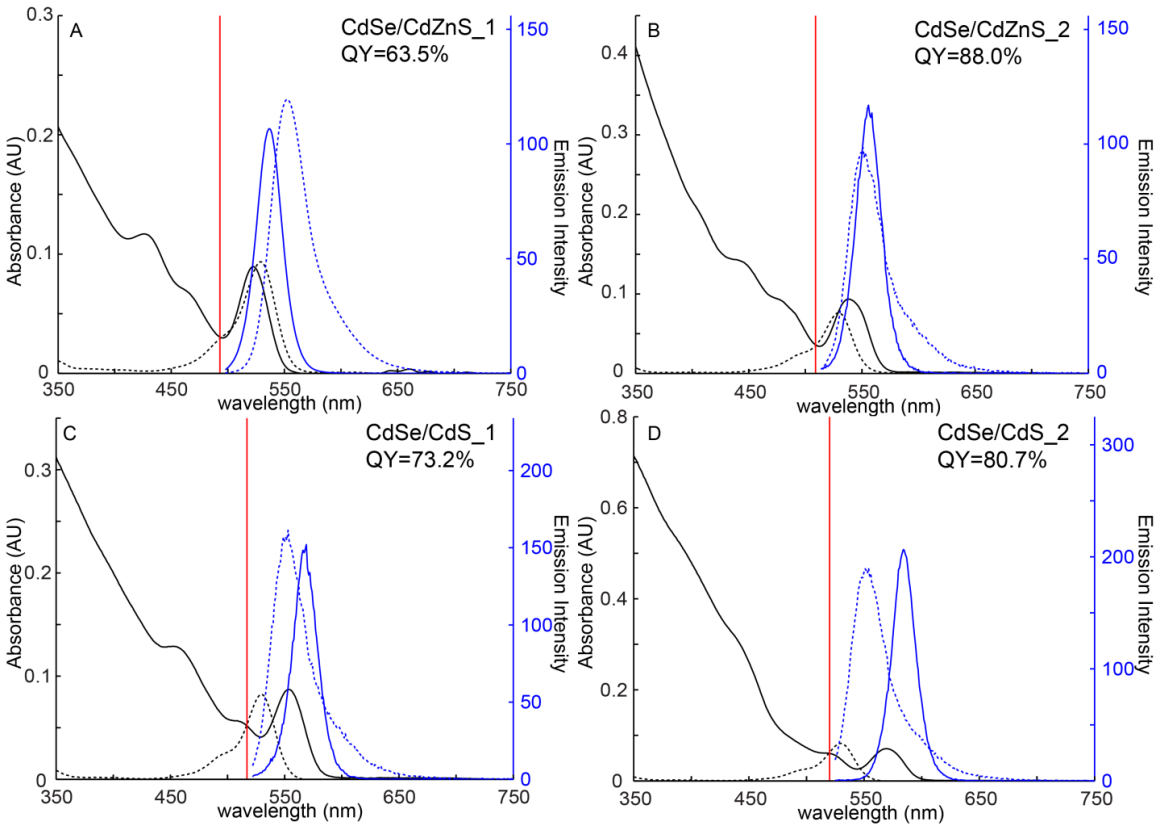

Figure 3.2 Quantum yield of **CdSe/CdZnS_1** (A), **CdSe/CdZnS_2** (B), **CdSe/CdS_1** (C) and **CdSe/CdS_2** (D) QD samples. The excitation wavelengths used for each measurement are marked by the red line. Absorption spectra (black) and emission spectra (blue) of QDs are shown as solid lines, while dashed lines indicate rhodamine 590 in ethanol as the reference dye.

Table 3.1 Characterizations of QD samples used before and after GPC purification.

QD samples	CdSe/CdZnS_1	CdSe/CdZnS_2	CdSe/CdS_1	CdSe/CdS_2
Core radius (nm) [a]	1.52	1.52	1.65	1.65
Shell thickness (ML) [b]	1.6	4	1.6	4
Absolute QY before GPC	64%	88%	73%	81%
Relative QY drop after GPC	−84%	−23%	−70%	−28%
Olefin proton to QD ratio drop after GPC	−93%	−94%	−93%	−95%
Removal of Phosphorus containing ligand after GPC?	Yes	Yes	Yes	Yes

[a] The core radius was estimated by a calibration curve describing the radius as a function of the position of the lowest-energy absorption peak. [b] "ML" is the abbreviation of monolayer equivalents.

purification by GPC. **Figure 3.3** shows the NMR spectra of **CdSe/CdZnS_1** before (**Figure 3.3A**) and after (**Figure 3.3B**) the GPC purification in toluene. In **Figure 3.3A**, four sharp signals representing free TOPO (53.48 ppm), TDPA (42.34 ppm), dialkylpyrophosphonate (28.74 ppm), and TOP (–32.34 ppm) can be identified in the ^{31}P NMR spectra[20,89,137]. A large amount of olefin-containing species (4.8-5.8 ppm, ~3950 olefin protons per QD, determined by quantitative NMR and UV-Vis as described previously) are represented in the ^{1}H NMR. However, after the GPC purification, all the

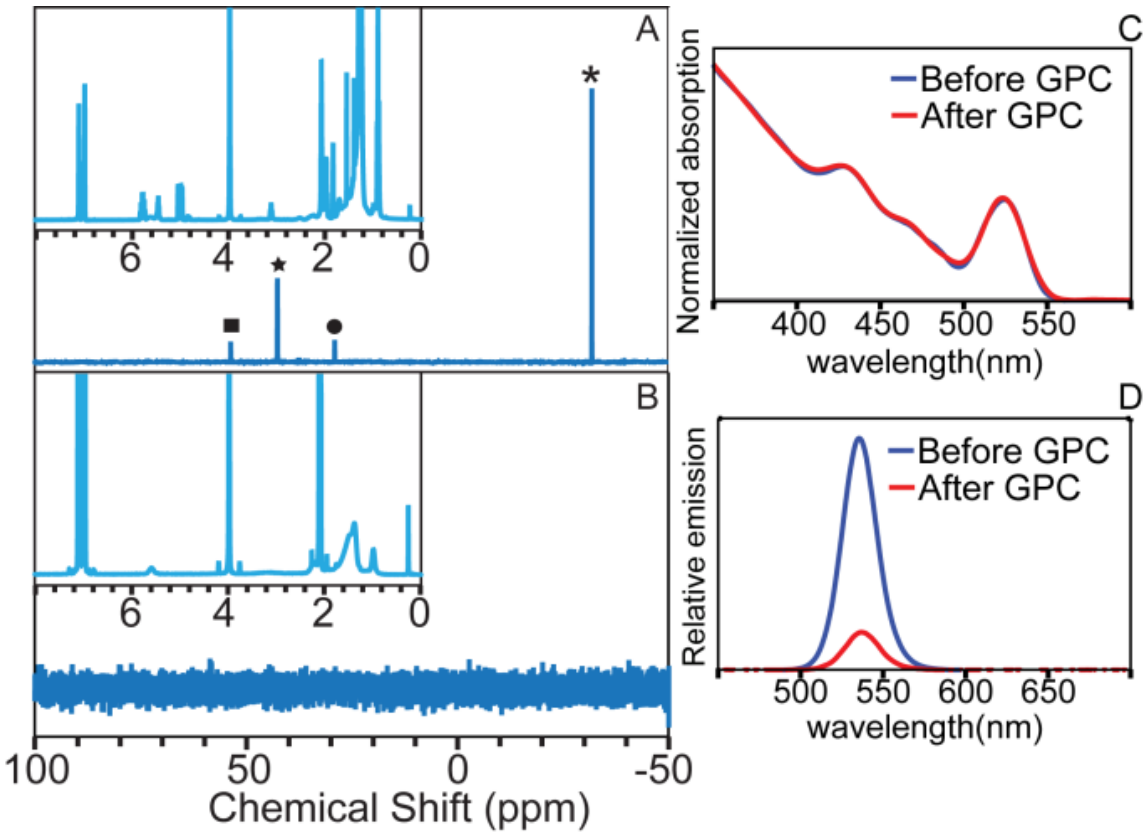

Figure 3.3 Characterization of **CdSe/CdZnS_1** sample before and after the GPC purification. The ^{31}P NMR spectra of the sample before the GPC purification (A) and after the GPC purification (B) with the ^{1}H NMR shown in the insets. The marks in (A) indicate the peaks associated with the phosphorus-containing molecules that are removed during the purification. (C) Absorption spectra of the sample (normalized to 365 nm) before and after the purification. (D) Relative emission spectra of the sample (normalized to the absorption of the excitation wavelength, 365 nm) before and after the purification. Copyright 2015 American Chemical Society.

phosphorus-containing ligands have been removed completely and the total amount of olefin proton has significantly decreased (**Figure 3.3B**). As mentioned previously, the rounded shape of the peak in the olefin region indicates that the only remaining olefin ligands are strongly interacting with the QD surface; we attribute this to an ionic (X-type) binding mode of residual oleate. The other three QD samples show similar NMR responses to purification (**Figure 3.4**), and all the results have been summarized in **Table 3.1**.

Concurrent with the removal of the neutral ligands, the emission intensities of the particles all decrease upon GPC purification. The relative QY of **CdSe/CdZnS_1** decreased by 84% after GPC with no shift in the absorption and emission spectra, which implies that the decrease of brightness is not associated with etching/aggregation (**Figure 3.3 C,D**). As discussed below, we attribute the QY decrease to an increase in nonradiative decay associated with the removal of weakly associating ligands. Similar results can also be observed in the other three samples (**Figure 3.5** and **Table 3.1**). Among the four samples, **CdSe/CdZnS_1** (84%) and **CdSe/CdS_1** (70%) samples show a higher emission intensity drop than **CdSe/CdZnS_2** (23%) and **CdSe/CdS_2** (28%) samples, which can

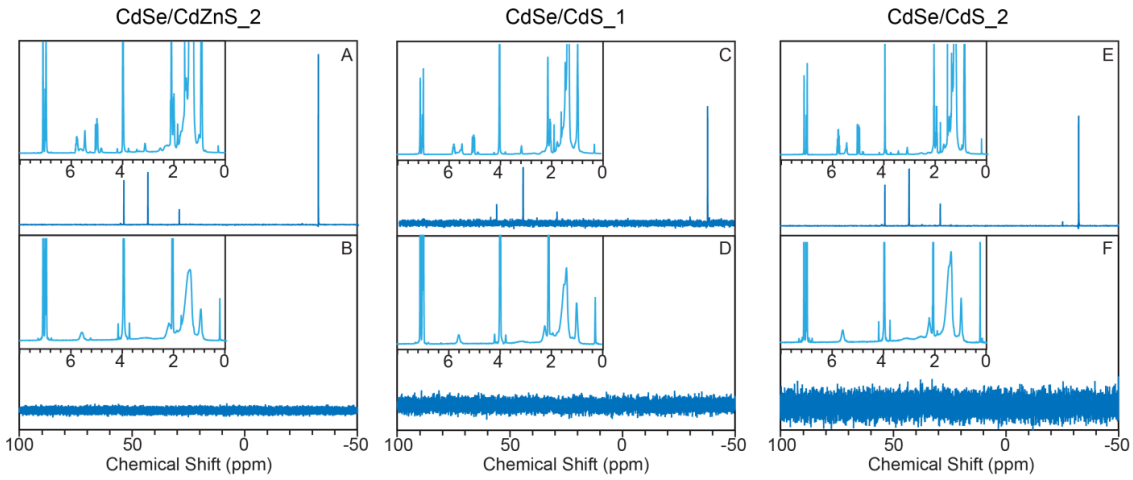

Figure 3.4 ^{31}P NMR spectra of samples before the GPC purification (A, C, E) and after the GPC purification (B, D, F) with the ^{1}H NMR shown in the insets for **CdSe/CdZn S_2** (A, B), **CdSe/CdS_1** (C, D) and **CdSe/CdS_2** (E, F).

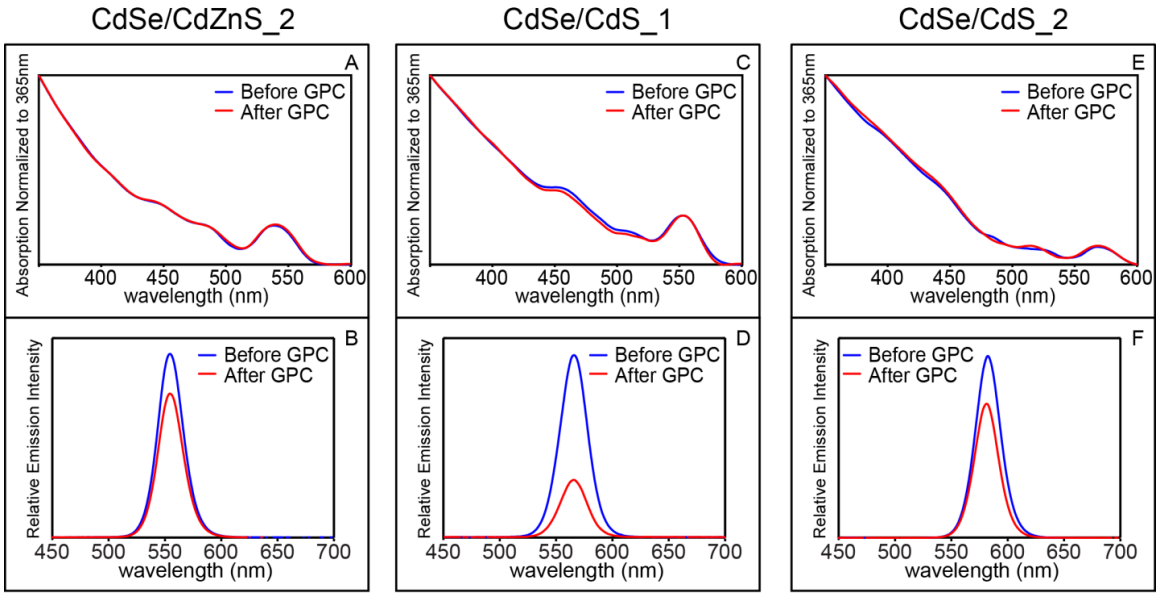

Figure 3.5 Absorption spectra of the samples (normalized to 365 nm) before and after the purification for **CdSe/CdZnS_2** (A), **CdSe/CdS_1** (C) and **CdSe/CdS_2** (E). Relative emission spectra of the samples (normalized to the absorption of the excitation wavelength, 365 nm) before and after the purification for **CdSe/CdZnS_2** (B), **CdSe/CdS_1** (D) and **CdSe/CdS_2** (F).

be explained by better isolation of the excitons from the surface traps with a thicker shell. Importantly, these changes are brought about in the absence of any change in solvent or precipitation of the QDs or introduction of protic or nucleophilic species that are known to displace ligands from QD surfaces[53,54,95]. These well-characterized and isolated QDs therefore provide a good model system to study whether the above process is reversible and which ligands are responsible for the initial high QY.

3.2.3 QY regeneration by introduction of neutral ligands

After the purification, the QDs were immediately transferred into a nitrogen-filled glovebox to suppress oxidation. According to the NMR spectra recorded before and after

the GPC process, the ligands that were removed by GPC include OA, CdOA, OAm, and ODE from the olefin-proton-containing group and TOP, TOPO, TDPA, and CdTDPA from the phosphorus-containing group. We sought to determine whether reintroduction of these species to the system could restore the QY. In order to avoid possible ligand exchange reactions, we chose not to include TDPA and CdTDPA among the neutral binders studied in this work since phosphonic acid is known to displace oleate from the surface of CdSe QDs[73]. Therefore, we have introduced the first six ligands individually, as well as a mixture of TOP and CdOA, back to QD solution with two different ligand-to-QD ratios (300:1 and 3000:1). The lower number is intended to be roughly comparable to the total number of surface sites per QD, while the larger number represents an excess[110,116,121]. After mixing the ligands and the purified QDs for a certain period of time (1 day and 7 days), the QY of each of the samples was measured and recorded. The relative QY among QDs with similar absorption spectra, emission spectra, and solvent can be measured with high precision, and therefore we reported this value. In particular, we measured the QY changes during the observation period by comparing each reaction sample to an as-synthesized QD solution reference. As shown in **Figure 3.6** (left column), the emission intensities of most of the GPC-purified QD solutions decreased upon storage in the glovebox for the longer period of time, though for sample **CdSe/CdZnS_2**, the QY increased slightly after 1 day of storage. The changes observed in purified samples during storage in dilute solution in the absence of ligand addition could be due to slow re-equilibration of the surface-bound and/or free metal oleate, and these samples serve as a control for the response to ligand addition.

We found that reintroduction of selected ligands resulted in a significant increase, or "regeneration", of QY in all samples tested. When we compare the response to introduction of the putative ligands, the QY is enhanced when TOP and CdOA are introduced in all four samples. The combination of TOP and CdOA always shows the

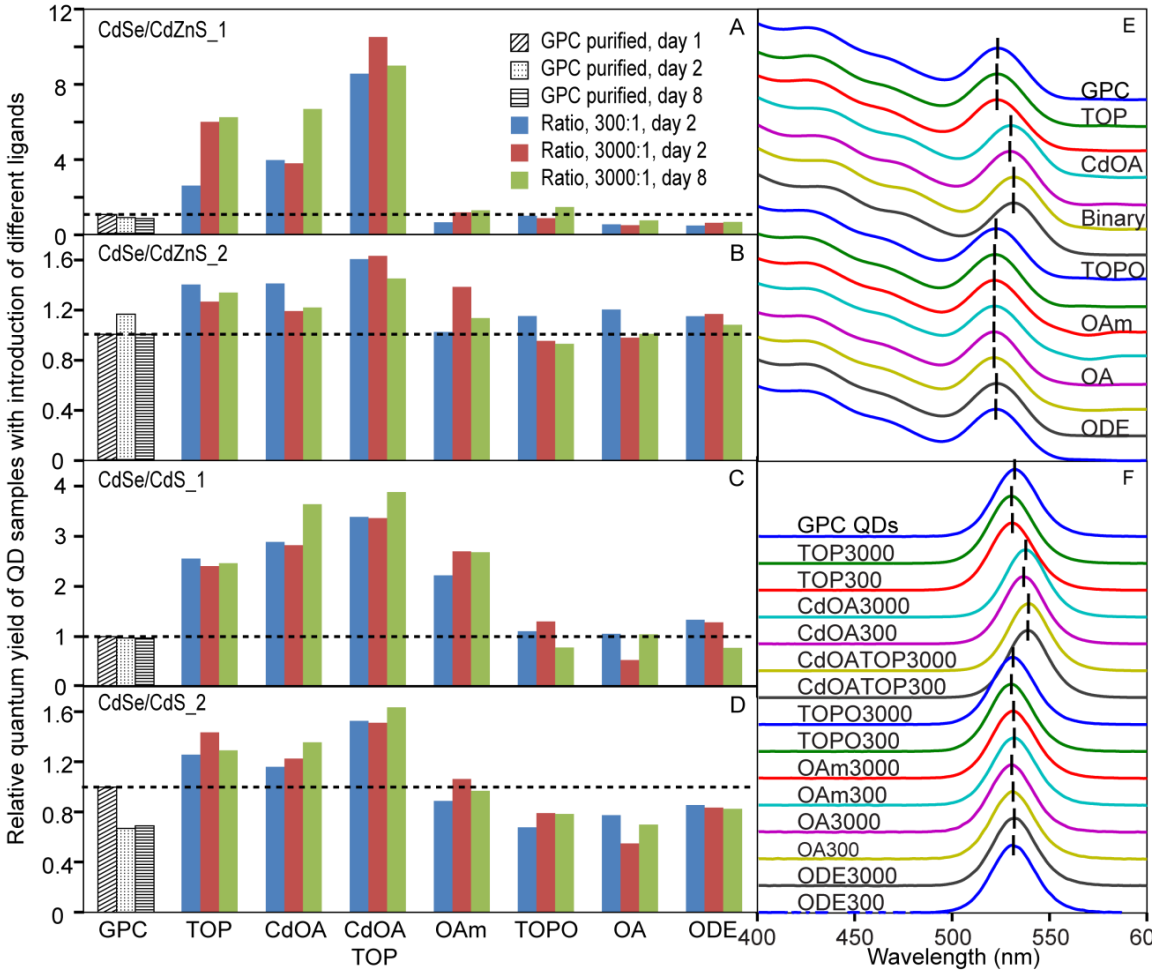

Figure 3.6 QY regeneration results with introduction of different ligands. (A-D) The relative QY of GPC-purified stock solution and ligand mixing solutions for CdSe/CdZnS_1 (A), CdSe/CdZnS_2 (B), CdSe/CdS_1 (C), and CdSe/CdS_2 (D). All of the results are normalized to the QY of the freshly GPC-purified samples shown with the dashed line. (E) Absorption spectra of the GPC purified CdSe/CdZnS_1 QDs mixing with different ligands on day 2. Here, the CdOA and TOP mixture is described as binary in short. The labeled curves have a 3000:1 ligand-to-QD ratio, while the curves below have a ratio of 300:1. (F) Emission spectra during the regeneration process for CdSe/CdZnS_1. The label is a combination of the ligand type and ligand-to-QD ratio. The samples are the same as the absorption measurements in (E). Both absorption and emission spectra are normalized to the lowest energy extinction peaks. Copyright 2015 American Chemical Society.

greatest amount of QY regeneration, which indicates that these two ligands are increasing the QY in a complementary manner. OAm can regenerate the QY in CdSe/CdS samples (especially **CdSe/ CdS_1**), but the QY did not significantly increase with the presence of OA, ODE, or TOPO. For example, as shown in **Figure 3.6A**, compared to the freshly GPC purified **CdSe/CdZnS_1** sample, the QY increased 6-fold when the higher amount of TOP is introduced and remained at a level close to the initial QY before GPC purification for the 7-day measurement period. The binary ligand system shows the highest amount of QY regeneration, up to ~12 times the GPC-purified control at the same time point for **CdSe/CdZnS_1** (the QY of the GPC stock solution decreased 16% after 1 day of storage). The QY regeneration of the thin-shell QDs is much higher than that of the thick-shell samples, which mirrors the observation of a smaller decrease in QY after the GPC purification. We did not observe a large difference in response to reintroduction at the two different ligand-to-QD ratios, which indicates that the surface has been completely saturated at the lower concentration of neutral ligands. All the ligands behave similarly for CdZnS and CdS shells except when OAm is introduced. When OAm is introduced to CdSe/CdZnS QDs, the QY does not increase; however, the QY does increase significantly when OAm is added to CdSe/CdS QDs. For **CdSe/CdS_1**, the response to OAm is close to that of TOP. One interpretation of the role of "L-type" ligands in maintaining QY is that ligand orbitals mix with interfacial localized states to move them outside of the bandgap[138,139]. In this interpretation, band-edge quantum-confined states are minimally affected. CdZnS has a larger bulk band gap than pure CdS, and so the interaction between OAm and the surface trap states is not strong enough to move the states outside of this

larger shell band gap. The influence of relative binding strength on QY will be further addressed below.

Figure 3.6E and **F** show the absorption and emission spectra of GPC-purified **CdSe/CdZnS_1** QDs after mixing with different ligands as described above. An important goal of our study is to detect differences in structure and composition between initially prepared and purified QD samples that could be responsible for QY changes. Consequently it is important to check whether the initial absorption and emission spectra, which did not change significantly on purification, are maintained upon reintroduction of putative ligands. Both absorption and emission spectra remain constant with the introduction of the L-type ligands we investigated; however, in the case of CdOA, which behaves as an electrophilic "Z-type" ligand, a significant red shift is observed. We observed similar results for pure CdS shell samples (**Figure 3.7A, B**). This indicates that the decreases in QY of the QDs after purification, which occurred without red or blue shift, are more directly related to the removal of the L-type ligands (TOP or OAm) than CdOA even though a higher coverage of Cd has also been shown to increase the brightness of CdSe and CdSe/CdS samples in published reports[71,95].

3.2.4 Lifetime analysis by time-resolved fluorescence spectroscopy

To gain additional insight on possible mechanisms for quenching and restoration of QY as a function of ligand concentration, we measured the PL decays of stirred QD samples in anhydrous toluene under 368 nm pulsed excitation, which is similar to the excitation wavelength we used for the relative QY measurements (365 nm). Since thin-shell QD samples display a larger response to the introduction of the ligands, we focused

on **CdSe/CdZnS_1** and **CdSe/ CdS_1** samples in this discussion, results shown in **Figure 3.8**; the thick-shell QD samples **CdSe/CdZnS_2** and **CdSe/CdS_2** behaved similarly and shown in **Figure 3.10**.

Data collected over 200 ns revealed multiple lifetime components (**Figure 3.8A, B** insets), including a long-lived tail with an apparent lifetime of > 50 ns. Previous reports of PL decays on QD samples with near-unity absolute QY[19,140] and reported decays of single QDs in the "on" state[100] support a radiative recombination lifetime $k_r^{-1} \approx$ 20-30 ns for

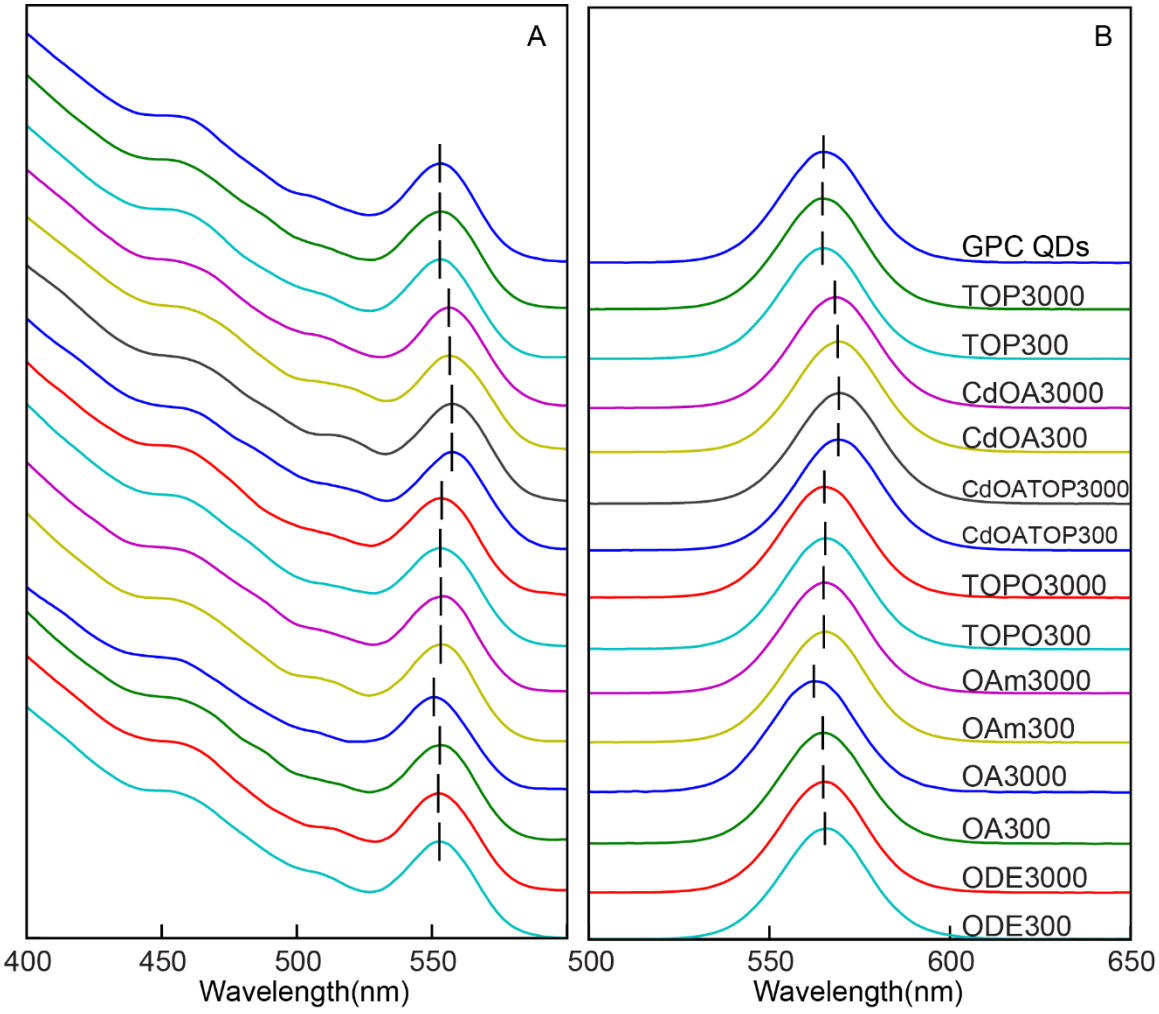

Figure 3.7 Absorption spectra (A) and emission spectra (B) of the GPC purified **CdSe/CdS_1** QDs after mixing with different ligands for 1 day. Both absorption and emission spectra are normalized at the position of the lowest energy peaks. Lifetime analysis by time-resolved fluorescence spectroscopy.

CdSe-based QDs similar to those described here. Accordingly lifetime components are likely a result of trapping/detrapping processes. In order to focus on the principal reasons for changes in ensemble QY, we chose to focus on the first 50 ns, which contain > 90% of the light emitted (**Figure 3.8A, B**). The lifetime curves of the samples mixed with TOPO, OAm, and TOP will be compared with the samples before and after the GPC purification. Since the introduction of CdOA results in a change in the band-edge electronic structure of the sample based on the absorption spectrum, the radiative recombination rate is not expected to be the same as in the other samples. Therefore, the lifetime result of CdOA cannot be directly compared to the above three ligands (see **Figure 3.9A, B**). Introduction of the ODE control resulted in only small changes in the decay traces (**Figure 3.9C**).

In general, the trend of the lifetime results is similar to the observation of the QY changes, where the samples with higher QYs have longer average lifetimes. The decays shown in **Figure 3.8A, B** show a relatively constant slope of the logarithm of intensity with respect to time in a window of ~20-50 ns, and this slope was similar among samples with different ensemble QYs. However, samples with lower QYs displayed significantly greater intensity loss within the first 10 ns. This trend is more clearly apparent when the decay traces are normalized at 30 ns to emphasize differences in decay rate at earlier times (**Figure 3.8C, D** and insets therein). After GPC purification, QY regeneration (as observed upon introduction of TOP in both samples and OAm in **CdSe/CdS_1**) is accompanied by reduction, but not complete elimination, of the accelerated decay at early times.

Analysis of rate dispersion in ensemble QD samples and time evolution of decay rates in single-QD photon counting experiments have supported an interpretation of rate dispersion as being primarily or entirely inhomogeneous in QD samples, the result of subpopulations

with varying decay rates[100,129]. Subpopulations with lower QYs are expected to display shorter lifetimes because of elevated nonradiative decay rates. In this case, it may be possible to constrain models of nonradiative decay by decomposing the observed decays into several lifetime components. We employed a reconvolution fit with multiple decay lifetimes to analyze the decays within the first 50 ns. Uncertainty in the lifetime values was examined with support plane analysis[141] (a detailed description of the analysis is available in **the materials section**). With this analysis, the longest lifetime approximates the decay seen in the ~15-25 ns window, while the shorter lifetimes describe the rapid decay seen at early times. By analyzing the rates and amplitudes of the lifetime components, we sought to distinguish whether quenching in GPC-purified samples and regeneration in ligand-introduced samples are associated chiefly with changes in lifetime among all lifetime components or with changes in the relative population fraction of QDs with different decay rates, as assessed from the amplitudes of the short and long lifetime components of the fit.

In the case of thin alloy shells (**Figure 3.8E**), we found that a three-component lifetime fit was statistically supported by the data, while the bright QD samples with pure CdS shell (**CdSe/CdS_1** before GPC, with TOP3000 and with OAm3000) required only two components (**Figure 3.8F**). We found that the change in QY between the samples before and after GPC, and between GPC and QY regenerated samples, is accompanied by a change in the amplitude of the lifetime components, with little change in the lifetime value. For example, the amplitude average lifetime of **CdSe/CdZnS_1** after the GPC purification is 3.77 ns; after mixing with TOP, the lifetime increases to 10.49 ns (we report

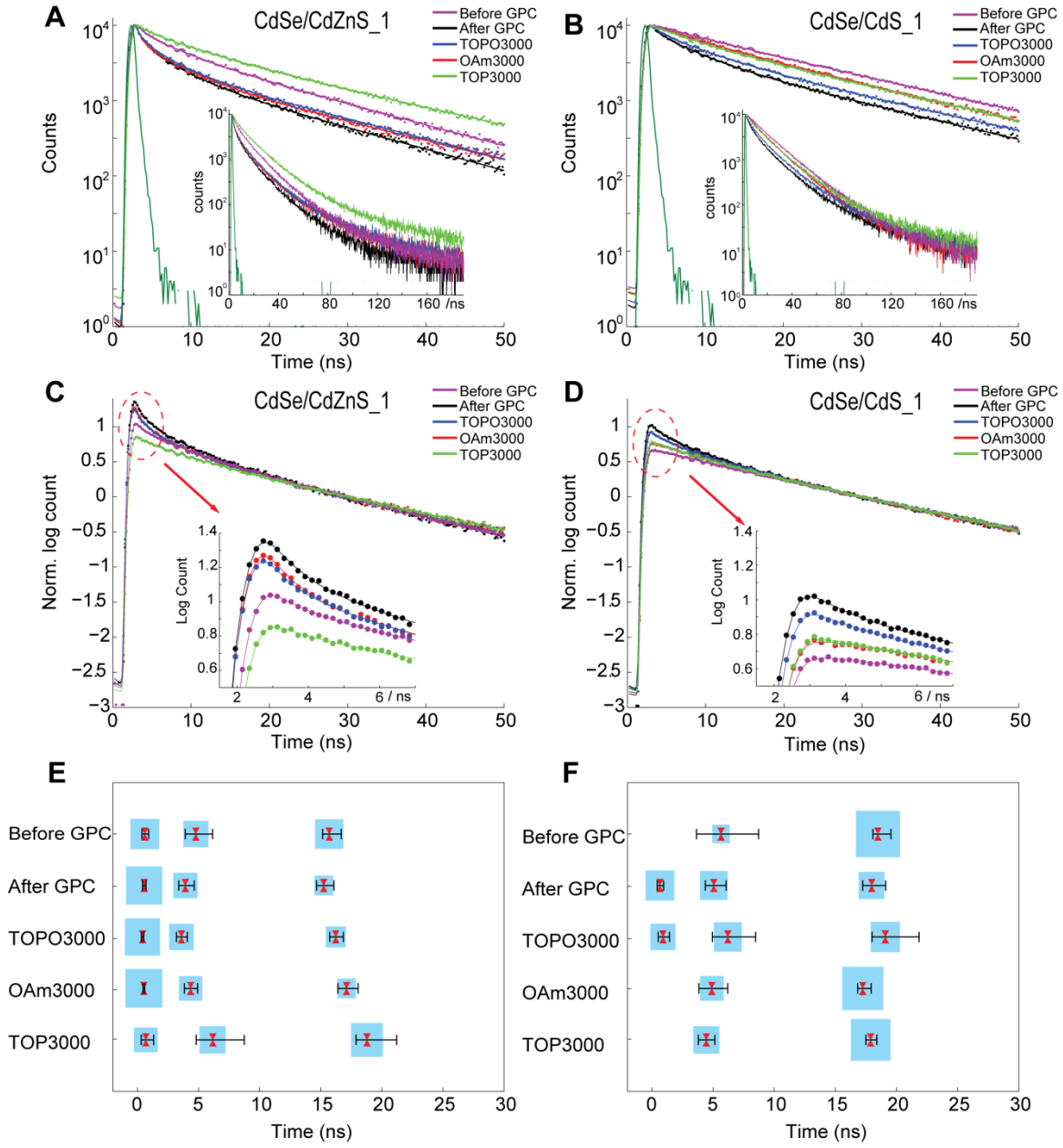

Figure 3.8 Comparison of fluorescence lifetime decays for **CdSe/CdZnS_1** (A) and **CdSe/CdS_1** (B) core/shell QDs before/after GPC purification and subsequently mixed with different ligands, focused on the first 50 ns. Data collected over 200 ns are shown in the insets. (C, D) Corresponding lifetime decays normalized at 30 ns; insets show detail. Lines are reconvolution fits. (E, F) Charts displaying lifetime values and corresponding amplitudes for reconvolution fits of PL decay traces for **CdSe/CdZnS_1** (E) and **CdSe/CdS_1** (F). The weighted amplitudes are represented by the areas of the blue squares, while the lifetime values are indicated by red marks at the center of each square. Error bars indicate the uncertainty of each lifetime component as obtained by support plane analysis with a confidence limit of 90%. (see **Table 3.2** for details).

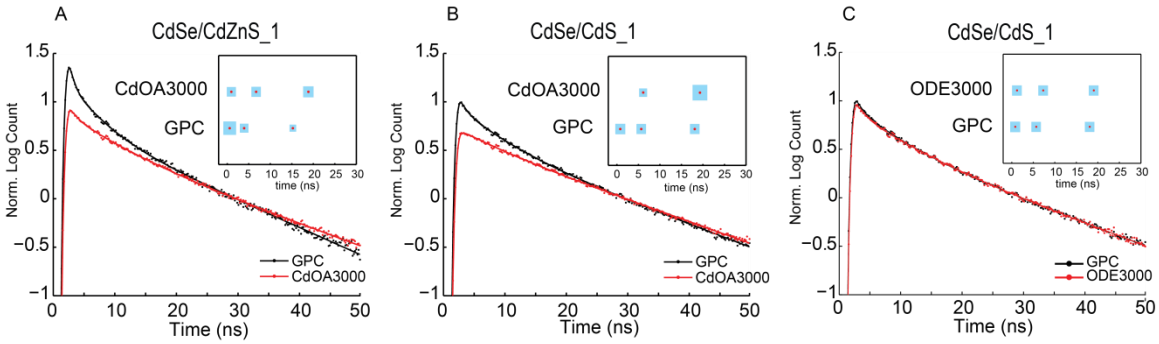

Figure 3.9 Fluorescence lifetime decays for **CdSe/CdZnS_1** (A) and **CdSe/CdS_1** (B) core/shell QDs after GPC and further mixed with CdOA. The lifetime decay curves are normalized at 30 ns. (C) Lifetime decays for **CdSe/CdS_1** after GPC and further mixed with ODE. The lifetime decay curves are normalized at 30 ns. Re-convolution fits of the corresponding decays are showed in the insets, where the weighted amplitude is proportional to the area of blue squares and lifetime value of each component is displayed as the red dot at the center of each square.

amplitude average lifetimes because they are nominally proportional to the steady-state fluorescence intensity[142]). The values of the component lifetimes change no more than 30%, but the amplitude ratio between the shortest and longest lifetime components increases by a factor of 6.7. Similar results can be observed in comparing GPC-purified QDs to the initial samples prior to GPC (see **Table 3.2** for detailed lifetime values and exponential amplitudes). Thus, the reduction in QY upon removal of L-type ligands appears to be driven primarily by a large increase in decay rate among a subset of the QDs.

We can use the PL decay profiles to consider possible models for quenching in QDs with vacant L-type ligand sites. One model is to consider each vacant site to contribute a similar nonradiative decay rate, in an additive manner[116]. In this case, the distribution of decay rates in the purified samples will reflect the distribution in the number of vacant sites per QD. But because each QD presumably contains numerous binding sites for L-type ligands and nearly all are vacant following GPC purification, it would seem improbable that a significant fraction of the purified QDs would have zero vacant sites and

thus remain unquenched. We therefore rule this model out. A second model considers a stochastic quenching process, such as the formation of charged QDs leading to Auger

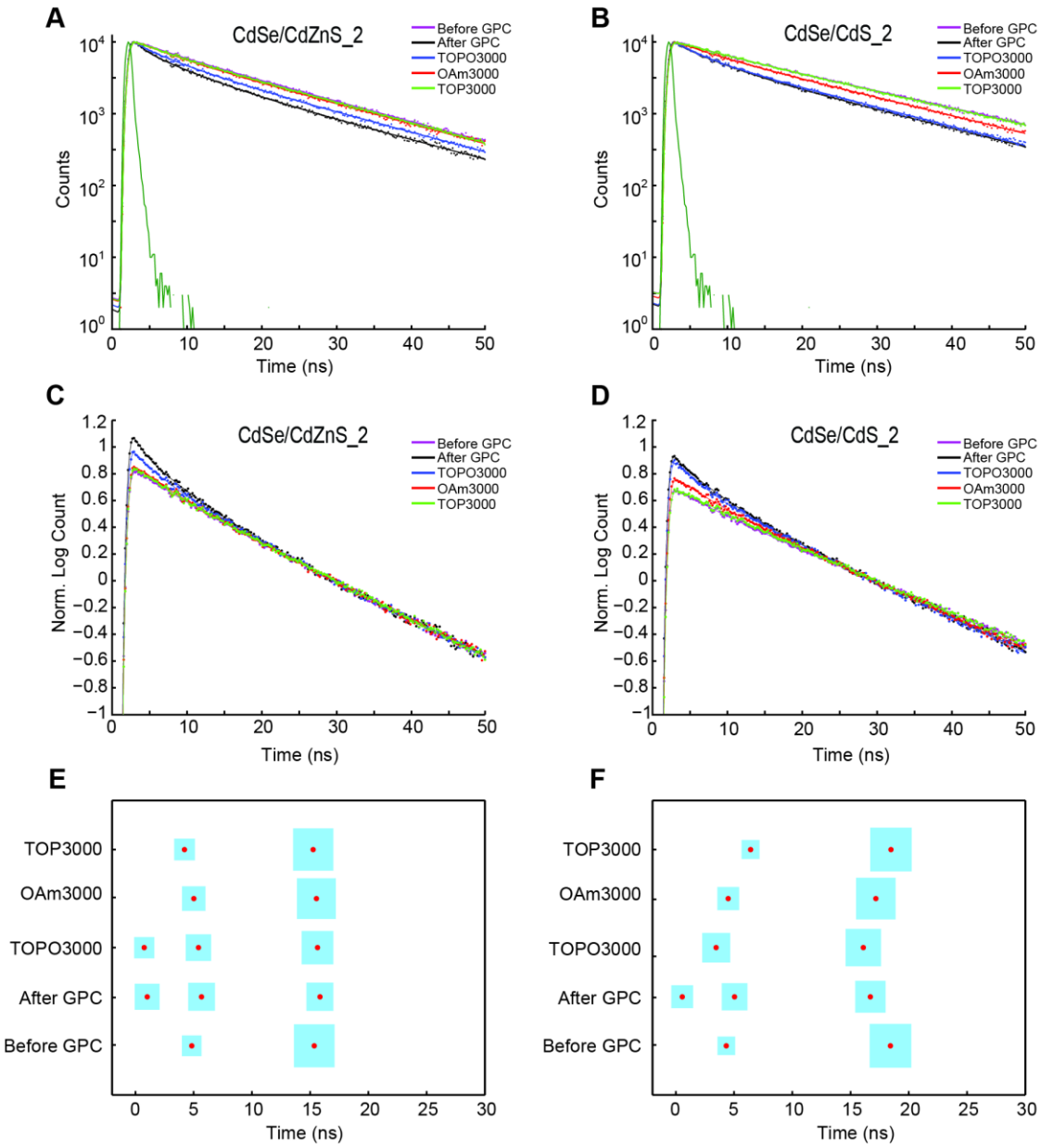

Figure 3.10 Comparison of fluorescence lifetime decays for **CdSe/CdZnS_2** (A) and **CdSe/CdS_2** (B) core/shell QDs before/after GPC and further mixed with different ligands (TOP, OAm and TOPO), focused on the first 50ns. (C, D) Corresponding lifetime decays normalized at 30 ns, emphasizing changes of the fast decay component with different ligands. (E,F) Re-convolution fits of the corresponding decays for **CdSe/CdZnS_2** (E) and **CdSe/CdS_2** (F) indicate the number of the exponential components as well as the weighted amplitude (area of blue squares) and lifetime value of each component (red dot at the center of each square).

recombination[97],whose probability is tuned by ligand coverage. In this model, ligand coverage does not significantly affect the component lifetimes, but rather tunes the population fraction that is in a bright or quenched configuration at a given time, in a manner analogous to the fluorescence intermittency seen in single-particle studies.[143] A third possibility is that the most significant changes in QY arise from vacancies at a subset of L-type ligand binding sites that occur rarely enough that some QDs in the ensemble lack such sites and do not experience quenching at low ligand concentration. Measurements that link structure and QY among individual QDs[144] may be of value in distinguishing among these models. Spectroscopic techniques such as transient absorption, upconversion PL decay measurements that can more precisely resolve rapid decay processes, and multiple-pulse experiments have been applied to the analysis of QD radiative and nonradiative decay[145,146]. It is clear from the results presented here that the ensemble QY, average decay rate, and rate dispersion of QDs change in response to ligand concentration. Thus, spectroscopic analyses must ideally be performed on samples with well-specified ligand populations and concentrations if the results of such studies are to be compared or applied to new systems.

While the results in **Figure 3.6** show that QY regeneration upon introduction of excess ligands can be maintained over a period of at least a week, we sought to study the time evolution of QY and PL decay profiles in greater detail. We focused on the thin-shell QD samples with introduction of 3000 equiv. of TOP, a treatment that improved the ensemble QY in all cases. As shown in **Figure 3.11A** and **B**, the brightness of the QD samples can be fully regenerated to the level prior to GPC purification after mixing with TOP for 1 h, which suggests that the high QY of the sample before the purification is due

to the presence of neutral ligands such as TOP. On the basis of the time evolution of the relative QY, the alloy shell sample requires a longer period of time to reach equilibrium; in this case the sample at 5 min is only halfway through its full regeneration, whereas at 5 min the pure CdS shell sample is close to its maximum brightness. The high QY in the TOP-introduced **CdSe/CdZnS_1** sample can be maintained for 7 days, but there is a decrease in QY with the TOP-introduced **CdSe/CdS_1** sample after 1 day. As shown in

Table 3.2 Detailed lifetime values and relative population of the reconvolution fits on the PL decay curves shown in **Figure 3.8E** and **3.8F**.

QD sample	Ligands	Tau1[a]	wt.A1[b]	Tau2[a]	wt.A2[b]	Tau3[a]	wt.A3[b]	Tau_avg[a]
CdSe/CdZnS_1	1ppt	0.61	36.92%	4.79	27.63%	15.70	35.45%	7.11
	GPC	0.57	58.22%	3.93	25.94%	15.25	15.84%	3.77
	TOPO	0.43	55.12%	3.61	27.16%	16.22	17.72%	4.09
	OAm	0.54	60.49%	4.37	24.18%	17.11	15.33%	4.01
	TOP	0.70	24.90%	6.16	30.04%	18.78	45.07%	10.49
CdSe/CdS_1	1ppt	---	---	5.65	13.59%	18.48	86.41%	16.74
	GPC	0.66	36.34%	5.06	33.92%	17.97	29.75%	7.30
	TOPO	0.91	28.07%	6.21	34.53%	19.08	37.40%	9.54
	OAm	---	---	4.91	24.19%	17.24	75.81%	14.26
	TOP	---	---	4.45	30.32%	17.89	69.69%	13.81

[a] Tau is the lifetime component τ shown in the previous lifetime analysis method discussion. The unit for each lifetime component is ns.[b] wt.A is the weighted amplitude. $Wt.A_i=(A_i/\sum A)\times 100\%$

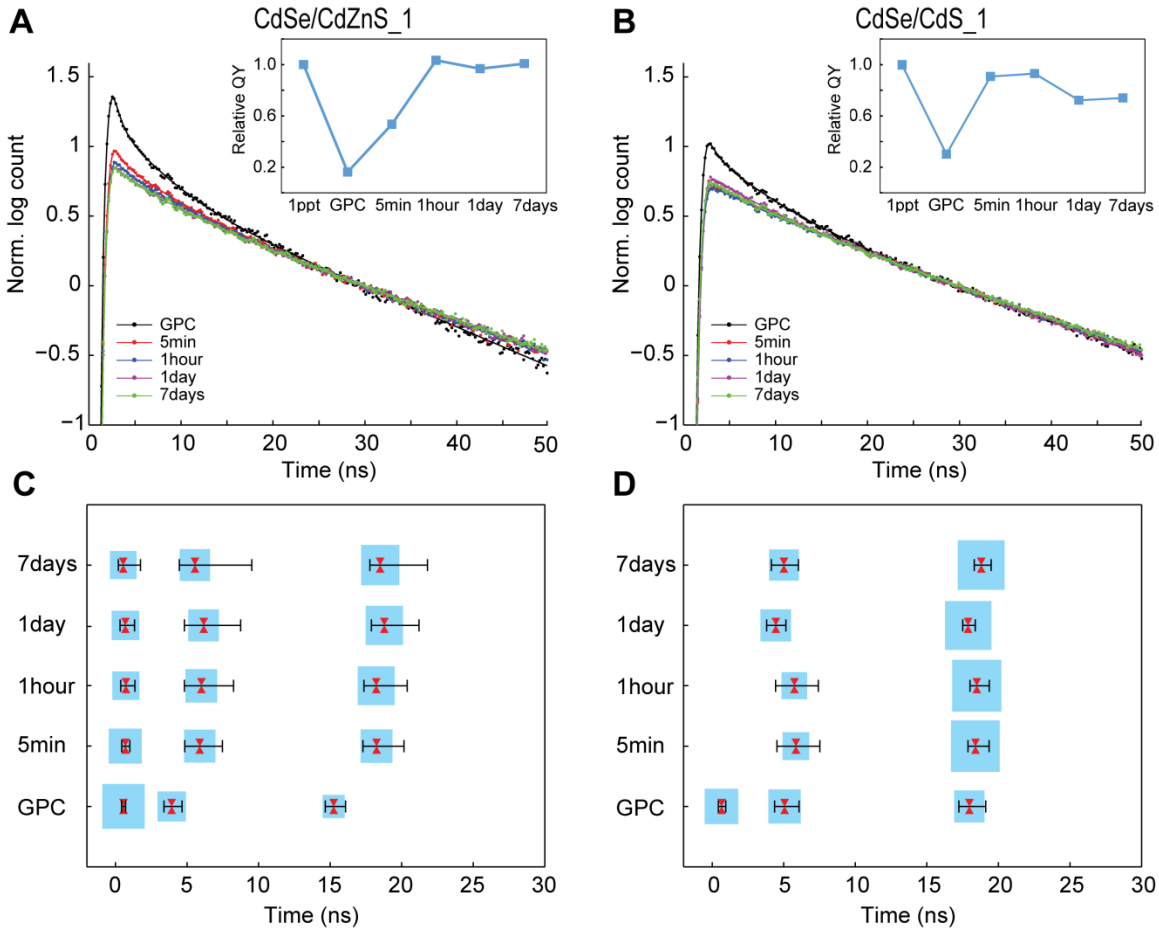

Figure 3.11 Fluorescence lifetime decays for **CdSe/CdZnS_1** (A) and **CdSe/CdS_1** (B) core/shell QDs after GPC purification, and then mixed with TOP at various time after introduction of TOP, normalized at 30 ns. Changes of relative QY are shown as insets. Here, the sample before GPC purification is described as "1ppt" in short. (C, D) A re-convolution fit of the corresponding decays gave the weighted amplitudes (area of blue squares) and lifetimes of each component (red marks at the center of each square) for **CdSe/CdZnS_1** (C) and **CdSe/CdS_1** (D) mixed with TOP over time. The uncertainties in each lifetime component was obtained by support plane analysis with confidence limit of 90%. Copyright 2015 American Chemical Society.

Figure 3.11C and **D**, the lifetimes of each component for the TOP introduced samples are fairly similar at different waiting times. These results are consistent with changes in the relative population fraction of QDs with different decay rates driving QY regeneration in the GPC-purified samples.

3.2.5 Reversibility test of the QY regeneration process

One concern is whether changes in ligand concentration lead to irreversible structural changes in the QDs. To investigate the reversibility of the regeneration process, a second round of GPC was used to repurify the QY-regenerated thin-shell QD samples, subsequent to introduction of CdOA, TOP, or OAm. By comparing the absorption and emission spectra before and after the second purification, we can detect irreversible changes in size or shape associated with changes in ligand concentration.

As shown in the initial QY regeneration results, when CdOA is introduced into both **CdSe/CdZnS_1** and **CdSe/CdS_1** samples, there is a red shift in the absorption spectra. As shown in **Figure 3.12A, B**, they did not shift back after the second GPC purification process, which indicates that the regeneration process with CdOA is not reversible. The small red shift in the **CdSe/CdS_1** sample on introduction of CdOA is analogous to that seen when CdOA is used as a Cd precursor in shell growth, but the irreversible nature could indicate some surface reconstruction. When CdOA is added to the **CdSe/CdZnS_1** sample, a larger red shift is observed, and one possible reason is a cation exchange reaction between Zn from the shell and CdOA in the solution[147–149]. To confirm this, purified **CdSe/CdZnS_1** treated with CdOA solution or pure toluene was precipitated, and the supernatant portions of these two samples were digested and characterized by inductively coupled plasma-mass spectrometry (ICP-MS). As shown in **Figure 3.12C**, a much higher amount of Zn is observed in solution when CdOA is introduced. The total amount of excess Zn detected in the supernatant corresponds to 25.3 % of the Zn equivalents introduced during shell synthesis; this suggests that at least 25.3 % of the Zn in the shell has been replaced by Cd. One interesting observation is that for GPC-purified **CdSe/CdS_1**, after

treatment with a large excess of CdOA, a subsequent GPC purification found a significant portion of the sample to be retained on the GPC column. Interactions between polystyrene

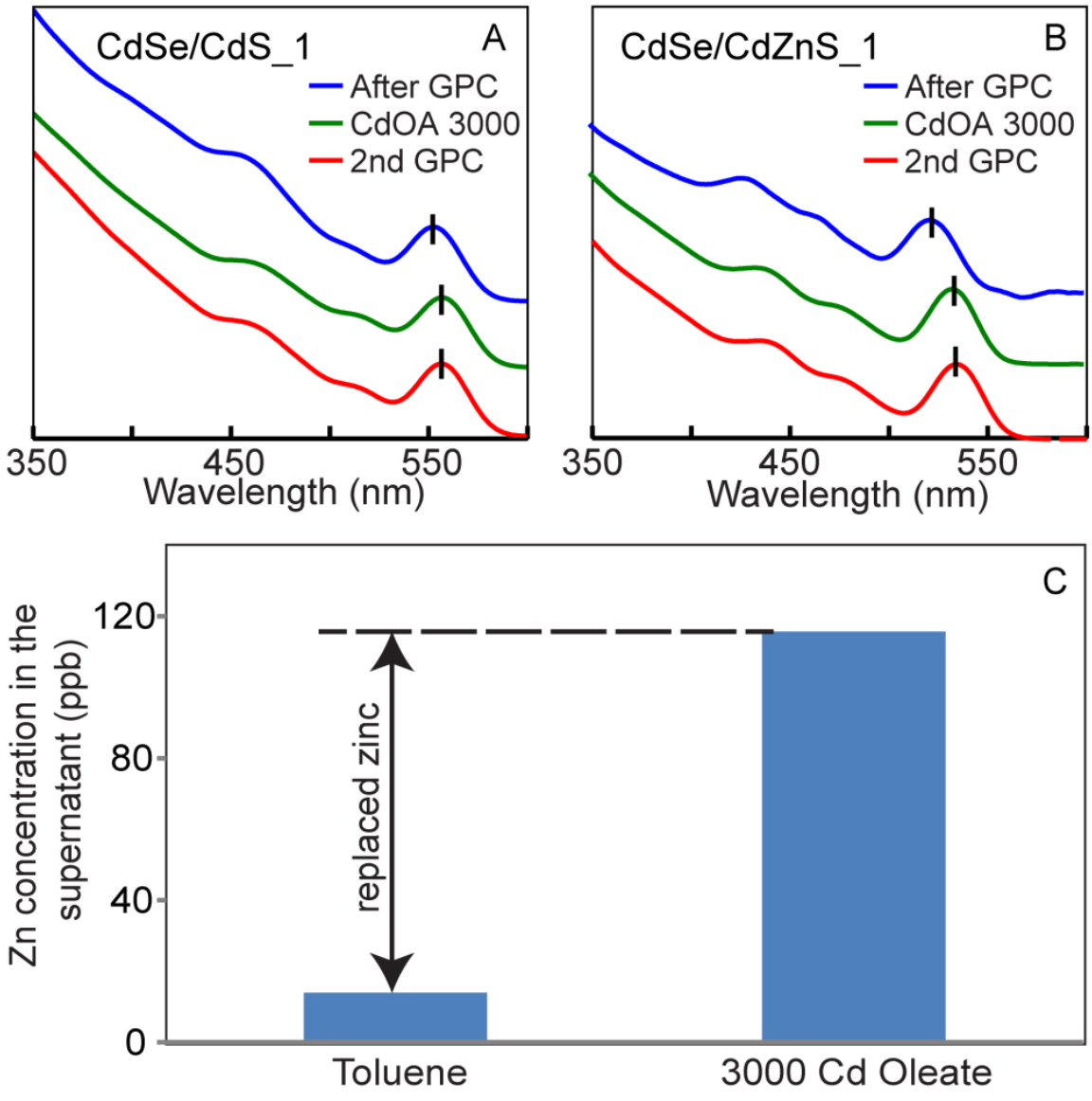

Figure 3.12 Reversibility test of CdOA. (A, B) The absorption spectra before and after the introduction of CdOA and after the second GPC purification for **CdSe/CdS_1** (A) and **CdSe/ CdZnS_1** (B). (C) ICP-MS analysis of the Zn content in digested supernatant of GPC-purified **CdSe/CdZnS_1** sample mixed with toluene or with 3000 equiv of CdOA solution. Copyright 2015 American Chemical Society.

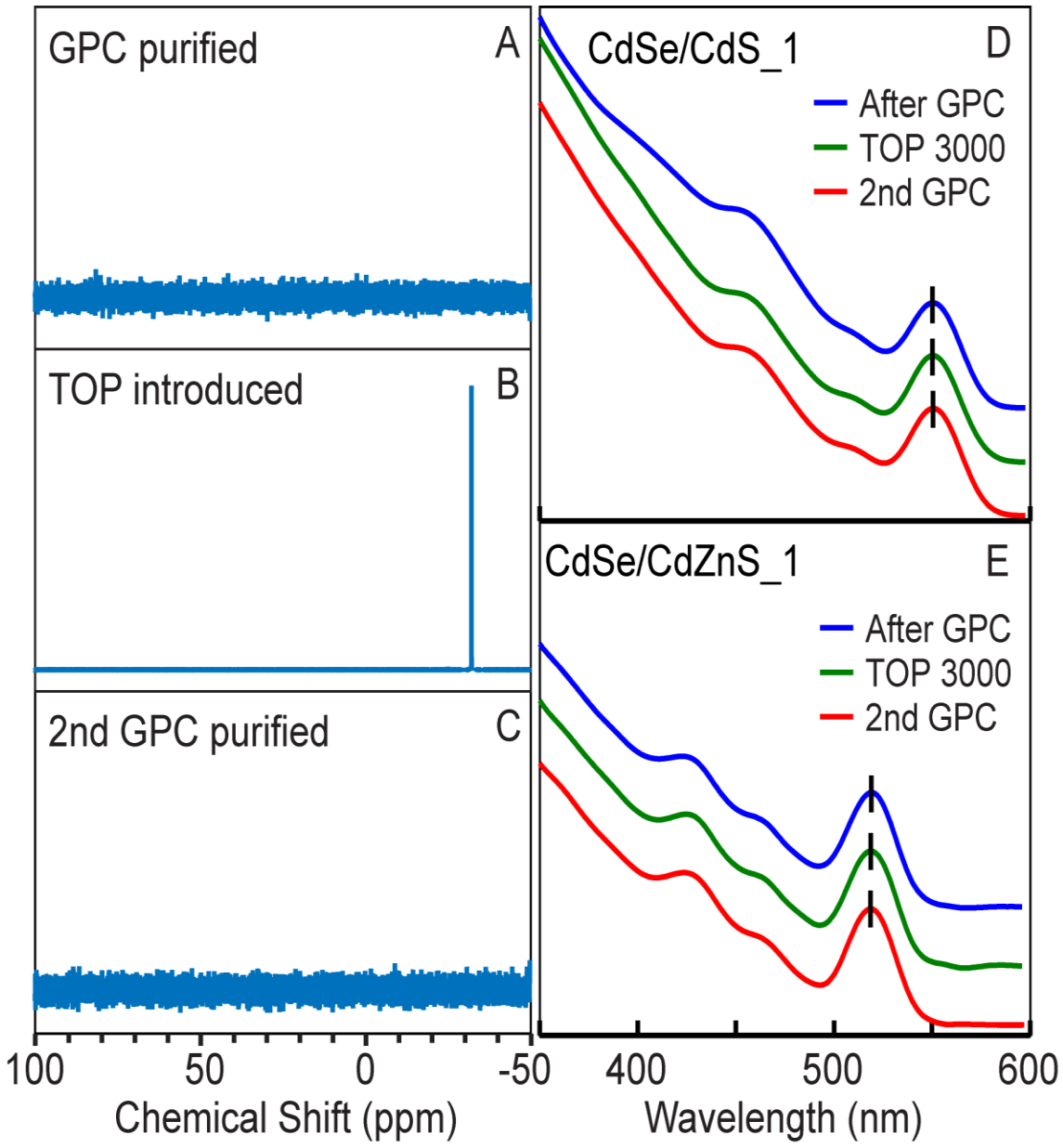

Figure 3.13 Reversibility test of TOP. ^{31}P NMR spectra before (A) and after (B) the introduction of TOP and followed by after the second GPC purification (C) of the GPC-purified **CdSe/ CdS_1** QDs. The absorption spectra during the process described above for **CdSe/CdS_1** (D) and **CdSe/CdZnS_1** (E).which showed no shifting of the bandgap absorption peaks. Copyright 2015 American Chemical Society.

GPC media and metal-rich samples have been reported in other systems.[70] We have observed similar results previously when attempting to purify QDs synthesized under

highly metal-rich conditions, which is consistent with CdOA adhesion to the CdSe/CdS QD surface in the present case.

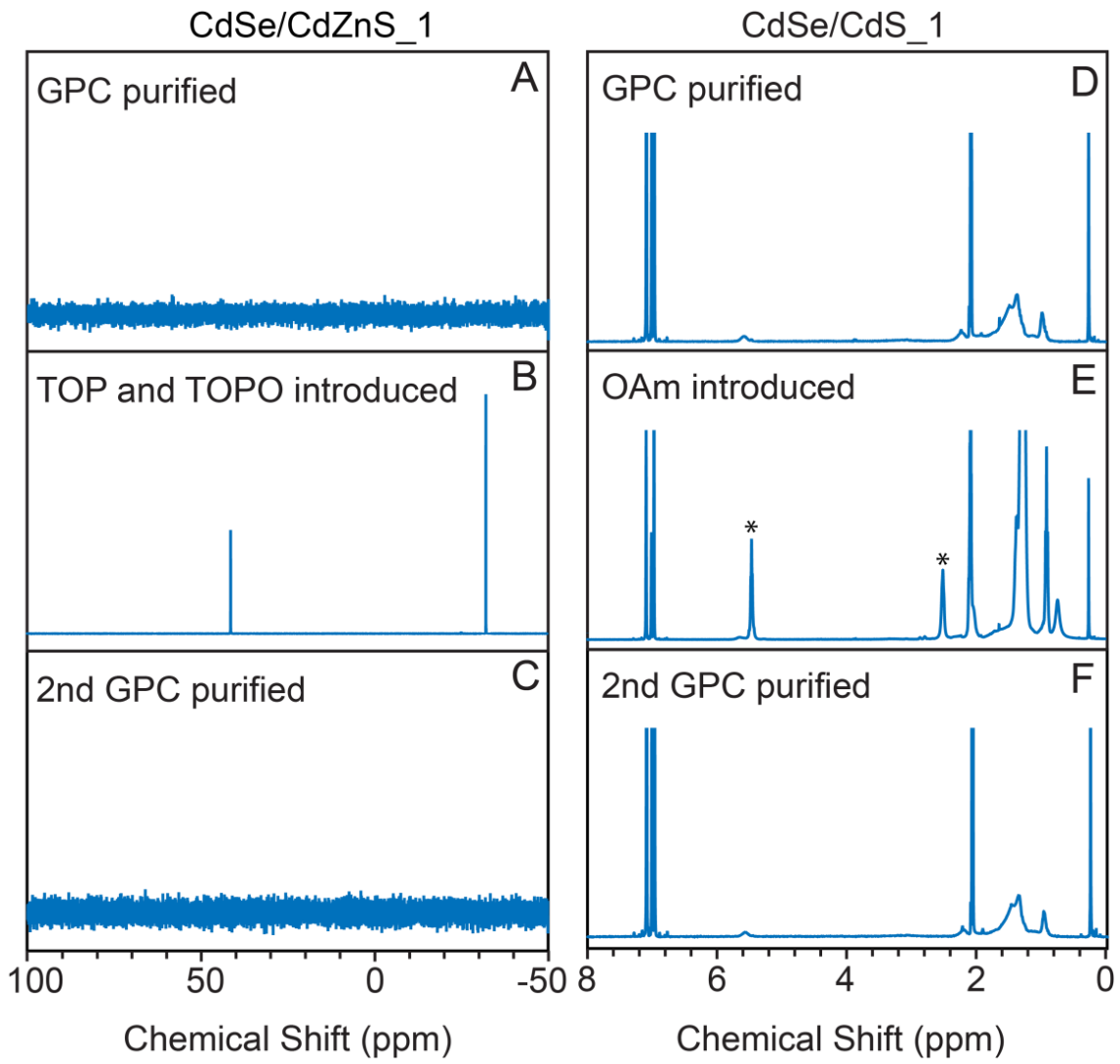

Figure 3.14 ^{31}P NMR spectra before (A) and after (B) the introduction of the mixture of TOP and TOPO, and after the 2nd GPC purification (C) for the GPC purified **CdSe/CdZnS_1** sample. ^{1}H NMR spectra before (D) and after (E) the introduction of OAm, and after the 2nd GPC purification (F) for the GPC purified **CdSe/CdS_1** sample. The marks in (E) indicate the free olefin proton and α-H in the OAm peaks that are removed during the 2nd GPC purification process. Absorption (G) and emission (H) spectra during the removal of the solvent and redissolution into deuterated solvent of the 2nd GPC purified **CdSe/CdS_1** sample.

On the other hand, **Figure 3.13D** and **E** show that, during introduction and removal of TOP, both CdSe/CdS and CdSe/CdZnS QD samples maintain their absorption features. This suggests that TOP does not change the effective size or size distribution of the quantum-confined band-edge states (there is an increase in relative absorption in the UV range, which may be associated with changes in higher energy excitations). After the second GPC purification, NMR confirms that TOP can once again be completely removed from the system and the absorption spectrum remains constant (**Figure 3.13A-C** and **Figure 3.14A-C**). On the basis of these results, we believe that the regeneration process with TOP is reversible. Similar results can also be observed with OAm, where the α-H disappeared after the second GPC purification (**Figure 3.14D-F**). According to the emission spectra, the QY decreased after removing TOP by the second GPC purification, but it remained higher than the first GPC-purified sample. This result suggests that the regeneration process with TOP might not be completely described as a simple adsorption reaction and the QD surface may reconstruct with the help of the introduced L-type ligands. Previous reports have identified a role of L-type ligands in displacing metal oleate from CdSe QD surfaces at high concentration.[95] Here, we also attempted to measure the oleate population after the second GPC purification, but due to the aggregation of the particles during the phase change process when switching to deuterated solvent, we were unable to obtain consistent results based on NMR and absorption spectra.

3.2.6 Isothermal titration calorimetry of ligand addition

On the basis of our results above, as well as previous literature reports, L-type ligands (including TOP, TOPO, and OAm) can reversibly attach to and detach from the

QD surface[106,110]. However, as shown in our regeneration and lifetime studies, not all of these ligands contribute equally to the photo-physical property changes in QDs. Ligand/ QD interaction is known to influence the energy levels and occupation of interfacial states, affecting electron and hole trapping rates and intraband decay rates. The effect of a certain total ligand concentration will depend on the adsorption isotherm and on the effect of such binding on the interfacial states. It is desirable to have an independent measurement of the extent of binding so that these factors can be distinguished. NMR has proven to be a powerful technique for the determination of the interactions between ligands and the nanocrystal surface. Diffusion-ordered NMR analysis (DOSY) has been employed specifically to characterize the bound and free ligand population on QDs in previous work[74,111]. However, in this study, we did not observe any significant difference in diffusion constant measured by DOSY (**Figure 3.15**), T_1 measurement on ^{31}P, or NOE response on ^{1}H spectra with selective saturation on the ^{31}P resonance (data not shown) upon introduction of GPC-purified QDs to TOP or TOPO solutions. Both behaved similarly to free ligand controls in these NMR experiments. These results suggest a fast dynamic adsorption/desorption equilibrium, where the bound ligands are exchanging rapidly with the excess of unbound ligands in the solution.[150] Therefore, we employed isothermal titration calorimetry to detect and characterize the binding between the neutral ligands and QDs. Although widely used in biochemistry, ITC has only recently begun to be applied to nanoparticles to assign parameters for multiple binding problems.[151] In this study, we titrated the same amount of TOPO, OAm, and TOP to the GPC purified **CdSe/CdZnS_1** sample to measure the heat response. Any response of the system as equilibrium is re-established that has nonzero enthalpy change, such as bond formation upon ligand binding,

will generate a heat response. The shape of the heat response over the course of the titration can be used to characterize the equilibrium constant and stoichiometry of reactions, while the sign and magnitude of the signal characterize the associated enthalpy change. Due to the intolerance of the machine toward toluene, anhydrous tetrahydrofuran (THF) has been used as the solvent for this study.

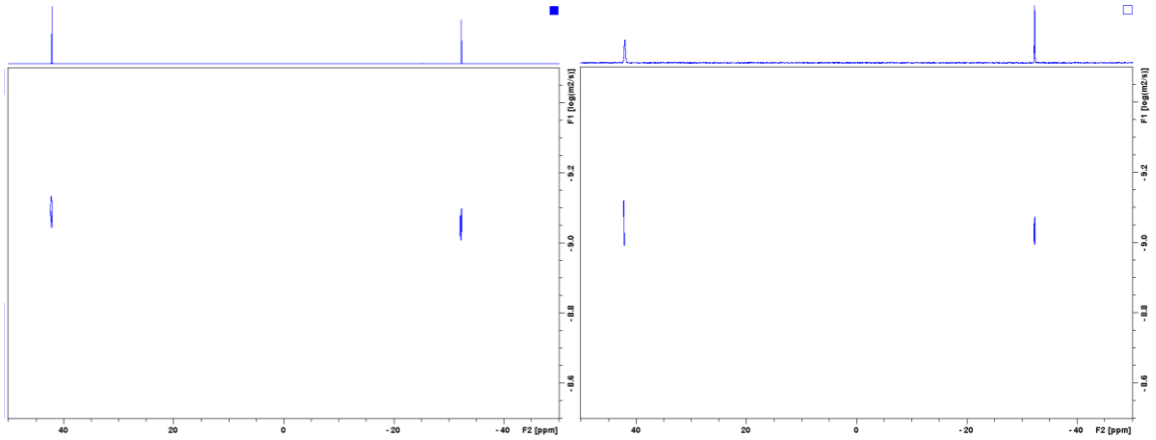

Figure 3.15 DOSY spectra on ^{31}P of free TOP/TOPO (left) and TOP/TOPO mixing with **CdSe/CdZnS_1** sample with a 300 ligand-to-QD ratio (right). Neither TOP nor TOPO can be distinguished from free ligands after mixing with QDs, where the diffusion constant of TOP is 9.3×10^{-10} m^2/s and TOPO is 8.6×10^{-10} m^2/s. The diffusion constant of QD is 1.9×10^{-10} m^2/s based on the DOSY measurement of the olefin proton. The diffusion constant of the solvent toluene is 2.4×10^{-9} m^2/s.

As shown in **Figure 3.16**, when TOPO is titrated, the overall heat response is small and no trend can be observed in the integrated curve, which indicates that there is no significant binding between TOPO and the QDs at these concentrations. The ITC trace for introduction of OAm shows a small exothermic response at low ligand concentration that rapidly saturates. This rapid saturation indicates a high association equilibrium constant. The thermogram was fit with the simple independent identical sites model by varying the number of sites per QD *N*, equilibrium constant *K*, and molar enthalpy change ΔH. The best fit was obtained when the number of sites is close to 10, with $K = 2.3 \times 10^4$ M^{-1} and

ΔH = –27 kcal/mol. However, since the magnitude of the equilibrium constant K is small and the QD concentration is low, the molar enthalpy changes ΔH and the number of sites N are correlated in the fit. In particular, the shape of heat response curves within this model are parametrized by Brandt's c parameter (c = [QD]KN, [QD] is the concentration of the QDs). For data that are characterized by c values smaller than 1 (indicating a small mole fraction of bound ligands out of the total added), the enthalpy change and the number of sites are correlated, but the equilibrium constant K is well constrained. When TOP is introduced, there is a much greater exothermic response than for the reaction with OAm (an overall exothermic heat approximately 14 times more than that of OAm). The greater heat indicates that TOP has a more negative molar enthalpy of binding and/or binds to a greater number of sites per QD than does OAm. As seen in the PL response during QY regeneration, slower kinetics are also observed in the raw heat signal, which does not rapidly return to baseline between injections when TOP is introduced to the **CdSe/CdZnS_1** QDs. The thermogram for TOP cannot be well-fit by a simple independent identical sites model. In order to compare the results for TOP and for OAm, one approach is to consider the difference in ΔH and K that would be required if the number of binding sites per QD is considered to be the same. In this case a fit with N fixed to 10 reveals $\Delta H_{TOP\_QD}/\Delta H_{OAm\_QD}$ = 37 and $K = 4.3 \times 10^3$ M^{-1} for TOP.

Despite an apparently larger equilibrium constant for OAm than for TOP, introduction of OAm leads to much less change in QY than TOP, particularly in alloy shell QDs. This could indicate that the ITC signal for OAm corresponds to binding to only a subset of active trapping/quenching sites or that binding of OAm does not sufficiently perturb the energy levels associated with trapping and recombination. However, due to the

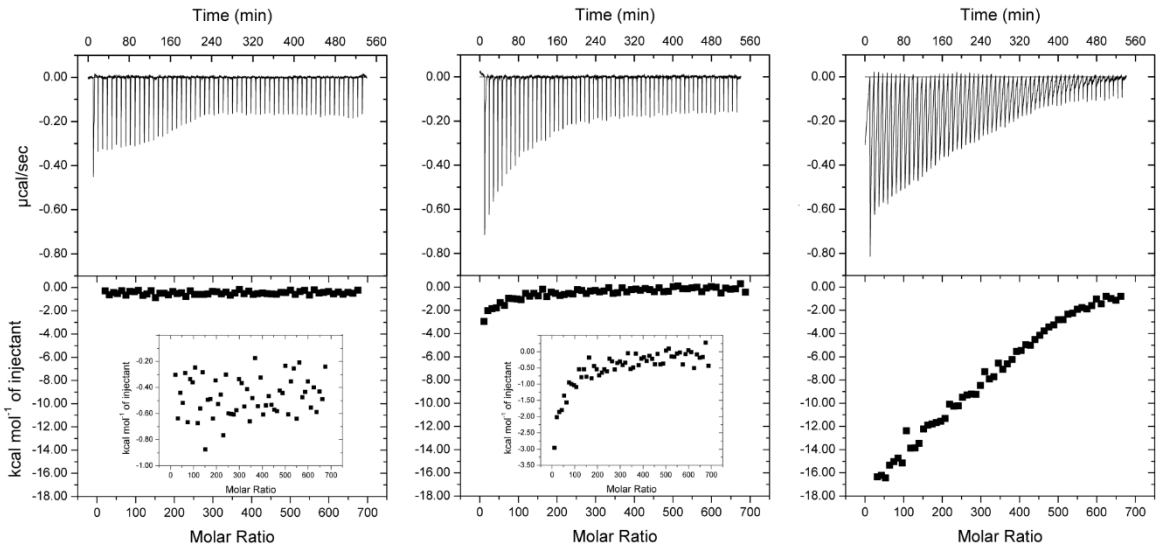

Figure 3.16 ITC traces for **CdSe/CdZnS_1** titrated with TOPO (A), OAm (B) and TOP (C) at the same concentrations. Top panel displays the raw heat per injection, while bottom panel shows the integrated curves adjusted to the scale for the TOP titration. Insets in bottom panels (A) and (B) show zoomed in integrated curves for TOPO and OAm titrations, respectively. Ligand-to-solvent reference titrations have been subtracted from the traces shown; solvent-to-solvent and solvent-to-QD runs gave negligible responses. Copyright 2015 American Chemical Society.

steric and electronic differences between these molecules, it is highly possible that OAm and TOP bind to different sites on the QD and the number of sites is not the same. The trends we observed in ligand binding strength are consistent with those predicted in Rempel's work for ligands binding to the Se-terminated (0001) surface of wurtzite CdSe.[152] The theoretical value of the binding energy between TOP to wurzite CdS S-terminated (0001) surface is 3.13 eV.[153] If we assume the binding behavior of TOP to the CdZnS alloy shell surface is similar to that for pure CdS, then the total heat response that we observe of about −200 eV/QD (obtained by integrating the response shown in **Figure 3.16C**) corresponds to about 60 available sites for TOP per QD. We believe that a more adequate model accounting for interactions among similar and dissimilar ligands is needed to describe such ligand association, dissociation, and exchange reactions more thoroughly,

and this could be an important target for future studies. Nevertheless, it seems reasonable to argue, particularly for ligands behaving as σ donors, that a strongly exothermic bond-forming step, leading to a large energy separation between bonding and antibonding orbitals, could assist in displacing electron traps from within the band gap. The trend of enthalpy change and QY regeneration that we observe supports this argument.

3.2.7 Conclusion

The maintenance of high PL QY is important to applications of QDs in lighting and displays, bio-imaging, and luminescent solar concentrators. In optoelectronic devices such as solar cells it is likewise important to passivate interfaces in such a way as to limit non-radiative recombination. Surface-adsorbed molecules (ligands) play at least two roles in the behavior of colloidal QDs: they maintain solubility and suppress aggregation, and except in QDs with very thick shells they are responsible for defining the electronic boundaries of the quantum well. In this study we used GPC purification to provide a well-defined initial state for association of neutral ligands to vacant sites. We have demonstrated that the decrease in QY observed on purification of QDs can be simply a result of ligand removal and is not necessarily due to irreversible changes or "damage" to the QD surface. Among the components of the CdSe-based core/shell samples tested here, the QY appears to be most critically affected by the loss of phosphine ligands on purification, because reintroduction of phosphine led to near-complete regeneration of QY with little change in absorption spectrum. In contrast, phosphine oxide and free carboxylic acid had a minimal effect on QY, and the primary amine showed significant QY regeneration only in the case of pure CdS shells. Introduction of Cd carboxylate equivalents led to a large increase in

QY in a manner complementary to phosphine, but was also associated with irreversible structural changes.

Time-resolved PL allows us to conclude that the reduction and regeneration in QY are not experienced uniformly among the QDs in the ensemble, but are rather associated with the changes in the relative populations between a subset with lifetime comparable to the radiative lifetime and a subset with significantly shorter lifetimes. A simple model of quenching by a binomially distributed number of recombination centers appears to be insufficient to describe the role of vacant sites in limiting QY.

We also show that ITC, a technique that does not require specific nuclei as spectroscopic probes or deuterated solvents, can be used to measure ligand interactions with QDs with nonzero molar enthalpy of binding. We expect ITC to become a versatile tool for studying ligand binding and interactions on nanoparticle surfaces. Due to its sensitivity, ITC does require a well-controlled reaction system, and it is important to identify purification methods and sample metrics that can ensure repeatable results for compound semiconductor nanocrystals.

3.2.8 Materials

The following chemicals were used as received. Cadmium oxide (CdO; 99.999%), Zinc oxide (ZnO; 99.999%), Trioctylphosphine (TOP; 97%) and Trioctylphosphine oxide (TOPO; 99%) were purchased from STREM Chemicals. Oleic Acid (OA; 99%), 1-Octadecene (ODE; 90% technical grade), and Selenium (Se; 99.999%) were purchased from Alfa Aesar. 1-Tetradecylphosphonic Acid (TDPA; >99%) was purchased from PCI synthesis. Bio-Beads S-X1 GPC medium was obtained from Bio-Rad Laboratories. Toluene-d_8 (D, 99.5%) was obtained from Cambridge Isotope Laboratories. Decylamine

(95%) was purchased from Sigma Aldrich. Oleylamine (80-90%) and Bis(trimethylsilyl)sulfide ($(TMS)_2S$; 95%) were purchased from Acros Organics. Rhodamine 590 chloride (R590, MW 464.98) was obtained from Exciton. Toluene (99.5%) and Tetrahydrofuran (THF, 99%) were purchased from Mallinckrodt Chemicals. 200 Proof Ethyl Alcohol (Ethanol) was obtained from Decon Laboratories. Acetone (99.9%) was purchased from VWR. Methanol (99.9%) was purchased from Fisher Scientific. Toluene was dried with activated 4A molecular sieves. THF was dried using the Puresolv system from Innovative Technologies. Synthetic or analytical procedures under inert conditions were carried out using Schlenk line techniques, in a glovebox, under N_2 atmosphere.

Optical spectroscopy. The optical absorption spectrum was recorded using a Thermo Scientific Evolution Array UV-Visible Spectrophotometer with toluene as the solvent as well as the blank in a 1cm path quartz cuvette. Routine emission spectra were recorded by an Ocean Optics USB 4000 spectrometer under ~365 nm excitation.

NMR analysis of QDs. Routine NMR samples of the QDs were prepared in toluene-d_8. The QDs' concentration is set at approximately 20 μM; the exact value in each case was measured by UV-Vis using the calculated molar extinction coefficient. The spectra were recorded on Bruker Avance III 400. The quantitative ^1H NMR spectra were measured with ferrocene as the internal standard and 30 s relaxation delay, allowing the system to reach a reliable equilibrium. The ^{31}P NMR spectra of QD samples were measured with 512 scans to increase the signal-to-noise ratio. T_1 is measured by the vendor-supplied inversion recovery pulse sequence experiment. Diffusion measurements and NOE difference measurements on ^1H spectra with selective saturation on the ^{31}P resonance were performed Bruker Avance III HD 400 and analyzed by the Topspin version 3.2 software.

Synthesis of CdSe QDs. The CdSe cores were prepared by a hot-injection method[3] using cadmium tetradecylphosphonate as the Cd precursor, trioctylphosphine selenide as the Se precursor and a mixture of TOP and TOPO as the solvent. The two precursors were mixed at high temperature (350 to 365 ℃) and cooled down with an air blower immediately after the injection. The lowest energy absorption peak for the CdSe cores used to prepare the CdSe/CdZnS samples was at 509 nm, while that of the CdSe cores used for the CdSe/CdS sample was at 522 nm.

CdZnS and CdS overcoating. Shells were grown using a selective ionic layer adhesion reaction (SILAR) method described previously. Briefly, a portion of as-synthesized CdSe cores was flocculated by methanol and acetone. After decanting the supernatant, the QDs were redissolved into hexane and stored in the freezer (4 ℃) for more than 12 hours. All the undissolved materials were removed by centrifugation and the sample was precipitated again by an addition of methanol and acetone. Afterward, the QDs were brought into a measured volume of hexane. The UV-Vis absorption spectrum was recorded at a known dilution of the sample to determine the size and quantity of QDs. The solution of QDs in hexane was transferred to a solvent of 1:2 oleylamine:ODE (v/v, 9 mL total) and degassed at 100 ℃ to remove hexane. Before the addition of the reagent *via* syringe pump, the system was heated to 200 ℃ under nitrogen. For the pure CdS shell growth, the Cd precursor is prepared by diluting 0.2 M $Cd(oleate)_2$ in ODE with 2 equivalents of decylamine and a volume of TOP to yield a concentration of 0.1 M. For the CdZnS alloy shell growth, the metal precursor is prepared similarly to the pure Cd precursor but using a mixture of $Cd(oleate)_2$ and $Zn(oleate)_2$ (the ratio of Cd:Zn is 3:7) to yield a metal concentration of 0.1 M. The S precursor was always a 0.1 M solution of

$(TMS)_2S$ in TOP. The volume increase associated with 1 monolayer coverage in both cases is calculated based on the radius increase of 3.37 Å, which is the half of the wurtzite *c*-axis unit cell dimensions for CdS. Alternating injections of metal precursor and sulfur precursor were performed, adding the metal precursor solution first, with injections starting every 15 minutes for CdS shell and 20 minutes for CdZnS shell. The flow rate was adjusted to complete each injection over the course of 3 minutes. The volume of each injection was calculated to apply 0.8 monolayers coverage each cycle (a cycle is defined as one metal precursor injection and one sulfur precursor injection). For the thin shell samples (**CdSe/CdS_1** and **CdSe/CdZnS_1**), two cycles were performed while five cycles were added to the thick shell samples (**CdSe/CdS_2** and **CdSe/CdZnS_2**). The growth processes were monitored by both UV-Vis absorption and fluorescence spectrometers. After the reaction, the mixture was cooled down to the room temperature and the molar extinction coefficient was estimated based on the amount of the core introduced at the beginning and the total volume of the solution after the synthesis.

Absolute quantum yield measurement. The absolute QY of QD samples was assigned by comparison to a rhodamine 590 standard (R590, QY= 99% in ethanol[154,155]). Fluorescence spectra of QD and R590 dye were taken under identical spectrometer conditions on a Varian fluorescence spectrometer in triplicate and averaged. The optical density was kept below 0.1 from the excitation wavelength to 800 nm to avoid internal filtering effects. The QY was calculated based on the integrated intensities of the emission spectra, the absorption at the excitation wavelength and the refraction index of the solvent using the equation:

$$\mathrm{QY_{QDs}} = \mathrm{QY_{dye}} * \frac{\mathrm{Absorbance_{dye}}}{\mathrm{Absorbance_{QDs}}} * \frac{\mathrm{Emission\ integral_{QDs}}}{\mathrm{Emission\ integral_{dye}}} * \frac{\mathrm{Refraction\ index^2_{toluene}}}{\mathrm{Refraction\ index^2_{ethanol}}}$$

The precision of this measurement in our case is limited by the precision of the absorbance measurement (~1%) while the accuracy among samples in different solvents will be limited by the accuracy of the refractive index correction term.

GPC purification of the QDs. The GPC column was packed by as previously described[6] with toluene as the eluent. The as-synthesized core/shell QDs were purified by 1 cycle of precipitation with acetone only and redissolution in toluene. Then the QD solution was added to the column and the sample was collected when the elution volume equaled ~1/3 of the total volume of the column (the expected void volume for irregularly spaced spherical beads); this volume corresponds to the fraction at which the purified QDs eluted. The GPC column was rinsed thoroughly (3 times the total volume of the column) between runs.

Preparation of pure Cd oleate. The cadmium oleate used as a ligand in the regeneration study was prepared as follows. CdO and oleic acid were introduced to a three neck flask (the ratio of CdO: OA is 1:5), where OA was used as both acid and solvent. The mixture was degassed and then heated to 270 ℃ under N_2 to form a colorless and clear solution. Then the sample was cooled and transferred to a refrigerator (4 ℃) to allow the product to precipitate. Excess oleic acid was separated by filtration and the insoluble $Cd(oleate)_2$ was washed with ethanol 5× to remove the remaining oleic acid. FTIR and ^1H NMR has been used to confirm the removal of oleic acid.

Quantum yield regeneration and relative quantum yield measurement. After GPC purification, the QD samples were transferred into sealed N_2 environment and pumped into glove box immediately to avoid any possible oxidation. The ligand solutions are also prepared in the glove box. For the regeneration process, the concentration of the

QD samples are fixed to be 0.5 μM and the ligand concentration is controlled to be 1.5 mM or 0.15 mM to provide two different ligand-to-QD ratios (1:3000 and 1:300). The total volume of the mixing solutions is 1 mL and the solutions were kept gently stirring for the 7 day measurement period. The relative QY is characterized by diluting a portion of the above solutions into dry toluene and measuring the absorption and emission spectra. The optical densities of the sample solutions were kept below 0.1 at wavelengths above the 365 nm excitation wavelength to avoid internal filtering effects. The relative QY is calculated by comparing the integration the emission spectrum divided by the absorption at 365 nm.

Time-resolved photoluminescence measurement. The PL decays of QDs in toluene were collected in front-face mode with 1 cm quartz cuvette in a lifetime spectrometer (Edinburgh Mini-τ) equipped with a 368 nm picosecond-pulsed-light-emitting diode. A stirring stage was set under the Mini-τ and a mini stirring bar was placed in the cuvette to stir the QD solution to avoid accumulation of photo-products during the measurement. The instrument response function (IRF) is recorded using Rayleigh scattering of pure water.

Analysis of photoluminescence decay lifetimes. Analysis follows the methods described in *Principles of Fluorescence Spectroscopy* by Lakowicz,J.R. The PL decays were fit with a multi-exponential function re-convoluted with the recorded instrument response function (IRF). For example, if the decay was fit with a tri-exponential function, then:

$$I(t) = \int_0^t IRF(t') \cdot \left(C + \sum_{i=1}^{3} A_i \exp\left(-\frac{t - t'}{\tau_i} \right) \right) dt'$$

where $I(t)$ represents the intensity at time t, and τ_i and A_i are the exponential lifetime and amplitude, respectively, of decay component i.

The amplitude average PL lifetimes were calculated based on Equation 9.

$$\tau_{avg} = \frac{(A_1\tau_1 + A_2\tau_2 + A_3\tau_3)}{(A_1 + A_2 + A_3)}$$

The goodness of the fit is determined by nonlinear least-squares analysis (NLLS) which tests whether the fit is consistent with the raw data and to obtain the lifetimes and amplitudes for the fit that provide the best match between the measured raw data, $N(t_k)$, and the calculated decay, $N_c(t_k)$, where N represents the discrete sequence of intensities measured at times t_k and k is an index. A reduced χ_R^2 is then minimized to find the best-matched fit:

$$\chi_R^2 = \frac{1}{\nu} \cdot \sum_{k=1}^{n} \frac{[N(t_k) - N_c(t_k)]^2}{N(t_k)} \qquad \nu = n - p$$

where $\nu = n - p$, is the number of degrees of freedom, n is the number of data-points, and p is the number of floating parameters. The reduced χ_R^2 is minimized for all the lifetime decay fits.

Support plane analysis was applied to obtain the uncertainty in the lifetime for each exponential component. The procedure is to change one lifetime τ_i (i=1~3) from its value where χ_R^2 is at a minimum, $\chi_{R,\min}^2$, to one of a series of possible lifetimes with offsets $\Delta\tau_k$ ($\tau_i \pm \Delta\tau_k$). Then, we re-run the least-squares fit, keeping $\tau_i \pm \Delta\tau_k$ constant, to minimize χ_R^2 again to $\chi_{R,par}^2$. The confidence probability was judged by the F_χ statistic:

$$F_\chi = \frac{\chi^2_{R,par}}{\chi^2_{R,\min}} \quad F_{\chi,P} = 1 + \frac{p}{\nu} F(p,\nu,P)$$

where $F(p,\nu,P)$ is the F statistic with p parameters and ν degrees of freedom with a probability P that F_χ is due to random errors in the data. In this work, the uncertainty in the lifetime is obtained using P= 10%, suggesting there is less than 10% probability that F_χ is due to random error, in other words a 90% confidence limit. Confidence limits were calculated for decays illustrated in the preceding narrative.

Reversibility test. CdSe/CdZnS_1 and CdSe/CdS_1. QD samples are purified by GPC and mixed with 3000 equivalents of ligand. After stirring inside the glovebox for 1 day, the mixtures are purified again by GPC. Absorption and emission spectra are monitored during the process.

Inductively coupled plasma-mass spectrometry analysis. Two samples were prepared. One is made by diluting 1 nmol of GPC purified **CdSe/CdZnS_1** QDs in 0.5 mL toluene; the other by mixing 1 nmol of the same QD sample with 3 μmol CdOA (3000:1 ratio) in 0.5 mL toluene. After stirring under N_2 overnight, these two samples were precipitated by acetone and the supernatants were transferred evacuated to dryness. 1 mL aqua regia was introduced and was allowed to digest the sample for 2 h. Then the solutions were brought to 50 mL in a volumetric flask with 2% HNO_3 in water. The concentrations of Zn were detected by a Thermo-Finnigan Element XR ICP-MS.

Isothermal titration calorimetry. Isothermal titration calorimetry (ITC) experiments were performed on a VP-ITC calorimeter (Microcal Inc., Northampton, MA). Ligand solutions were titrated from the 300 μL injection syringe to the sample cell loaded to its 1.8 mL filling capacity, and the heat response to maintain a constant temperature

between the sample cell and reference was monitored. The sample cell was purged with nitrogen before loading the GPC purified QD solution to minimize the influence of the oxidation reactions. Each experiment was conducted at 22 ℃ and midrange reference power; allowed to equilibrate prior to an initial 600 seconds delay; and in order to allow adequate equilibration between each injection, 8-9 min intervals were set between each injection for a total 60 injections in 5 μL increments. Dry THF was chosen as the solvent for both the ligands and QDs, as well as the blank solvent in the reference cell. Reference titrations were conducted to determine any significant heat of dilution between the solvent, ligand solution and QD solutions that may have accounted for signal in the final ligand-QD titrations. Only ligand-solvent reference titrations were subtracted from ligand-QD titrations, as other reference titrations were determined negligible. The QD solutions loaded in the sample cell were 0.5 μM (same as for QY regeneration) and ligand solutions loaded in the syringe were 1.5 mM.

3.3 Reducing competition by coordinating solvent promotes morphological control in alternating layer growth of CdSe/CdS core/shell quantum dots

3.3.1 Introduction

The formation of core/shell structures in colloidal semiconductor nanocrystals is important in maintaining the spectroscopic properties of colloidal quantum dots (QDs) and defining new functions. When using selective ionic layer adhesion and reaction (SILAR) based techniques, conversion of shell precursors to surface-adsorbed equivalents should be maximized for effective control of shell growth. Our group has previously demonstrated that the commonly used cadmium precursor $Cd(oleate)_2$ has low conversion yield when

added in monolayer-equivalent quantities during the growth of CdSe/CdS core/shell QDs via the SILAR technique[20]. The growth solvent could potentially play an important role in governing precursor conversion, in particular by controlling precursor solubility and through competition for nanocrystal surface sites. Primary amines such as oleylamine[19,23,99], octadecylamine[18,27] and hexadecylamine[156] have long been used as coordinating solvents for nanocrystal growth, with oleylamine a common choice for shell growth on CdSe QDs by SILAR[19,20].

The role of the primary amine in the nanocrystal growth has been studied extensively and there have been contradictory conclusions, which have recently been well summarized by Garcia-Rodriguez et al[157]. Additionally, Hollingsworth's and Vela's groups have reported that switching to a secondary amine (dioctylamine) improved the synthetic yield when growing CdS shells on CdSe QDs, especially for larger shell thicknesses[23,158]. Foos et al. have shown that the use of secondary and tertiary amines can result in an improved size distribution during growth of CdSe nanocrystals.[159] One possible mechanism is that the reactivity of the Cd precursor was reduced due to the strong coordination of the primary amine. Liu's and Vela's groups have suggested that primary amines such as oleylamine may stabilize $Cd(oleate)_2$ in solution through the formation of six-coordinate complexes[157,158]. Solution-phase complexes could be sterically restricted in the case of secondary or tertiary amines. However, as shown previously, amines can improve the fluorescence quantum yield by coordination to the nanocrystal surface[55,106] and it is possible that such surface coordination is competing with precursor conversion as well.

In this work, we grew CdSe/CdS core/shell quantum dots in solvent mixtures with three different representative amines—primary, secondary, and tertiary—via a SILAR technique. We selected oleylamine (OAM), dioctylamine (DOM) and trihexylamine (THM) for our studies. The three amines were chosen to 1) represent primary/secondary/tertiary amines; and 2) have similar molecular weight and molar volume, so that similar amine:QD ratios (~50000:1) could be achieved at similar QD concentrations. The course of the growth was monitored by UV-Vis absorption and photoluminescence (PL) emission spectroscopy. Emission peaks at wavelengths shorter than the effective band-gap ("blue peaks") appeared in the PL spectrum when QDs were grown in primary amine, suggesting nucleation of small CdS particles as a result of cross-reaction of the shell precursors as seen previously, and such nucleation was suppressed and no CdS particles were present in the QDs grown in tertiary amine. Scanning transmission electron microscopy (STEM) proved the yield of the shell was highest when using the tertiary amine (trihexylamine) as the growth solvent. In order to explain these observations, proton NMR was applied to understand the interaction of different amines with the CdSe surface. We demonstrated that the interaction between the solvent molecules and the nanoparticle surface is an issue influencing shell growth by SILAR, since the shell precursor must compete with such interactions in order to saturate the surface prior to introduction of the complementary precursor for growth of the shell compound.

3.3.2 Shell growth as monitored by absorption and emission spectroscopies

During the course of the growth, aliquots with a consistent volume of 50±5 μL were drawn and diluted in 2.0±0.2 mL of hexane for monitoring by absorption and PL

spectroscopy. This method resulted in diluted samples with < 25% error in concentration. The nominal concentration of core/shell particles in each aliquot can be calculated based on the quantity of cores introduced at the start of the reaction; the nominal concentration decreases over the course of shell growth due to the increase in total volume as shell precursor solutions are introduced. The band-edge absorbance peak of all aliquots remained less than 0.1 AU such that little fluorescence light is re-absorbed when the samples are excited. Absorption and PL spectra of core/shell particles grown in the three amines are shown in **Figure 3.17**. To facilitate comparison, the absorption and PL spectra of successive aliquots have been scaled to compensate for the difference in nominal concentration of core/shell particles. In particular, the absorbance and intensity values plotted should be representative of the signals seen at the same QD concentration (0.42 μM), with a scaling error of less than 25%. In all three shell growth experiments, the absorption spectra indicate a red shift in the lowest-energy (1S) exciton resonance is observed with increasing shell thickness, accompanied by an increase in the height of the scaled 1S absorbance. An increase in the 1S molar extinction coefficient with increasing size of CdSe QDs has been described and modeled by Jasieniak et al[160]. The trend for the same model applied to the evolution of the 1S absorbance in the CdSe/CdS core/shell particles is indicated by the black curves in **Figure 3.17A-C**, with 25% error indicated by dashed lines.

Figure 3.17D-F shows that in all three growths, the PL emission intensity of CdSe/CdS core/shell particles continuously increased with increasing CdS shell thickness; this is a result of an increasing quantum yield as well as an increasing excitation rate at the same concentration due to enhanced absorption at short wavelengths due to the CdS shell.

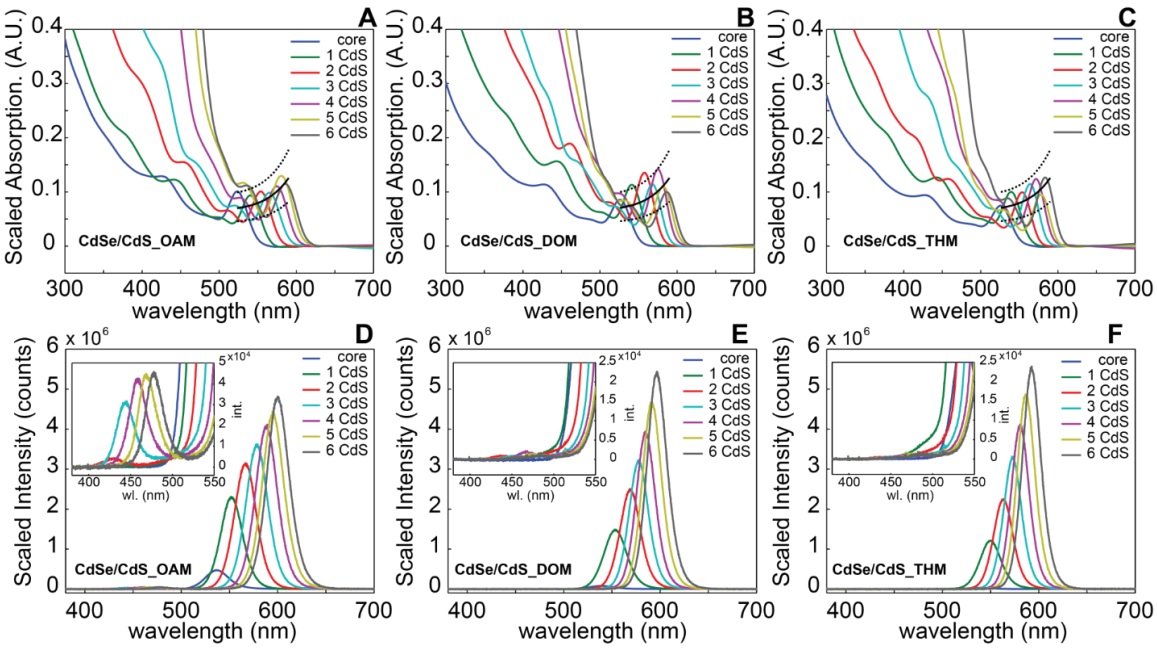

Figure 3.17 Scaled absorption and emission spectra over the course of CdSe/CdS core/shell QDs growth in three amines. (A, D) **CdSe/CdS_OAM** grown in oleylamine; (B, E) **CdSe/CdS_DOM** grown in dioctylamine; (C, F) **CdSe/CdS_THM** grown in trihexylamine; Absorptions and emissions are normalized to the concentration of QDs in each aliquot, so that all the absorption and emission represent the absorption and intensity of the same amount of QDs, the dash lines represent the upper and lower band of 25% error for the QD concentration in each aliquot. The insets zoomed in the region of emission where "blue-peaks" appeared for **CdSe/CdS_OAM** and **CdSe/CdS_DOM**, and no "blue-peaks" in **CdSe/CdS_THM**. Copyright 2015 American Chemical Society.

Despite superficially similar absorption spectra and band-edge PL spectra among the three samples, a close examination of the emission spectra reveals a PL peak appearing between 400-500 nm ("blue peak") that is present in the oleylamine case (**Figure 3.17D**), greatly diminished (~50× less intense) with dioctylamine, and nearly absent with trihexylamine. The blue peaks are absent prior to introduction of shell precursors, are centered at wavelengths shorter than the emission of the CdSe cores used, and shift to longer wavelengths as additional shell precursors are introduced. These characteristics are all consistent with the appearance of a CdS nanoparticle side product. The wavelengths of the

blue peaks fall within the range of emissions for CdS nanoparticles with diameters 3.5-4.5 nm[161,162].

3.3.3 STEM images of the core/shell QDs grown in three amines

In order to support the above hypothesis that the blue peaks are PL from a CdS nanoparticle side product that is abundant in the case of oleylamine, scanning transmission electron microscopy (STEM) has been used to record the images from CdSe cores as well as the three core/shell products prepared in three different solvents. As shown in **Figure 3.18**, the radius histograms are determined by analysis of STEM images of the same magnification at 6-7 randomly selected regions; *N* is the number of particles analyzed. In comparing STEM images **Figure3.18A-D** and the radius histograms **Figure 3.18E-H**, the differences in particle sizes and distributions are clearly displayed. We characterize the average radius and peak radius for particles; the average radius is obtained directly from the distribution (including small particles), while the peak radius is the center of a Gaussian fit (red curve, **Figure 3.18E-H**) to the distribution and represents a characteristic radius for core/shell particles in the sample.

A majority of particles in the core/shell samples showed a radius larger than that of the cores and commensurate with shell growth; however, CdSe/CdS_DOM (**Figure 3.18C**) and CdSe/CdS_THM (**Figure 3.18D**) showed larger average and peak radius as compared to CdSe/CdS_OAM (**Figure 3.18B**). Additionally, both CdSe/CdS_DOM and CdSe/CdS_THM showed narrower size distributions and showed particles with more uniform shapes. Inspection of the STEM images reveals the presence of a significant number of particles smaller than the CdSe cores in CdSe/CdS_OAM. Although the STEM images cannot clearly resolve CdS from CdSe, we can assign the smallest particles as a

CdS nanoparticle side product. These small particles contribute to the smaller average radius in this sample. The peak radius primarily describes the core/shell product; it is the smallest in CdSe/CdS_OAM as well, indicative of thinner CdS shells due to loss of material to the side product.

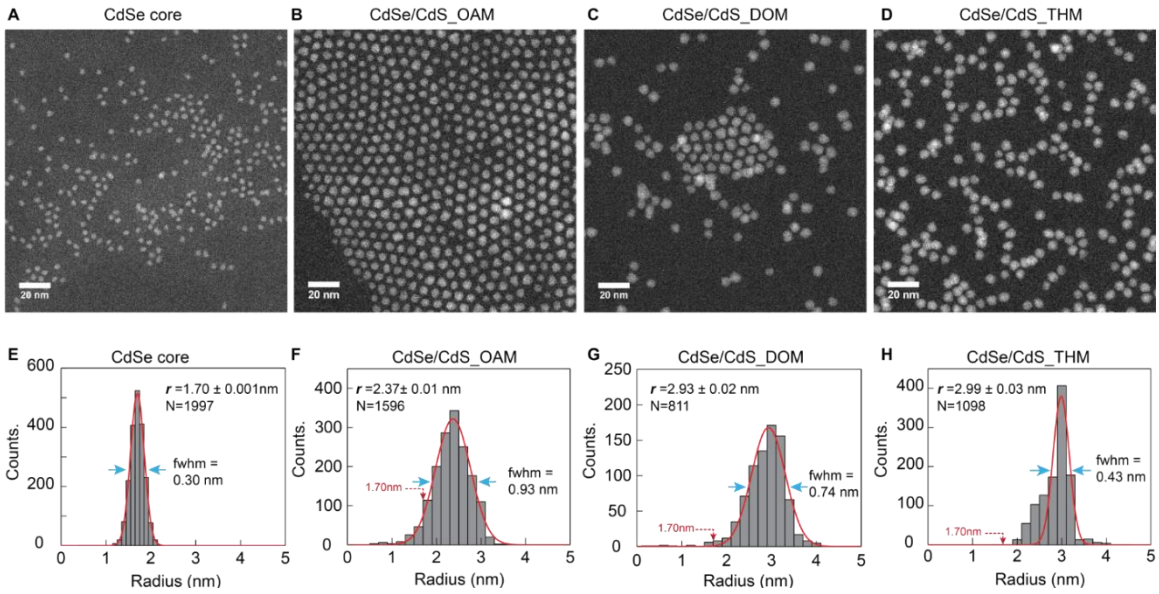

Figure 3.18 STEM images and radius histograms for CdSe cores (A,E) and core/shell samples **CdSe/CdS_OAM** (B, F), **CdSe/CdS_DOM** (C, G), and **CdSe/CdS_THM** (D, H). The histograms are fitted by Gaussian functions (red curves, E-H) to determine the peak radius; the FWHM is indicated by blue arrows. Copyright 2015 American Chemical Society.

At the same time, the distribution of radius for CdSe/CdS_OAM (fwhm = 0.93 nm) is broader than that for CdSe/CdS_DOM (fwhm = 0.74 nm) and CdSe/CdS_THM (fwhm = 0.43 nm). Core/ shell particles growing in trihexylamine maintained a very narrow size distribution, nearly as good as the cores (fwhm = 0.30 nm), although a small fraction of particles with radius down to 2.5 nm (**Figure 3.18H**) remained present. The STEM results confirm that the more highly substituted amines dioctylamine and especially trihexylamine were effective in suppressing the nucleation of small particles during shell growth, and the observation of small particles in the CdSe/ CdS_OAM and CdSe/CdS_DOM samples

corroborates the assignment of the blue PL peaks as radiative recombination from CdS nanoparticles. Examination of the shapes of nanocrystals in the three core/shell samples appears to show greater roundness in CdSe/CdS_DOM and CdSe/CdS_THM, suggesting that conditions that suppress nucleation also help to enforce isotropic shell growth.

3.3.4 Proton NMR characterization of amine interactions with QD surface

The results from the optical spectra and STEM images confirm that by using different amines as the coordination solvents, the shell formation process varies significantly. In order to probe this ligand/nanocrystal interaction directly under mild and controlled conditions, we recorded ^{1}H NMR spectra of mixtures of CdSe cores with each of the amine solvents diluted in d_8-toluene (**Figure 3.19**). Reference spectra of the amines in d_8-toluene without QDs were recorded for comparison. The QDs were purified by gel permeation chromatography (GPC, toluene/polystyrene) to minimize the impact of any impurities and isolate interactions between the amines and the CdSe QD surface. In the presence of the QDs, the α-proton and olefin peaks of oleylamine are significantly broadened, which is evidence of a strong interaction between oleylamine and the nanoparticle surface. In contrast, a mixture of dioctylamine with the CdSe cores shows only a small degree of broadening and a small downfield shift, and a mixture of trihexylamine with the CdSe cores shows almost no change versus the free molecule. These results indicate that the interaction affinities of amines to the nanoparticle surface are in the order of oleylamine > dioctylamine > trihexylamine from strong to weak. This implies that replacing oleylamine with dioctylamine or trihexylamine in SILAR shell growth effectively destabilizes the neutral nanocrystal surface, which facilitates binding of the

Cd(oleate)$_2$ precursor independently of differences in solution-phase interactions that may also be present.

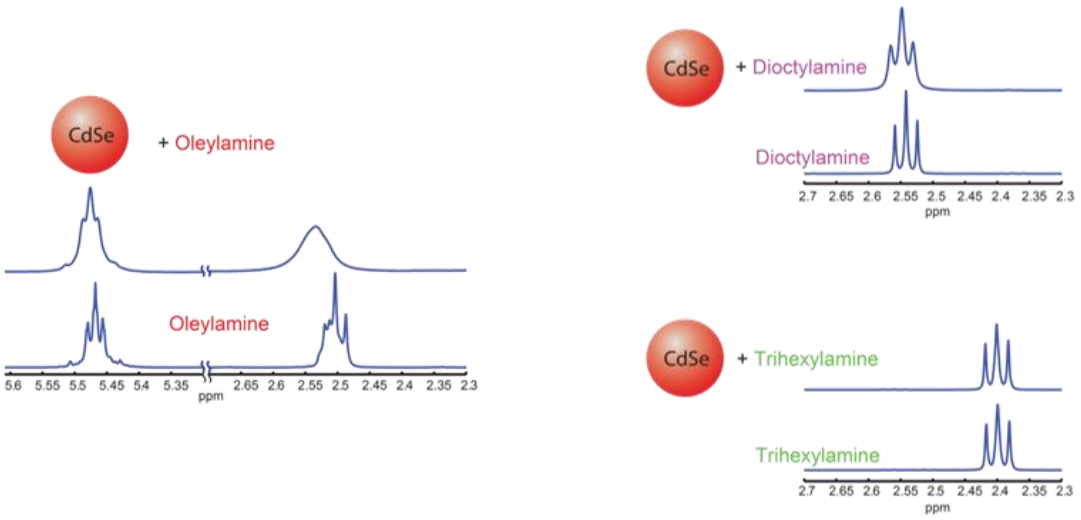

Figure 3.19 ^{1}H NMR for α-proton for the three amines studied in the presence and absence of CdSe cores. Solvent is d_8-toluene. Copyright 2015 American Chemical Society.

3.3.5 Conclusion

We have confirmed that replacing oleylamine with a secondary amine, dioctylamine, suppresses nucleation and improves core/ shell growth, and we have shown that moving to a tertiary amine, trihexylamine, is even more effective. We have also shown through NMR spectroscopy that the more highly substituted amines bind less strongly to the CdSe QD surface and permit greater precursor conversion under experimental conditions. On the basis of these results, we can conclude that oleylamine effectively competes with the precursor Cd(oleate)$_2$ for occupation of nanocrystal surface sites, leading to a significant amount of cross-reaction and nucleation of CdS particles during CdS shell growth by SILAR. Studies that separately quantify QD−amine and Cd

precursor−amine interactions could be used to differentiate their relative contributions to control of precursor conversion and growth.

3.3.6 Materials

The following chemicals were used as received. Cadmium oxide (CdO; 99.999%), trioctylphosphine (TOP; 97%), and trioctylphosphine oxide (TOPO; 99%) were purchased from Strem Chemicals. Oleic acid (OA; 99%), 1-octadecene (ODE; 90% technical grade), 1-tetradecylphosphonic acid (TDPA; 98%), and Se (99.999%) were purchased from Alfa Aesar. Di-n-octylamine (98%) and tri-n-hexylamine (97%) were purchased from Alfa Aesar. Decylamine (95%) was purchased from Sigma-Aldrich. Oleylamine (80−90%) and bis(trimethylsilyl) sulfide ($(TMS)_2S$; 95%) were purchased from Acros Organics. Toluene-d8 (D, 99.5%) was purchased from Cambridge Isotope Laboratories, Inc. 200 proof ethyl alcohol (ethanol) was obtained from Decon Laboratories, Inc. Methanol (99.8%) was purchased from BDH. Acetone (99.9%) was purchased from VWR. Ethanol (99.9%) was purchased from Fisher Scientific. TOPSe (2.2 M) was prepared by dissolving Se in TOP. A stock solution of $Cd(oleate)_2$ (0.2 M) in ODE was prepared by heating CdO in ODE with 2.2 equiv of oleic acid at 260 ℃ under nitrogen, followed by degassing under vacuum at 100 ℃ for 20 min. The sulfur precursor was 0.1 M solution of $(TMS)_2S$ dissolved in TOP. Nanocrystal core and shell growth was carried out under nitrogen (N_2) using Schlenk line techniques; air-sensitive reagents were prepared in a nitrogen filled glovebox.

Optical Spectroscopy. The optical absorption spectrum was recorded using a Thermo Scientific Evolution Array UV−visible spectrophotometer with hexane as the solvent as well as the blank in a 1 cm path quartz cuvette. Routine emission spectra were recorded by an Ocean Optics USB 4000 spectrometer under ~365 nm excitation.

Synthesis of CdSe Cores. A hot-injection technique was applied for synthesis of CdSe nanocrystals (NCs) cores.4 For a representative synthetic route, CdO (0.12 g) was heated with TDPA (0.5500 g) at 330 ℃ in a solvent of TOP (6 mL) and TOPO (6 g) under nitrogen flow until the solution became colorless. Following removal of evolved H_2O under vacuum at 130 ℃, the solution was heated again to 360 ℃ under nitrogen. As-prepared TOPSe (1.3 mL) was injected rapidly into the reaction pot, which was immediately allowed to cool to room temperature and stored as a yellow waxy solid. The Cd:TDPA:Se molar ratio is 1:2:3. The core radius was estimated by a calibration curve describing the radius as a function of the position of the lowest-energy absorption peak. One batch of cores provided sufficient material for several core/shell growth experiments; all core/shell particles were made on the basis of the CdSe QD cores taken from the same batch.

Synthesis of Core/Shell Nanoparticles in Different Amines. The method for CdSe/CdS core/shell particle growth was modified from our previous work. The difference was switching different types of amines (oleylamine, dioctylamine, trihexylamine) in the solvent mixture. The Cd precursor was prepared by diluting $Cd(oleate)_2$ stock solution in a solvent of 50:50 ODE and TOP with 2 equiv of the same amine in the solvent mixture (vs Cd) added to yield a Cd concentration of 0.1 M. The sulfur precursor was 0.1 M solution of $(TMS)_2S$ dissolved in TOP. The CdS shell was grown by alternatively introducing Cd and sulfur precursors into the reaction flask, 1 ML equiv of precursors added per cycle, and forming 6 ML of CdS shell in total after six cycles. Reaction progress was monitored by periodically withdrawing a small aliquot of a measured volume (typically 50 μL) from the reaction flask and diluting it in hexanes at room temperature; these aliquots were analyzed for UV−vis absorption and fluorescence emission in hexanes solution.

Scanning Transmission Electron Microscopy Imaging. After purification, the CdSe or CdSe/CdS core/shell QDs were brought into hexane to form a dilute solution (1.1 μM), and one drop of the solution was drop-casted on a clean TEM grid (400 mesh Cu grid with ultrathin carbon support film, Type-A, Ted Pella, Inc.) and pumped dry under vacuum for 2 h. The STEM samples were imaged by JEOL 2100F 200 kV FEG-STEM/TEM equipped with a CEOS CS corrector on the illumination system. Prior to high magnification observation, a large specimen area was preirradiated with electrons for 10 min to polymerize surface hydrocarbons and therefore prevent their diffusion to the focused probe. High angle annular dark-field (HAADF) STEM images were acquired on a Fischione model 3000 HAADF. A pixel dwell time of 16 μs was chosen.

3.4 Conclusion

As shown in this chapter, the neutral ligands are influencing both the synthesis of the core/shell QD samples and later photo-physical performance of the materials. Stronger binding ligands tend to assist in displacing electron traps from within the band gap and improve the brightness of the QDs; while the weak coordinating ligands open up more sites on the surface, allowing better precursor conversion efficiency during the shell growth process. This information is important for preparing bio-compatible QDs sample in both fabrications of the QDs and design of suitable hydrophilic capping ligands. Future work including study the binding strength between different amines and nanocrystals by ITC, and detail transient absorption spectroscopy study on the QY regeneration experiments will be valuable to better understand the effect of the neutral ligands on the QDs' properties.

CHAPTER 4

FABRICATION OF BIOCOMPATIBLE QDS WITH METHACRYLATE BACKBONE POLYMERIC IMIDAZOLE LIGANDS

4.1 Introduction

Quantum dots (QDs) are always considered as an attractive candidate in biolabeling applications. Compared to typical fluorescent dyes, QDs possess greater excitation cross-sections and better photo-stability, which is advantageous in imaging over an extended time. There are two common strategies to prepare water-soluble QDs, namely direct synthesis in aqueous phase and post-surface modification with hydrophilic coatings. Mulimani's group[163] and Donegan's group[164] have proposed using thioalkyl acids as the stabilizer to prepare CdSe and CdTe QDs in aqueous solution. However, the water-based synthetic routes tend to provide QDs with large size distribution and low quantum yield (QY). The other approach is to water-stabilize the QDs prepared in hydrophobic solvents. This process has been widely studied and can be grouped into two main strategies: one is removal of the native surfactant and replacing them with the hydrophilic ligands, or in short ligand exchange; the other approach is encapsulation of the particles with surfactants, silica shells, or amphiphilic copolymers[91]. The encapsulated QDs can maintain their brightness and stability in water over an extend period of time, but the hydrodynamic radius of these samples is considerably large, which limits their application in the biological system.[165–167] Bio-compatible QDs can also be made via ligand exchange with hydrophilic ligands

bearing nucleophilic anchoring groups such as thiol[21] and amine[2]. This strategy has shown smaller hydrodynamic radius than is achieved by the encapsulation strategies in which the initial ligand coating is retained.

The most widely studied hydrophilic ligands are thiol based molecules. Bawendi's group has shown that as-synthesized CdSe/CdZnS QDs can be coated with cysteine to form a biologically compatible and highly fluorescent probe for imaging[21]. Mattoussi's group designed water soluble CdSe/ZnS QDs based on surface exchange with dihydrolipoic acid (DHLA) for use in immunoassays[168]. In order to improve the long term stability of the QDs in water, several groups have explored using multiply binding (multidentate) polymeric ligands instead of traditional mono- and di-thiol based ligands[40,41,169]. One promising class of polymeric ligands utilizes imidazoles as anchoring groups, or often referred to as polymeric imidazole ligands (PILs)[2].

In this chapter, two projects related to PIL capped QDs will be described. The first project described here is a simple approach for the preparation of methacrylate backbone polymeric imidazole ligands (MA-PILs) with improved control on the composition and molecular weight, which can provide robust attachment to the QDs. The polymer is prepared by a copolymerization of N-methacryloxysuccinimide (NMS) and poly(ethylene glycol) methacrylate (PEGMA), followed by a post-modification to replace the NMS group with the histamine. These novel copolymers combine water solubility and robust attachment to QDs to provide narrow size distributions and good quantum yields. We have also explored the effect of polymer length and monomer composition on its complexation to quantum dots and display the utility of these copolymer functional materials through excellent dispersions in protic environments. The biocompatibility of these samples has

also been evaluated through scalable nonspecific binding and cell viability assays. In the second project, I will describe a mild and reproducible method for membrane-enveloped virus labeling with QDs. A ternary copolymer version of the MA-PILs that can incorporate PEG sidechains for steric stabilization in water, imidazole anchoring groups, as well as primary amines that are available for further modification has been used. This polymer has been functionalized with dibenzocyclooctyne (DBCO) and then attached to the QDs. We labeled the measles virus (MV) envelop with azido groups by incorporating an azide-bearing azidoethyl-choline (AECho) into the MV phospholipid bilayer via host cells. The exchanged QDs (QDs-DBCO) were attached to the azide-labeled MV (N_3-MV) through a copper-free, strain-promoted azide-alkyne cycloaddition (SPAAC) reaction. The QD-labeled MV maintains its infectious ability against host Vero cells.

4.2 Preparation of methacrylate backbone polymeric imidazole ligand capped quantum dots with low cytotoxicity and low nonspecific binding

4.2.1 Introduction

As described previously, PILs have been considered as a promising candidate in preparation of bio-compatible QDs. Krull's group has used such PIL-capped QDs as a fluorescence resonance energy transfer (FRET) donor for biosensors[170–172]; Bawendi's group and Mattoussi's group have shown that PIL-capped QDs can be used to label cells and that brightness can be maintained over an extended time[2]. Cai's group has used PIL-capped QDs to label viruses and shown that the viruses maintain their infectivity both in vitro and in vivo[41,173]. However, these PILs are prepared either by direct modification of poly(maleic anhydride), which leaves residual carboxylic acid side chains that may

influence the overall charge of QDs after ligand exchange reaction[41]; or through a boc-protected histamine based monomer via RAFT polymerization reaction, which requires several synthetic steps, including protection of the imidazole amine for successful RAFT polymerization and the corresponding de-protection[2] to access the imidazole for quantum dot attachment.

In this work, PILs bearing poly(ethylene glycol) (PEG) side chains were prepared using RAFT polymerization. A versatile post-modification strategy using activated ester units of NMS and PEGMA in the polymer chain afforded copolymers ranging from 6K to 50K with low polydispersities, along with tailored composition of each monomer along the copolymer chain. By controlling the monomer ratio, PEGMA molecular weight, time, and temperature, the composition could be tuned to study its effect on quantum dot functionalization. Representative oleate-capped CdSe/CdZnS QDs purified by gel permeation chromatography (GPC) method were used to test the effectiveness of the histamine-bearing polymers for preparation of water-soluble QDs. Successful ligand exchange of the QDs was characterized by good dispersions in water, lack of aggregation between QDs, and good quantum yields in water. The nonspecific binding and toxicity of the QDs toward human endothelial cells have also been characterized. The result illustrates the potential of methacrylate-based polymeric ligands to form bio-compatible nanocrystals for targeting and sensing applications.

4.2.2 Preparation of MA-PILs

MA-PILs were prepared by Dr. Anand Viswanath from Dr. Brian Benicewicz's group in the Chemistry Department here at USC. The synthetic procedure can be described

into three steps. In the first step, NMS and PEGMA were copolymerized in DMF with 4-cyano-4-[(dodecylsulfanylthiocarbonyl)sulfanyl]pentanoic acid (CDTPA) as the RAFT chain transfer agent and 0.1 equiv of AIBN at 80 ℃.

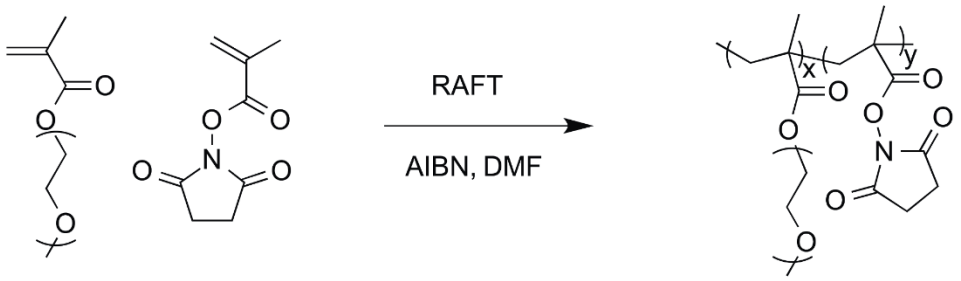

The polymerization was quenched in ice water, and the mixture was precipitated in ether. The mixture was centrifuged at 3000 rpm for 5 min and redispersed in THF. The RAFT agent was removed by reaction with an excess of AIBN at 64 ℃ for 1 h. Thus, the polymer was capped with a 2-cyanoisopropyl moiety to prevent side reactions with the original trithiocarbonate end group. The polymer was purified by several precipitations in ether and was redispersed in THF for subsequent use.

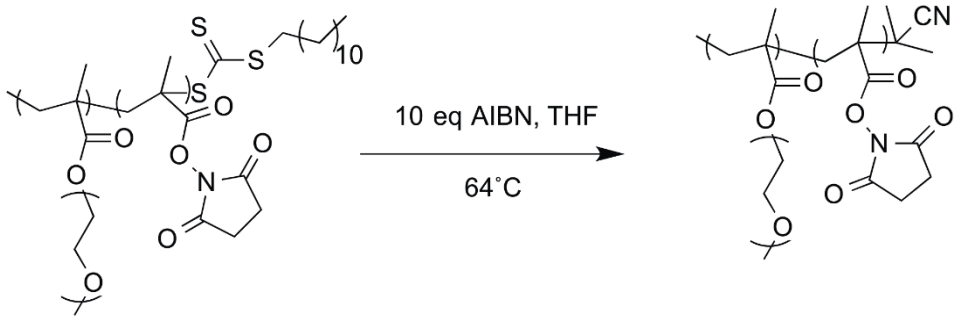

The last step is the modification of the NMS group with the histamine group. The above polymer is mixed with histamine 2HCl in DMSO and heated overnight at 70 ℃.

The polymer was purified by dialysis for 24h and followed by several precipitations before attaching to the QDs.

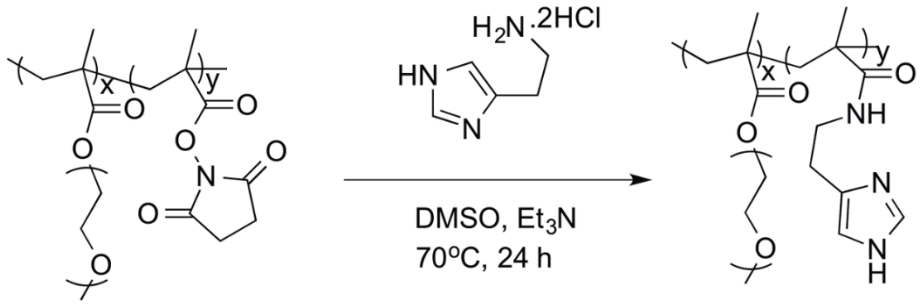

A series of polymers with different composition and molecular weight have been prepared and summarized in **Table 4.1**.

Table 4.1. Polymer characteristics used for the ligand exchange of QDs

Ligand Mn	PDI	Mol% Imidazole	Mol% PEGMA	# of imidazole units	# of PEGMA units	QY (%)	HR/nm
A, 10,680	1.24	54.29	45.71	32	9	36	8.6
B, 17,950	1.21	44.10	55.90	44	18	31	8.0
C, 30,700*	1.35	61.35	38.65	104	12	34	15.2
D, 50,550*	1.34	46.95	53.05	134	29	27	17.0

4.2.3 Ligand exchange and characterization of the PIL capped aqueous QDs

The CdSe/CdZnS QDs were prepared by the SILAR method as described previously. Totally 5 monolayers of the alloy shell were grown onto the CdSe core surface. The QY of the as-synthesized QDs was found to be 81% compared to rhodamine 590 (R590, QY=99% in ethanol). The sample was purified by the GPC method to remove the

excess ligands and impurities before the ligand exchange. After purification, the QY drops to 56%, which is in line with the previously described QY regeneration result. According to TEM (**Figure 4.1A**) and absorption spectrum, the QDs retained their monodispersity and narrow size distribution after purification. The initial ligand density was found to be 296 oleate species per QD by NMR with ferrocene as the internal standard. The hydrodynamic radius of QD was approximately 5.0 nm based on dynamic light scattering (DLS) volume distribution measurements (**Figure 4.1B**).

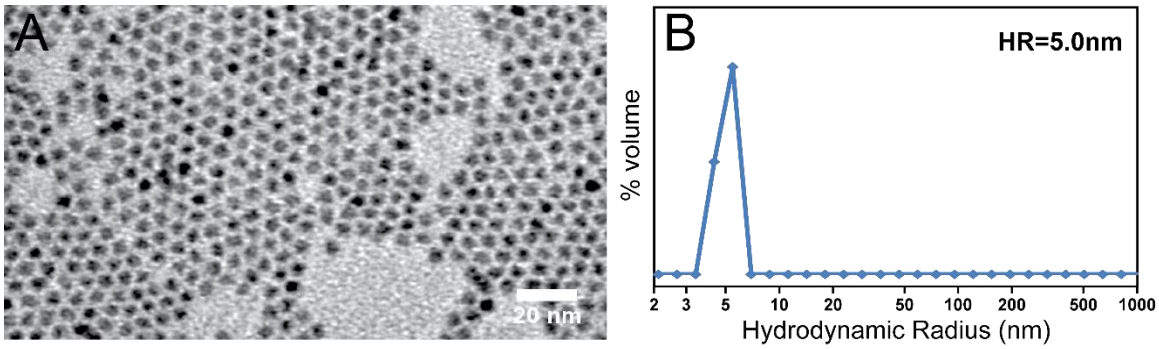

Figure 4.1 The TEM image (A) and DLS measurement (B) of GPC purified CdSe/CdZnS QDs.

After the QD purification by GPC, the ligand exchange reactions were done with four different molecular weight poly(PEGMA-co-imidazole) samples (11K, 18K, 30K, and 50K) by using a modification of the method published previously for acrylate based imidazoles. After the reactions, all of QDs in each sample could be well dispersed into pH = 7.4 buffer to form clear solutions that remained stable for more than 1 month when stored at 4 ℃. According to the absorption spectrum, there was no size change after the ligand exchange reaction. We further confirmed the monodispersity of the various polymeric imidazole ligand (PIL) coated aqueous QDs by TEM and DLS analysis. **Figure 4.2** shows the TEM of quantum dots drop-cast from aqueous solution, which revealed discrete

inorganic cores in all samples. In parts C and D, where the polymers involved higher number average molecular weight (Mn) and higher imidazole content (**Table 4.1**), the quantum dots displayed higher interparticle separation and decreased abundance of aggregated structures compared to those seen in parts A and B. DLS analysis showed lower hydrodynamic radii in parts A and B (8−8.6 nm), indicating that the quantum dots diffuse as discrete particles in solution. We note that the higher interparticle distance and higher hydrodynamic radii in parts C and D (15.2−17 nm) indicate a prominent role of the chain length and imidazole content in determining dispersion (**Figure 4.3**). The polymer compositions were calculated via NMR, and the repeat units of imidazole ranged from 32 to 134. The 11K and 18K polymers utilized a 550 g/mol PEG side chain, while the 30K and 50K incorporated a 950 g/mol side chain. The 30K and 50K polymers both have

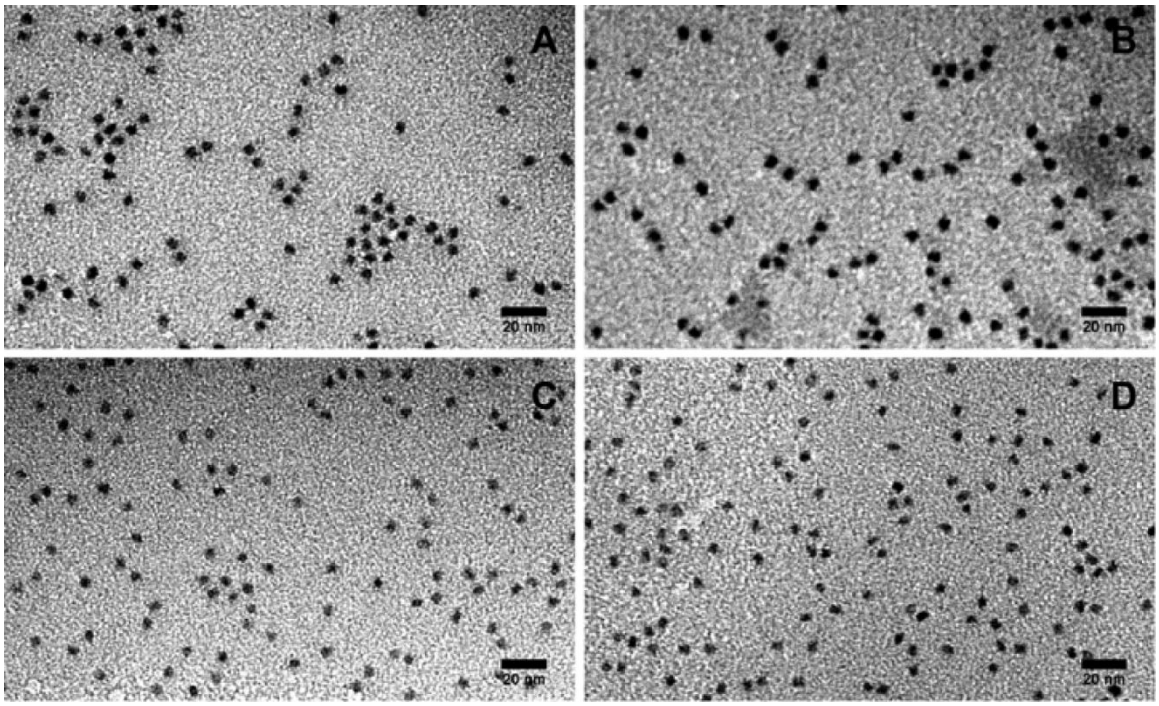

Figure 4.2 TEM images of aqueous CdSe/CdZnS QDs with different molecular weight polymeric imidazole capping ligands with molecular weight (Mn) A: 11K MW; B: 18K MW; C: 30K MW; D: 50K MW (scale bar = 20 nm). Copyright 2014 American Chemical Society.

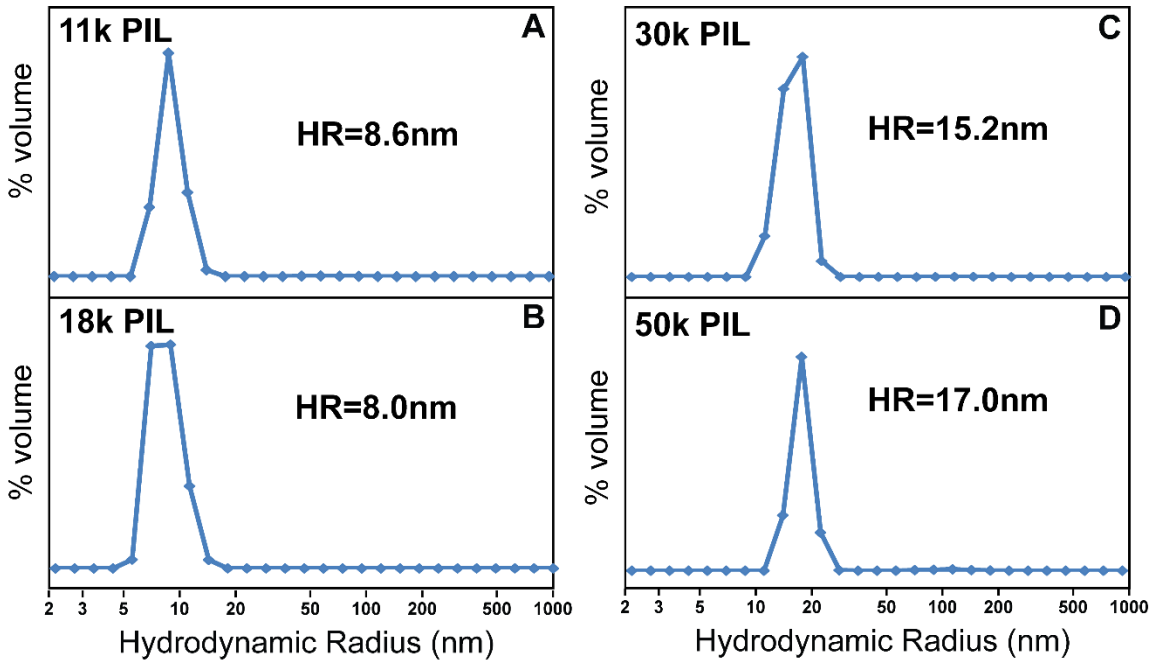

Figure 4.3 The DLS measurement of aqueous CdSe/CdZnS QDs with different molecular weight polymeric imidazole capping ligands. A: 12k MW; B: 18k MW; C: 30k MW; D: 50k MW.

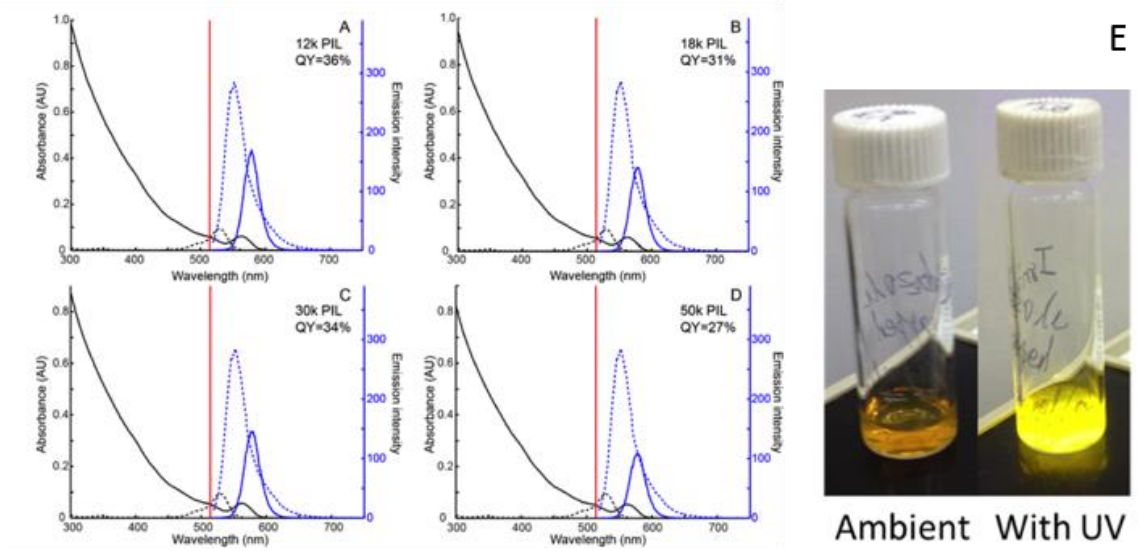

Figure 4.4 Quantum yield measurements of different molecular weight polymeric imidazole ligand capped QDs. A: 11K MW; B: 18K MW; C: 30K MW; D: 50K MW. The excitation wavelengths used for each measurement are marked by the red line. Absorption spectra (black) and emission spectra (blue) of QDs are shown as solid lines, while dashed lines indicate rhodamine 590 in ethanol. Figure E shows comparison of photographs displaying the fluorescent properties of the quantum dots in an aqueous medium in the presence of ambient light and UV light. Copyright 2014 American Chemical Society.

significantly higher loadings of the imidazole (104 and 134 as compared to 32 and 44 for the 11K and 18K, respectively) and may be helpful in obtaining superior dispersions. The improvement of the dispersion as the molecular weight and binding group content increases is congruent with the earlier work on functionalized polymers on various nanomaterials[174–176]. The brightness of the QDs was also maintained after the ligand exchange reaction. As shown in **Figure 4.4**, the QY of these four samples was around 30% (compared to a QY of 81% after synthesis and 56% after purification), which is suitable for applications of water-soluble QDs as fluorophores and as energy-transfer donors.

4.2.4 Toxicity and nonspecific binding test of the PIL capped QDs

Before using the PIL-capped QDs in any biological sensing or imaging, the toxicity and nonspecific binding of the particles need to be characterized. The biological tests described here were done in collaboration with Colin Johnson from the Chemistry Department and Kayla Pate from Department of Chemical Engineering at USC.

We implemented two fluorescence-based assays to evaluate the biocompatibility of MA-PIL coated QDs under conditions that are typical of a cell-surface labeling experiment. The model QDs we used here were CdSe/CdZnS QDs (shell thickness: 9 monolayers) and the PILs were prepared the same way as described in Chapter 4.2.2. The fluorescence-based assays were executed on a plate reader platform, permitting multiple replicates of each data point and potential scalability to a large number of polymer formulations to facilitate screening and optimization of putative biocompatible QDs. Since a common delivery method of QDs is via intravascular injection, such that the QDs come in contact with human umbilical vein endothelial cells (HUVEC), these have been utilized in a host

of previous studies to assess QD toxicity[177–179]. In order to quantify the degree of cytotoxicity that the MA-PIL QDs elicited in HUVECs, a Calcein AM cell viability assay was utilized. The Calcein AM probe becomes fluorescent upon hydrolysis by esterases found in viable cells. Thus, cell viability can be assessed by the intensity of the fluorescence in the wells using a plate reader. **Figure 4.5** shows the fluorescence signal from wells containing monolayers treated with QDs coated with varying molecular weight MA-PILs (10K, 22K, 34K); fluorescence is normalized to the signal from wells with equivalent DI water (vehicle control). None of the cells treated with 100 nM QDs demonstrate a significant difference from vehicle after 24 h exposure. In addition, results were compared to a positive control in the form of a solution of 0.025 mM cadmium acetate. In soluble forms, cadmium is a highly cytotoxic and carcinogenic element; its presence in many varieties of nanocrystal QDs has been a source of concern in biological applications. Indeed, we observed significant toxicity for low micromolar concentrations of aqueous cadmium ion. In contrast, the total cadmium concentration in the QD samples is 0.68 mM based on the number of Cd atoms per QD; the absence of toxicity by QDs suggests that Cd remains effectively sequestered in the QDs throughout the timescale of the experiment. We note that as free polymers, PEG-MA derivatives have been shown previously to exhibit very low cytotoxicity, comparable to or better than linear PEGs.[180]

To assess the propensity of the MA-PIL QDs to bind nonspecifically, the samples were introduced at a relatively high concentration (200 nM) to HUVECs in a medium containing 1% FBS and, following 5 min incubation, were decanted and rinsed so that any QDs that remained nonspecifically bound could be detected by virtue of their intrinsic fluorescence (**Figure 4.6A**). In order to focus on nonspecific adsorption and avoid

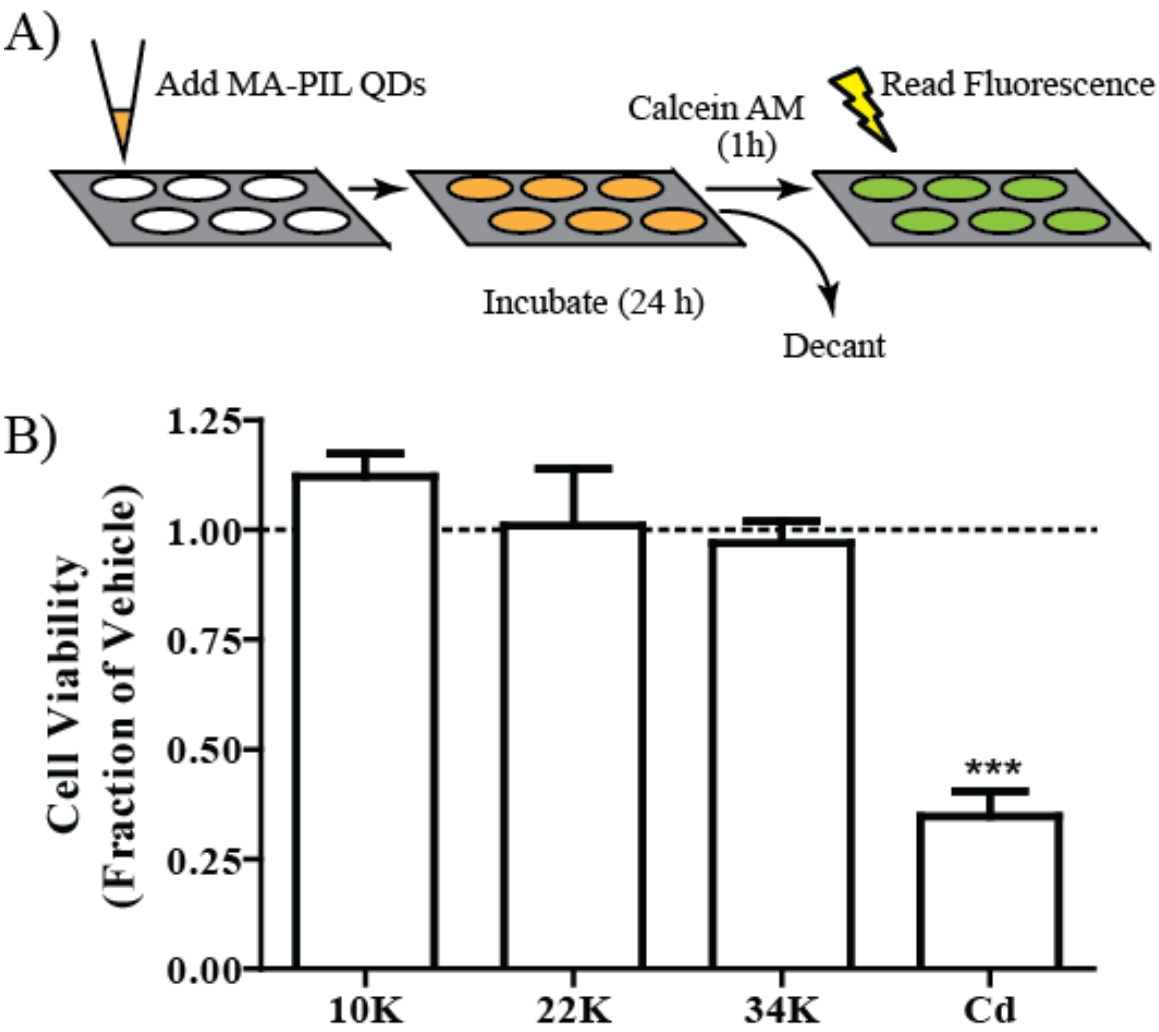

Figure 4.5 Effect of MA-PIL QDs on cell viability. A, HUVEC monolayers were incubated for 24 h (37°C) with 100 nM QDs coated with MA-PIL ligands exhibiting molecular weights of 10K, 22K, or 34K or with 25 μM cadmium acetate (Cd, positive control). Cell viability was then assessed using Calcein AM. B, Cell viability is reported as the experimental Calcein AM fluorescence normalized to the Calcein AM fluorescence observed for cells treated with vehicle only. Dashed line represents average cell viability of the vehicle. Error bars indicate SEM, n=3. ***p<0.001 vs. vehicle. Copyright 2015 Elsevier.

complications introduced by uptake via endocytosis, the incubation was conducted at low temperatures where endocytosis is less active. After three washes with PBS, the cells (treated with QDs with each coating, in triplicate) were analyzed via a plate reader to detect

fluorescence at the QD emission channel. Any QDs remaining after the washes, for example as a result of nonspecific binding to cell surfaces or the culture substrate, would result in a contribution to the fluorescence that is absent in the wells exposed to vehicle only. **Figure 4.6 B** shows the plate reader results for each of the three MA-PIL QD samples. A fluorescence reading was also taken prior to washing, as an internal control for variation in the brightness of the QD samples. The results are expressed as a fraction of the vehicle. No significant increase in residual fluorescence was observed compared to vehicle (both

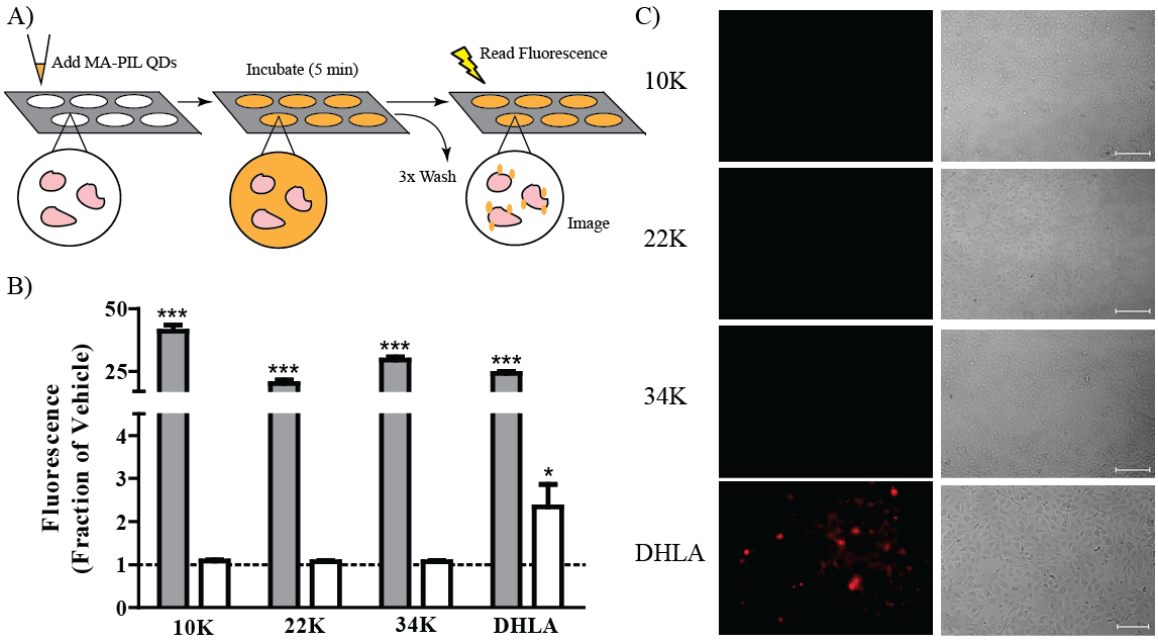

Figure 4.6 Nonspecific binding of MA-PIL QDs to HUVEC monolayers. (A) HUVECs were incubated for 5 min at 4 C with 200 nM QDs coated with MA-PIL ligands or with 200 nM QDs coated with DHLA ligands (positive control). The presence of MA-PIL QDs was quantified via self-fluorescence (panel B) and also visualized using fluorescence microscopy (panel C, left column). Fluorescence quantification was performed both before (grey bars) and following (white bars) three washes, with the latter representative of nonspecifically bound QDs. Phase contrast images (panel C, right column) were acquired to verify intact cell monolayers. Fluorescence was normalized to that observed for monolayers treated with a DI water equivalent (vehicle). Dashed line represents the normalized, average fluorescence observed for the vehicle. Error bars indicate SEM, n = 3–4. Some error bars lie within symbols. *$p < 0.05$ and ***$p < 0.001$ vs. vehicle. Images are representative of 3–4 independent experiments; scale bars represent 200 μm. Copyright 2015 Elsevier.

sample and vehicle values include a similarly small but non-zero contribution from autofluorescence and background).

The plate reader measurement provides a scalable, ensemble measurement of nonspecific binding that is immune to sampling bias that could be encountered in methods relying solely on fluorescence microscopy. As a positive control to confirm the ability of the method to detect nonspecific binding, we tested QDs coated with DHLA ligands. The carboxylate on DHLA is deprotonated at neutral pH, providing anionically stabilized QDs with a strongly negative zeta potential; DHLA-coated QDs have previously been observed to exhibit strong nonspecific binding to human cells.[38] Here, we confirm this observation with significant residual fluorescence detected at more than twice the vehicle.

4.2.5 Conclusion

In this work, we presented a facile copolymerization and post-modification method to prepare multidentate histamine copolymers which were shown to act as excellent ligands for CdSe/CdZnS QDs in aqueous solutions. The ligand exchange reactions were demonstrated using quantum dot starting materials with well-defined metrics including the type and average number of initial ligands as achieved by gel permeation chromatography. From the ligand exchange results and bio-compatible study, we did not observe any significant difference in QDs' performance over the range of polymer molecular weight. This result will be a valuable point of reference for further optimization of biocompatible QDs, including those introducing specific targeting functions through introduction of bio-affinity groups or bio-orthogonal linking chemistries.

4.2.6 Materials

The following chemicals were used as received from Fisher Scientific unless stated otherwise below. Cadmium oxide (CdO; 99.999%), Zinc oxide (ZnO; 99.999%), Trioctylphosphine (TOP; 97%) and Trioctylphosphine oxide (TOPO; 99%) were purchased from STREM Chemicals. Oleic Acid (99%), 1- Octadecene (ODE; 90% technical grade), 1-Tetradecylphosphonic Acid (TDPA; 98%), Selenium (Se; 99.999%) were purchased from Alfa Aesar. Bio-Beads S-X1 GPC medium was obtained from Bio-Rad Laboratories, Inc. Chloroform (D, 99.8%) was obtained from Cambridge Isotope Laboratories, Inc. Decylamine (95%) was purchased from Sigma Aldrich. Oleylamine (80-90%) and Bis(trimethylsilyl) sulfide ($(TMS)_2S$; 95%) were purchased from Acros Organics. Rhodamine Chloride 590 (R590, MW 464.98) was obtained from Exciton. Toluene (99.5% ACS analysis grade) was purchased from Mallinckrodt Chemicals. 200 Proof Ethyl Alcohol (Ethanol) was obtained from Decon Laboratories, Inc. Acetone (99.9%) was purchased from VWR. AIBN was purchased from Sigma-Aldrich and recrystallized thrice from methanol. Poly(ethylene glycol) methacrylate (500 and 950 g/mol) were obtained from Sigma-Aldrich and passed through a neutral alumina column to remove inhibitors before use.

4-Cyano-4- [(dodecylsulfanylthiocarbonyl)sulfanyl]pentanoic acid was obtained from Strem Chemicals, Inc. All media components were from Sigma Aldrich. 96 well plates with clear plastic bottoms and black walls were obtained from VWR. Calcein AM was obtained from Invitrogen.Synthetic or analytical procedures either under nitrogen (N2) or vacuum environment were carried out using Schlenk line techniques, or a glovebox.

Synthesis of CdSe/CdZnS QDs. The CdSe core was prepared by hot-injection method as described previously. CdZnS shell was coated by selective ionic layer adhesion and reaction (SILAR) approach. A portion of as-synthesized CdSe core was diluted with hexane and flocculated by methanol and acetone. After decanting the supernatant, the QDs were redissolved into hexane and held at 4 ℃ for more than 12 hours. All the undissolved materials were removed by centrifugation and the sample was precipitated again by an addition of methanol and acetone. Afterward, the QDs were brought into a measured volume of hexane. The UV-Vis absorption spectrum was recorded at a known dilution of the sample to determine the size and quantity of QDs.

The solution of QDs in hexane was transferred to a solvent of 1:2 oleylamine:ODE (v/v, 9mL total) and degassed at 100 ℃ to remove hexane. Before the addition of the reagent via syringe pump, the system was heated to 190 ℃ under nitrogen. The metal precursor is prepared by diluting 0.2M $Cd(oleate)_2$ in ODE and 0.2M $Zn(oleate)_2$ in ODE (ratio of Cd:Zn is 1:1) with 2 equivalents of decylamine and a volume of TOP to yield a metal concentration of 0.1M. The S precursor was a 0.1M solution of $(TMS)_2S$ in TOP. The volume increase associated with 1 monolayer coverage of $Cd_xZn_{1-x}S$ is calculated based on the radius increase of 3.37Å, which is half of the wurtzite *c*-axis unit cell dimensions for CdS. Alternating injections of metal precursor and sulfur precursor were performed, adding the metal precursor solution first, with injections starting every 15 minutes. The flow rate was adjusted to complete each injection over the course of 3 minutes. The volume of each injection was calculated to apply one monolayer coverage each cycle (a cycle is defined as one metal precursor injection and one sulfur precursor injection). The growth process is monitored by the absorption and emission spectra. After

the reaction, the mixture was cooled down to the room temperature and the molar extinction coefficient was estimated based on the amount of the core introduced at the beginning and the total volume of the solution after the synthesis.

PIL ligand exchange reaction for CdSe/CdZnS QDs. The ligand exchange reaction was performed by a modification of a published method.[2] Approximately 3 nmol purified QDs samples were pumped dry to remove toluene and brought to 0.3 mL chloroform/PIL solution (the molar ratio of PIL to QD is ranging from 150 to 200). The single phase mixture was stirred vigorously at room temperature for 30 min, after which methanol was introduced followed by stirring for additional 20 min (the amount of methanol is equal to 30% of the total volume of the chloroform). The QDs were precipitated once by addition of ethanol/hexane, redissolved in pH=7.4 aqueous phosphate buffer solution, filtered by polyethersulfone membrane (pore size: 0.2 μm), and then dialyzed by a centrifugal tube with 50000 nominal molecular weight cutoff (MWCO) membrane for further analysis.

Optical Spectroscopy. The formation of CdSe QDs and CdZnS shell on the surface was monitored by the absorption spectrum from UV-Vis spectroscopy. The optical absorption spectrum was recorded using a Thermo Scientific Evolution Array UV-Visible Spectrophotometer with toluene as the solvent as well as the blank in a 1cm path quartz cuvette. The fluorescence spectra were also used to monitor the growth and size distribution of the QDs. Emission spectra were recorded by an Ocean Optics USB 4000 spectrometer under ~365 nm excitation.

NMR Analysis of QDs. NMR samples of the QDs were prepared in $CHCl_3$-d. The ^1H NMR spectra were recorded on a Varian Mercury/VX 400 NMR with ferrocene as the internal standard. The relaxation delay used is 30s and the acquisition time is 3s, allowing the system to reach a reliable equilibrium.

Quantum Yield Measurement. The quantum yield (QY) of the CdSe/$Cd_xZn_{1-x}S$ QD samples was measured relative to rhodamine 590 (R590, QY=99% in ethanol). The excitation wavelength was chosen at 514nm. Fluorescence spectra of QD and R590 dye were taken under identical spectrometer conditions on Varian fluorescence spectrometer in triplicate and averaged. The optical density was kept below 0.1 between 500 and 800nm to avoid internal filtering effects. The QY was calculated based on the integrated intensities of the emission spectra, the absorption at the excitation wavelength and the refraction index of the solvent using the equation:

$$QY_{QDs} = QY_{dye} * \frac{Absorbance_{dye}}{Absorbance_{QDs}} * \frac{Emission\ integral_{QDs}}{Emission\ integral_{dye}} * \frac{Refraction\ index^2_{toluene}}{Refraction\ index^2_{ethanol}}$$

The precision of this measurement in our case is limited by the precision of the absorbance measurement (~1%) while the accuracy among samples in different solvents will be limited by the accuracy of the refractive index correction term.

Transmission electron microscopy. After purification, the original ligand capped and PIL capped CdSe/$Cd_xZn_{1-x}S$ QD samples were brought into toluene or water to form a dilute solution (0.15 μM). One drop of the solution (~20 μL) was drop-casted on a clean TEM grid (400 mesh Ni grid with ultrathin carbon support film, Type-A, Ted Pella, Inc.). After allowing the sample to deposit on the grid for 30 min, the excess solution has been winkled away with a tissue. The grids then have been pumped dry under vacuum for

2 hours. The samples were imaged by Hitachi H8000 scanning transmission electron microscope.

Dynamic light scattering measurement. The hydrodynamic radius of the purified QD samples were measured via dynamic light scattering (DLS) using a DynaPro-MSX instrument with 690nm laser wavelength (Wyatt Technology Corporation, Santa Barbara, CA). The sample was exposed to an appropriate laser intensity to determine the size and sized distribution of particles.

Cell Culture and Preparation. Human umbilical vein endothelial cells (HUVECs) (American Type Culture Collection) were maintained in Ham's F12K medium supplemented with 10% fetal bovine serum (FBS), 0.1 mg/mL heparin, 30 μg/mL endothelial cell growth supplement, 100 units/mL penicillin, and 100 μg/mL streptomycin. Prior to experimentation, HUVECs were seeded at a density of $5x10^4$ cells/well onto black-sided 96-well tissue culture plates and maintained for 24 h in supplemented Ham's F12K medium with 1% FBS to allow formation of confluent monolayers. All cultures were maintained at 37 ℃ in a humid atmosphere of 5% CO_2 and 95% air.

Calcein AM Cell Viability Assay. To characterize the potential toxicity of MA-PIL QDs, Calcein AM was used to assess cell viability following exposure to QDs. Confluent HUVEC monolayers were incubated (37 ℃, 5% CO_2) with QDs coated with MA-PILs exhibiting effective molecular weights of 10K, 22K, or 34K. QD solutions were prepared by adding small aliquots of MA-PIL QD solutions in DI water to supplemented medium containing 1% FBS to achieve an ultimate concentration of 100 nM QDs. Monolayers incubated with equivalent dilution of DI water or with 25 μM cadmium acetate

served as the vehicle and positive controls, respectively. Following 24 h incubation, treatments were decanted and replaced with 1 μM Calcein AM diluted in phenol red-free, serum-free media. When taken up by living cells, the non-fluorescent Calcein AM probe is hydrolyzed by endogenous esterases to yield fluorescent acetoxymethyl ester, thereby allowing for a quantifiable measurement of cell viability. After 1 h incubation (37 ℃, 5% CO_2), fluorescence was measured using a BioTek Synergy 2 multi-mode microplate reader equipped with excitation and emission filters of 485 ±20 nm and 530 ±25 nm, respectively, and using baseline (media containing Calcein AM) subtraction. Cell viability is reported as Calcein AM fluorescence normalized to the fluorescence observed for the vehicle. Each treatment was performed in triplicate, and results shown are the mean ± SEM of three independent experiments.

Nonspecific Binding Assay. To evaluate nonspecific interactions between MA-PIL QDs and cells, a static adhesion assay was implemented. Confluent HUVEC monolayers were incubated for 5 min with MA-PIL QDs exhibiting molecular weights of 10K, 22K, or 34K. QD solutions were prepared by adding small aliquots of MA-PIL QD solutions in DI water to supplemented medium containing 1% FBS to achieve an ultimate concentration of 200 nM. Incubations were performed at 4 ℃ to induce a state of cellular stasis, thereby preventing the endocytosis of MA-PIL QDs. Monolayers incubated with equivalent dilution of DI water or 200 nM of QDs coated with dihydrolipoic acid (DHLA) served as vehicle and positive control for nonspecific binding, respectively. Immediately following incubation, fluorescence was measured to serve as an internal positive control for each QD's self-fluorescence. Cells were then washed three times using PBS, pH 7.4, and fluorescence was measured again to evaluate nonspecific binding. Fluorescence was

measured using a BioTek Synergy 2 multi-mode microplate reader equipped with excitation and emission filters of 530 ±25 nm and 590 ±35 nm, respectively. Fluorescence measurements were normalized to the fluorescence observed for the vehicle. Each experiment was performed with three or four replicates, and results are shown as the mean ± SEM of these independent experiments. To corroborate fluorescence results and assess sensitivity, monolayers were additionally imaged using a Nikon Eclipse Ti-E inverted microscope equipped with a 20X objective lens. Bright field and TRITC laser (excitation = 555 ±10 nm; emission = 600 ±20 nm) images were acquired for each sample. Images shown are representative of three to four independent experiments.

4.3 Surface labeling of enveloped virus with polymeric imidazole ligand-capped quantum dots via metabolic incorporation of phospholipid in host cells

4.3.1 Introduction

As mentioned in Chapter 1, in order to use QDs for selective labeling in bio-imaging applications, the linker needs to have at least three different functional groups: one group to stabilized QDs in water; one group providing binding ability with the QDs surfaces; and the last group for attachment onto the biological target. As shown in the previous part of this chapter, PIL capped QDs have shown good dispersity in water, high quantum yield (QY), and low toxicity and non-specific binding to the cells. Those characteristics make PIL-QDs an attractive candidate for labeling. However, the previously established PEG-imidazole bi-polymer is lacking one group for biological targeting attachment. Therefore, a ternary copolymer version of the MA-PILs, which incorporates PEG side chains for steric

stabilization in water, imidazole anchoring groups, as well as primary amines that are available for further modification, has been prepared.[181]

The target virus we selected is measles virus (MV). Measles virus (MV) is a member of the morbillivirus subgroup of paramyxoviruses, containing glycosylated envelope proteins hemagglutinin (H) and fusion (F) that are embedded on the phospholipid bilayer envelope.[182] Live attenuated MV has been shown to possess promising oncolytic activity against many tumor cells,[183] which enables the possibility of virotherapy for cancer treatment.[184] For the sake of virotherapy, it is urgent to develop labeling strategies to site-specifically modify the virus surface with functional handles such as a folate and folate receptor-specific antibody, which can achieve targeting to tumor cells while avoiding normal cells.[185] The surface modification of enveloped virus in literature has focused on both surface proteins and on the phospholipid envelope. The covalent linkage of functionalities to surface proteins that is achieved by chemical modification[186], genetic engineering[187] and metabolic incorporation of azido sugars,[188,189] likely affects the normal properties of viruses including their interaction with host cells. Since the virus envelope is derived from a host cell membrane,[190] the metabolic incorporation of phospholipids that carry functional groups into the host cell membrane has enabled the subsequent modification of virus envelopes during virus replication and assembly[191].

Until now, little work has been done using QDs to label enveloped virus. Wang's group and Pang's group have utilized the streptavidin-conjugated QDs to modify the vesicular stomatitis virus and influenza virus successfully for the study of the tracking of labeled virus into host cells.[192–194] Similarly, Cai's group has labeled the enveloped baculovirus with PIL-capped QDs through copper-free click chemistry and maintained

their infectivity.[41] Xie's group and Pang's group have also modified the vaccinia virus, influenza virus and vesicular stomatitis virus with QDs that were functionalized by direct modification of amine and carboxylic-acid functionalized QDs.[186,195,196] However, all of these works are using genetic or chemical modification of a surface protein to label the virus. Additionally, except for Cai's work, the studies all employed acyl transfer chemistry to install clickable handles on water soluble QDs with amine-bearing coatings. In such cases, the synthetic yield for functional group attachment may be limited due to competing interactions on the QD surface environment.

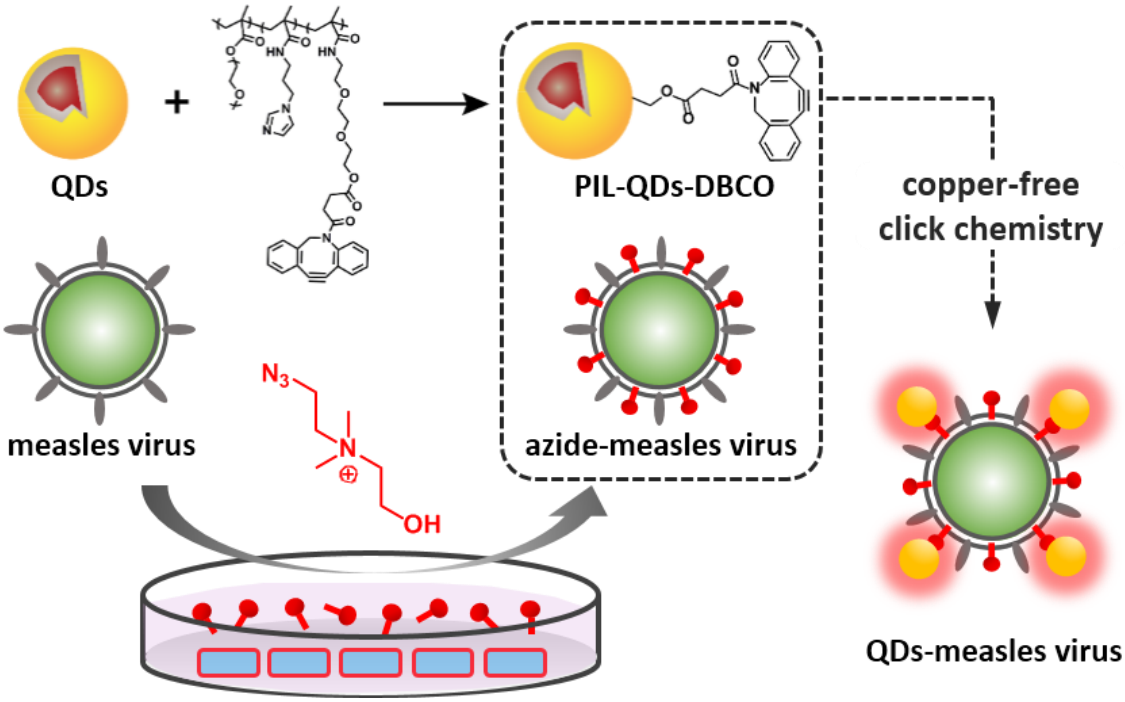

Figure 4.7 Schematic illustration of the synthesis of PIL-QDs-DBCO, the azide labeling of measles virus assisted by host cells and the strategy for labeling virus with QDs via copper-free click chemistry.

In this work, we labeled a live attenuated MV envelope with azido groups by metabolically incorporating an azide-bearing choline analogue AECho into the MV

phospholipid bilayer via host cells. Then the as-synthesized CdSe/CdZnS QDs were purified by gel permeation chromatography and subsequently exchanged with dibenzocyclooctyne (DBCO) functionalized MA-PILs.[197,198] The exchanged QDs (PIL-QDs-DBCO) were attached to the azide-labeled MV (N_3-MV) through a copper-free, strain-promoted azide-alkyne cycloaddition (SPAAC) reaction (**Figure 4.7**). The QD-labeled MV maintains its infectious ability against host Vero cells. We believe the present study demonstrates the feasibility of the metabolic labeling approach, and the viability and utility of a mild and reproducible method for membrane-enveloped virus labeling with QDs.

4.3.2 Fabrication and characterization of PIL-QDs-DBCO

The QDs were prepared by a selective ionic layer adhesion reaction (SILAR) method as described previously, and in total, 9 monolayers of CdZnS shell were grown to achieve the desired emission wavelength. The formation of the shell was monitored by the absorption and emission spectra of the aliquots taken during the growth (**Figure 4.8**). The ternary polymer version of the PILs was prepared as described previously. The as-synthesized polymer was purified and functionalized with DBCO though the active ester NMS group.

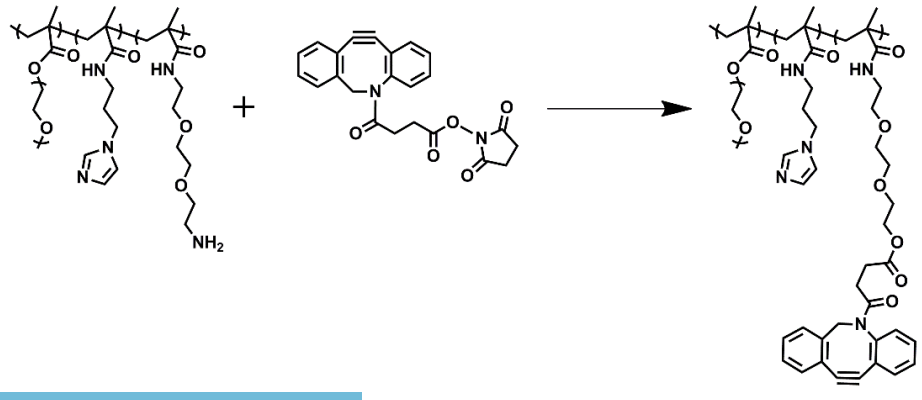

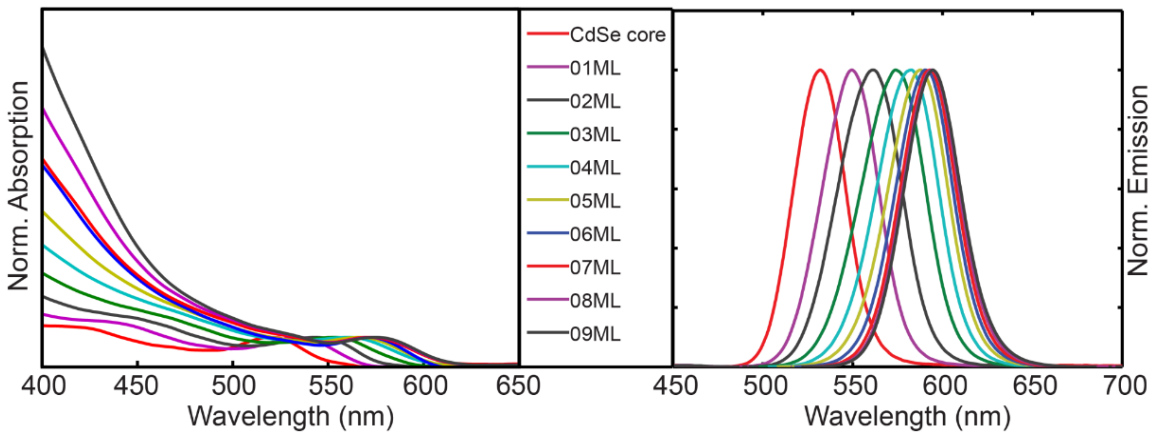

Figure 4.8 The absorption (left) and emission (right) spectra of aliquots taken during the overcoating processes of CdSe/CdZnS QD samples. Aliquots were taken after CdSe core purification at room temperature, prior to the shell synthesis at reaction temperature and after each injection of the SILAR process. The spectra were normalized to the position of the lowest energy extinction peak.

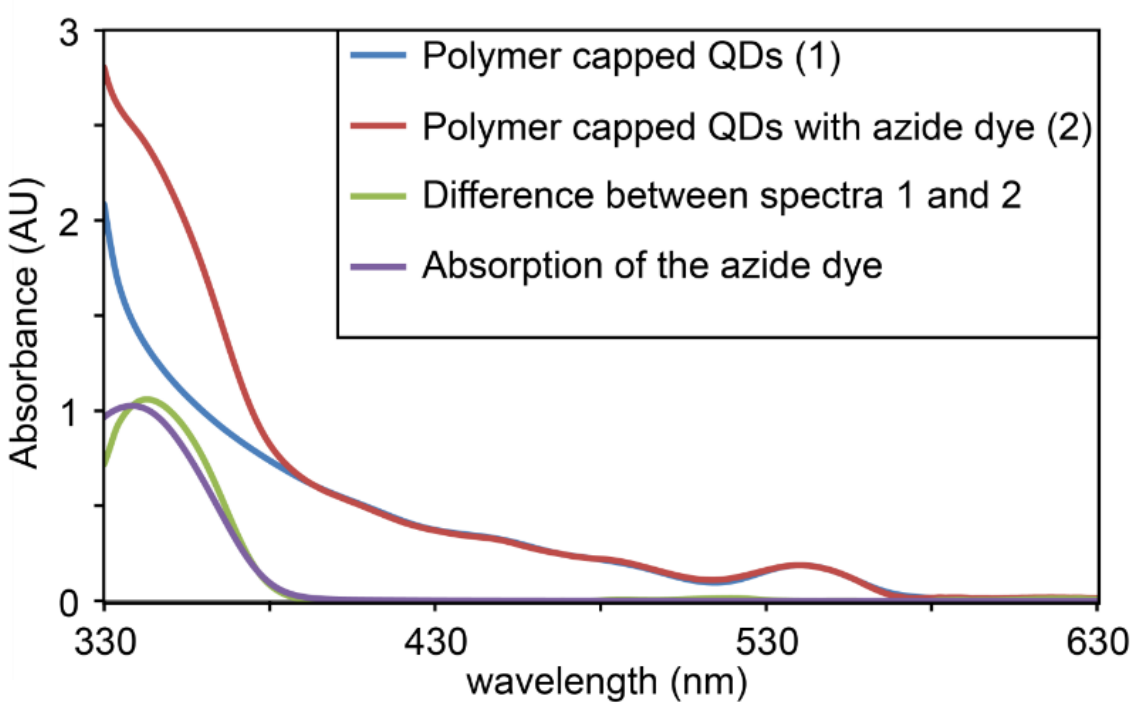

Figure 4.9 The DBCO group on PIL-QDs-DBCO detected by absorbance measurement using an azide dye.

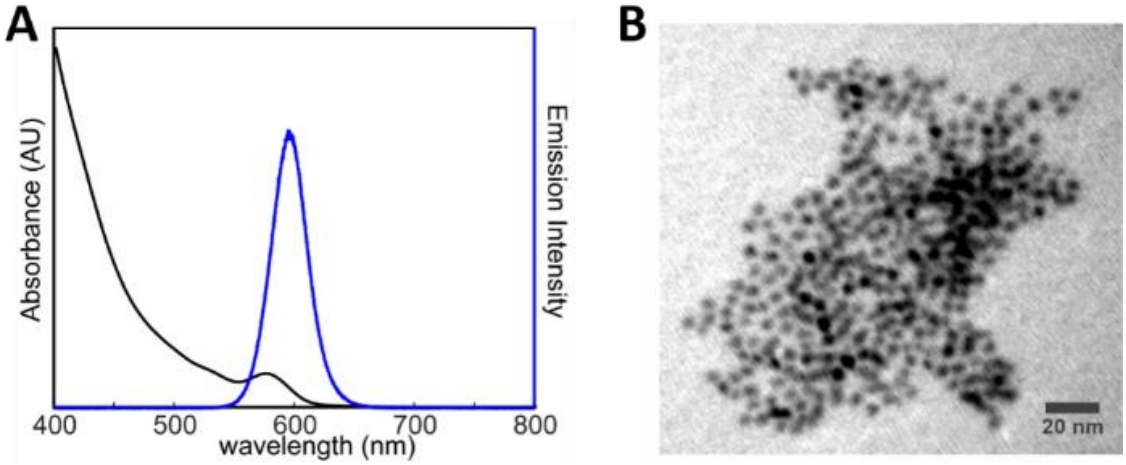

Figure 4.10 The absorbance (black) and emission (blue) spectra of PIL-QDs-DBCO in PBS. (B) TEM image of PIL-QDs-DBCO in aqueous solution. Scale bar indicates 20 nm.

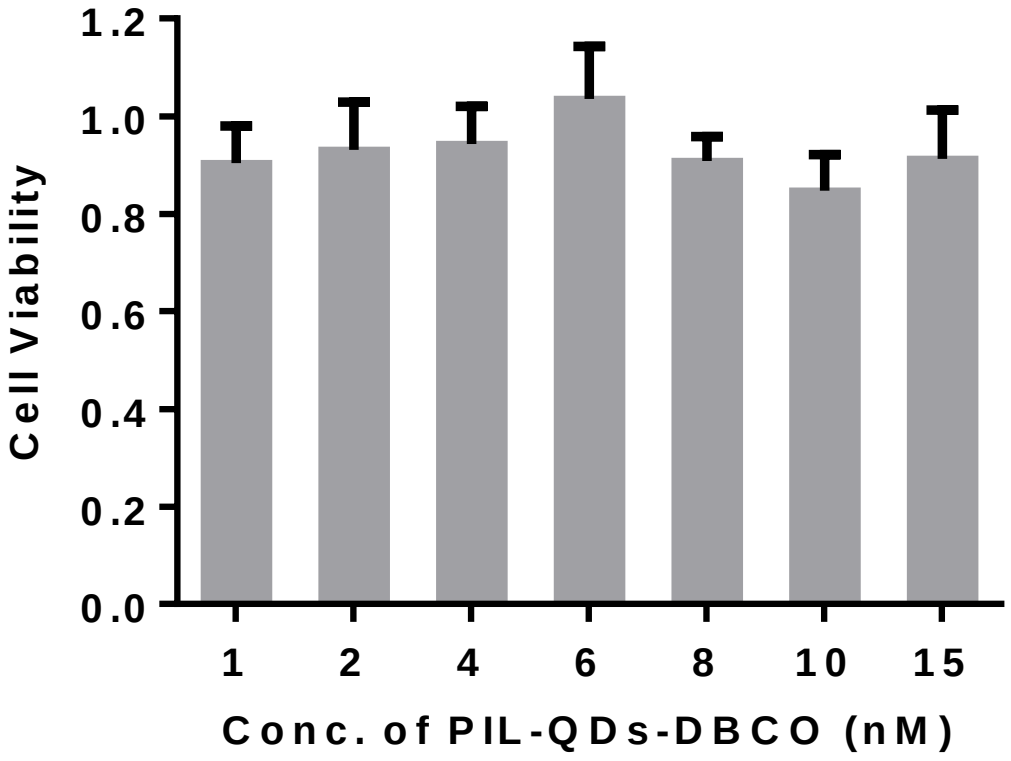

Figure 4.11 The Cell viability assay of PIL-QDs-DBCO at different concentrations.

The QDs were purified by GPC and then functionalized with the above DBCO-containing MA-PIL polymer. In order to confirm the ligand-exchanged QDs can be used to label the virus through SPAAC reaction, an azido dye was introduced to a separated PIL-QDs-DBCO solution. As shown in **Figure 4.9**, the absorption feature of the azido dye can be observed after a series of dialysis processes, which confirms that the DBCO group has been successfully attached onto the QDs and maintains its reactivity toward organic azides. According to the absorption spectrum and TEM image, the PIL-QDs-DBCO remained their monodispersity and narrow size distribution in PBS (pH=7.4) without any visible sign of aggregation (**Figure 4.10**). The sample remained stable for more than 6 months when stored in a 4 ℃ refrigerator, which maintained its quantum yield at 19% and hydrodynamic radius at around 17.3 nm with minimal aggregation based on DLS measurements. The toxicity of the PIL-QDs-DBCO was detected by cell viability assay, which indicated an absence of cytotoxicity to Vero cells (**Figure 4.11**).

4.3.3 Biolabeling of PIL-QDs-DBCO with Vero cells and measles virus

The choline analogue azidoethyl-choline (AECho) was synthesized following the reported procedure. Vero cells were used as host cells for MV propagation and were grown in complete Dulbecco's modified Eagle's medium (DMEM) supplemented with AECho at certain concentrations. After co-incubation with AECho for 48 h, the Vero cells were fixed and stained with PIL-QDs-DBCO via SPAAC reaction. The staining showed strong fluorescence signal of QDs on the cell membrane, demonstrating the successful incorporation of azido group into cell membrane (**Figure 4.12D**). Since we did not observe any nonspecific binding with the imidazole-PEG copolymer coated QDs, we believe that

the minute binding of PIL-QDs-DBCO on normal cells is due to the interaction between cell surface and DBCO/amine group, which does not influence the imaging results. The cell viability could be kept above 90% when incubated with AECho at 600 μM for 48 h, indicating its biocompatibility (**Figure 4.12A**).

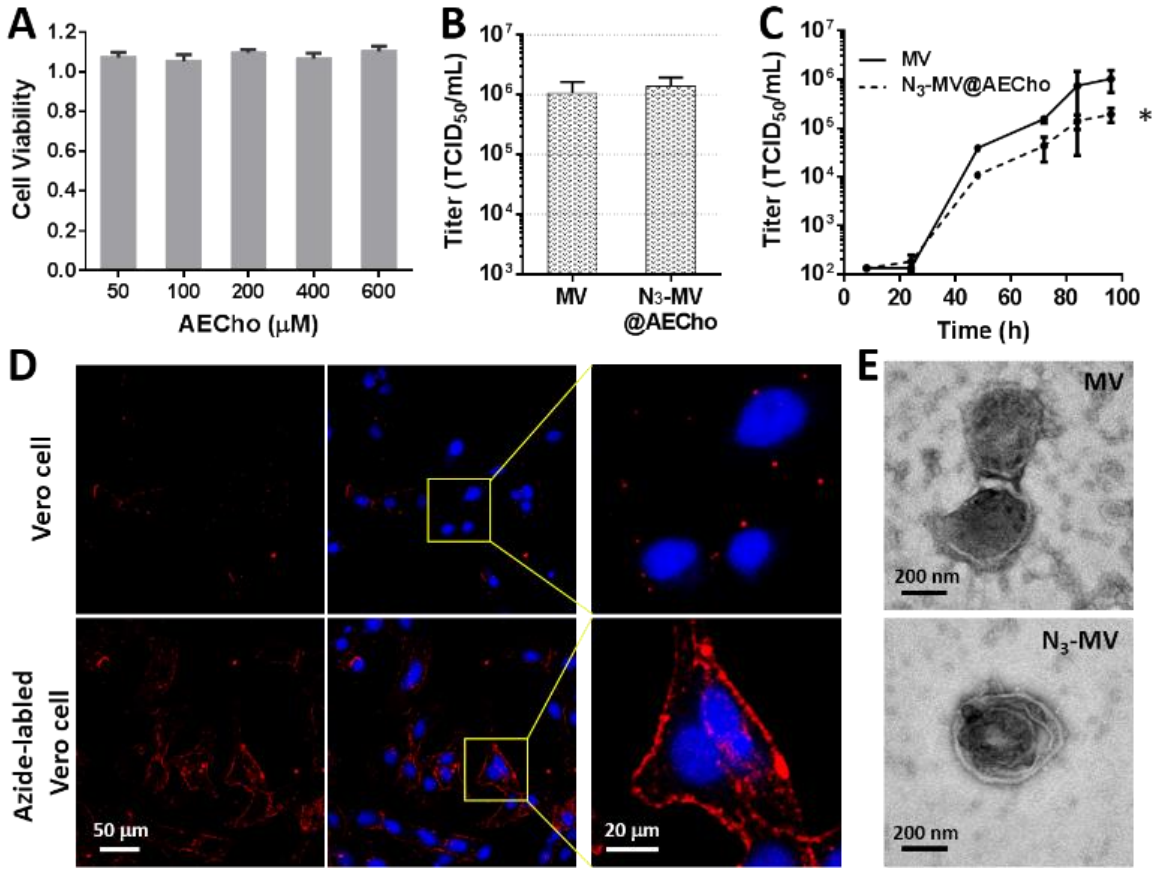

Figure 4.12 (A) CellTiter-Blue viability assay of Vero cells incubated with AECho at different concentrations for 24 h. (B) Production of control MV and N_3-MV. (C) One-step growth curves of control MV and N_3-MV. *p=0.14. (D) Fluorescence imaging of azide-labeled Vero cells stained with PIL-QDs-DBCO (red) and DAPI (blue). Scale bars indicate 0.05mm of regular views and 0.02mm of enlarged views. (E) TEM images of control MV (top) and N_3-MV (bottom). Scale bars indicate 200 nm.

To achieve azide labeling of the MV envelope, viruses were propagated on azide-labeled Vero cells incubated with 400 μM AECho. The progeny viruses that are grown in

AECho-treated Vero cells should be propagated with azido groups incorporated into their envelope upon release from their host cells, producing the azide-labeled MV (N_3-MV). The N_3-MV were purified from the cell culture medium on 20%-60% sucrose gradient.[199] To evaluate the production of N_3-MV, 50% tissue culture infective dose ($TCID_{50}$) of viruses were detected based on the Reed-Muench formula. The data showed that control MV and N_3-MV were at a comparable titer that around 10^6 $TCID_{50}$ mL^{-1}, suggesting metabolic labeling did not affect the propagation of MV in host Vero cells (**Figure 4.12B**). The infectivity of N_3-MV was evaluated by one-step growth kinetics.[200] As shown in **Figure 4.12C**, the N_3-MV could reach 2×10^5 $TCID_{50}$ mL^{-1} at 96 h post-infection, which did not indicate a statistically significant difference from that of control MV. In addition, the N_3-MV retained the intact structure of the control virus (**Figure 4.12E**). These results suggested that the azide labeling via metabolic incorporation of choline analogue AECho did not disturb virus production or infectivity.

A co-localization assay was performed to evaluate whether the N_3-MV could indeed be functionalized via the SPAAC reaction. The viruses were overlaid on coverslips for 60 min at 37 ℃, then fixed, permeabilized, and stained with both DBCO-Fluor 488 for azido group and propidium iodide (PI) for nucleic acid. The fluorescence imaging results showed that most of the fluorescence signal of PI co-localized with that of Fluor 488 for N_3-MV, appearing as yellow in a merged image. In contrast, there was no Fluor 488 signal observed for the control MV. (**Figure 4.13A**).Therefore, it was further verified that virus produced from azide-labeled Vero cells had azido group incorporated into virus surface, which was available for further chemical modification with DBCO derived functionalities through SPAAC reaction.

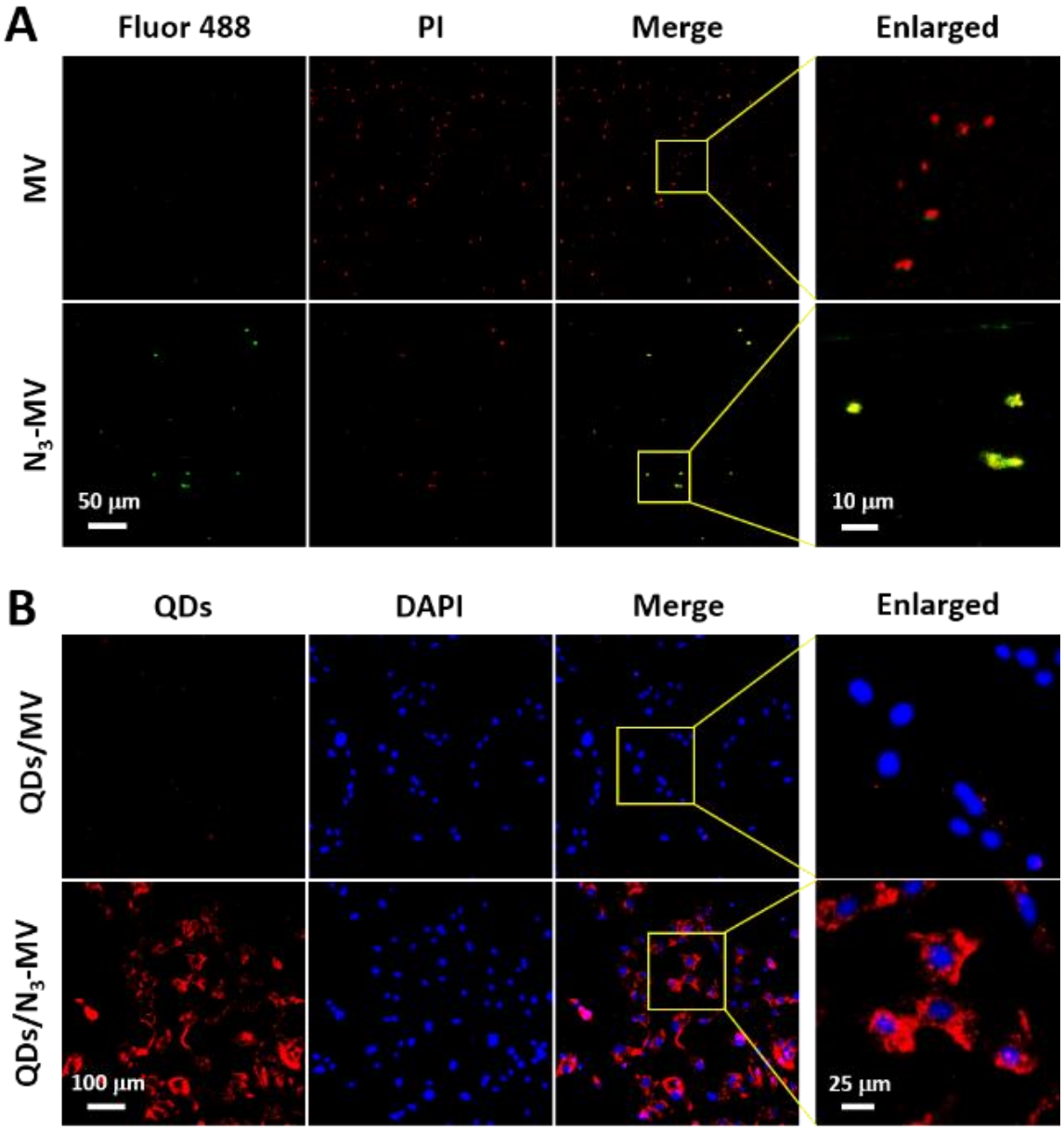

Figure 4.13 (A) Fluorescence imaging of control MV and N_3-MV stained with DBCO-Fluor 488 (green) and propidium iodide (red). Scale bars indicate 0.05mm of regular views and 0.01mm of enlarged views. (B) Fluorescence imaging of Vero cells co-incubated with QDs-labeled MV (red, QDs; blue, DAPI labeled cell nucleic acid). Scale bars indicate 0.1mm of regular views and 0.025mm of enlarged views.

We further labeled the azide modified virus with PIL-QDs-DBCO, followed by co-incubating with a new set of Vero host cells. The fluorescence imaging showed a

remarkably prominent signal of QDs on the cell membrane, indicating that QDs-labeled MV could interact with Vero cells. Conversely, there was no signal of QDs when the cells were co-incubated with a mixture of control MV and PIL-QDs-DBCO, suggesting that no obvious nonspecific adsorption of the PIL-QDs-DBCO on the cell surface occurs (**Figure 4.13B**). The interaction between the QDs-labeled MV and Vero cells demonstrates that the covalent attachment of QDs onto N_3-MV did not compromise the infectious ability of the virus against host cells.

4.3.4 Conclusion

We have proposed a mild and reproducible method to prepare QD-labeled viruses. We demonstrated that enveloped MV could be metabolically labeled with a choline analogue AECho assisted by host cells. The azide incorporation into viral surface did not affect production and activity of progeny N_3-MV. The QDs can be functionalized with DBCO-bearing methacrylate-based polymeric imidazole ligand, and subsequently maintain brightness and colloidal stability for more than 6 months. The QDs and virus can be linked together through SPAAC reaction without the addition of a copper catalyst, and the infectious ability of virus does not change. The remarkable ease of this metabolic labeling approach makes it accessible to other membrane-enveloped viruses, and the MA-PIL capped QDs have also been proven to be a reliable bio-imaging probe. It is envisaged that this labeling strategy will greatly facilitate the development of new anticancer agents that can retarget oncolytic viruses specific to cancer cells for cancer virotherapy.

4.3.5 Materials

Cadmium oxide (CdO; 99.999%), zinc oxide (ZnO; 99.999%), trioctylphosphine (TOP; 97%) and trioctylphosphine oxide (TOPO; 99%) were purchased from STREM Chemicals. Oleic acid (99%), 1- octadecene (ODE; 90% technical grade), and selenium (Se; 99.999%) were purchased from Alfa Aesar. Bio-Beads S-X1 GPC medium was obtained from BioRad Laboratories. Oleylamine (80-90%) and Bis(trimethylsilyl) sulfide ($(TMS)_2S$; 95%) were purchased from Acros Organics. Rhodamine chloride 640 (R640) was obtained from Exciton. Toluene (99.5% ACS analysis grade) was purchased from Mallinckrodt Chemicals. AIBN was purchased from Sigma Aldrich and recrystallized thrice from methanol. Poly(ethyleneglycol) methacrylate (500 g mol^{-1}) was obtained from Sigma Aldrich and passed through a neutral alumina column to remove inhibitors before use. Measles virus (MV) and Vero cells were obtained from the U.S. Centers for Disease Control and Prevention (CDC). DBCO-NHS ester and DBCO-Fluor 488 were purchased from Click Chemistry Tools. All the other chemicals were purchased from Fisher and used as received. Procedures under nitrogen (N_2) or vacuum environment were carried out using Schlenk line techniques or a glovebox.

Transmission electron microscopy (TEM) imaging, DLS measurements and QY characterizations were done in the same way as described in **Chapter 4.2**. CellTiter-Blue cell viability assays were measured with Tecan Infinite M200 microplate reader. Fluorescence images were obtained using Carl Zeiss LSM 700 confocal laser scanning microscope.

Preparation of PIL-QDs-DBCO. The CdSe/CdZnS core/shell QDs were synthesized through a selective ionic adhesion and reaction (SILAR) method. The growth

process was monitored by absorption and emission spectra. Totally 9 monolayers of CdZnS shells were coated onto the CdSe core. The MA-PIL ternary polymer was prepared as described previously, which includes 40% imidazole for QD binding, 20% amine for post-modification and 40% PEG for water solubility. The number average molecular weight of the polymer was 33.5 kD and the polydispersity index (PDI) was 1.19. The PIL polymer was purified by dialysis and precipitation/redissolution, and then functionalized with DBCO by stirring the polymer with DBCO-NHS ester (polymer to DBCO mole ratio is 1:10) in a mixture of DMSO and chloroform (1:4) overnight. The as-synthesized QDs were purified by one cycle of precipitation and redissolution followed by GPC purification in toluene solvent. After this, the QDs were pumped dry and mixed in the above DBCO-polymer solution (mole ration QD:polymer = 1:100). The mixture was stirred for 1 h, after which 0.5 mL methanol was injected into the solution and stirring was continued for another 30 min. The resulting PIL-QDs-DBCO were precipitated by hexane and ethanol and redispersed by phosphate buffer saline (PBS). The water soluble dots were further purified by dialysis and filtration with a 0.2 μm membrane.

Cell culture and azide labeling. Vero cells were cultured in Dulbecco's modified Eagle's medium (DMEM, Hyclone) supplemented with 10% fetal bovine serum (FBS, Atlanta Biologicals), 100 IU/mL penicillin and 100 μg/mL of streptomycin (Hyclone). The azide labeling of Vero cells was achieved by cultivating cells in the DMEM containing certain concentrations of AECho. For fluorescence imaging, the azide-modified Vero cells were washed with PBS and fixed with 4% (w/v) paraformaldehyde. Upon that, cells were stained by 10 μM DBCO-Fluor 488 or 10 nM PIL-QDs-DBCO for 1 h, then washed with PBS. The nucleic acid of the cells was stained with 1 μg/mL DAPI for 10 min. After

washing, the cells were imaged by a Carl Zeiss LSM 700 confocal laser scanning microscope imaging system. The PIL-QDs-DBCO was excited using a 555 nm laser, emitting 550-650 nm fluorescence. DBCO-Fluor 488 was excited using a 488 nm laser, emitting 500-600 nm fluorescence. The DAPI was excited with 405 nm laser, emitting 420-500 nm fluorescence.

Virus propagation and azide labeling. MV was propagated in monolayer of Vero cells in the presence of 2% FBS. Generally, Vero cells were infected with wild type MV with a multiplicity of infection (MOI) of 0.1 pfu/cell. For the azide-labeled MV (N_3-MV) propagation, the medium was supplemented with 400 μM AECho. The infected cells were scraped into medium 72 h post-infection and the cell debris was removed by centrifugation at 3000 g for 15 min (4 ℃). The control MV and N_3-MV were purified over a gradient of sucrose centrifuged at 30,000 rpm for 3 hours (4 ℃).

Virus titer assay. The titers of MV and N_3-MV were quantified by 50% tissue culture infective dose ($TCID_{50}$). Vero cells were cultured in 96-well plates in complete medium until the cells reached 80-90% confluence, followed by replacement of DMEM containing 2% FBS. The virus samples prepared in DMEM by 4-fold serial dilutions were added to Vero cells. After culture for 3 days, the cells were stained with 0.1% crystal violet and observed under an inverted microscope. The well number that had cytopathic effect (CPE) on Vero cells were counted for the $TCID_{50}$ calculation according to the Reed and Muench method.

One-step growth assay. MV and N_3-MV were inoculated in Vero cells monolayer at MOI of 0.2 pfu/cell for 8, 24, 48, 72, 84 and 96 h, respectively. At the end of each time

point, the infected cells were scraped into medium and the cell debris was removed by centrifugation at 3000 g for 15 min at 4 ℃. The one-step growth curve of these viruses were titrated by $TCID_{50}$ on normal Vero cells according to a previous report.

Transmission electron microscopy imaging of the virus. The morphology of the viruses were characterized by transmission electron microscopy (TEM). 5 μL of MV or N_3-MV was dropped onto a carbon coated copper grid that pre-treated by 1% alcian blue for 5min. After 10 min, unabsorbed virus was removed with filter paper. Grids were fixed by 2% paraformaldehyde for 5 min; after that, 10 μL of 0.5% uranyl acetate was applied for 30 sec. The samples were then observed with the TEM.

Fluorescence co-localization assay. The purified MV or N_3-MV solution was dropped onto cover glasses for 1 h at 37 ℃. Excess viruses were then washed away with PBS solution, and the remaining viruses were fixed with 3% paraformaldehyde for 30 min at room temperature. After being permeabilized with 0.5% Triton X-100 in PBS, the viruses were incubated with 10 μM DBCO-Fluor 488 for 1 h. The nucleic acid of the virus was stained with 10 μg/mL propidium iodide (PI) for 15 min. Excess fluorophores were washed away with PBS. Fluorescence images were acquired using a Carl Zeiss LSM 700 confocal laser scanning microscope imaging system. DBCO-Fluor 488 was excited using a 488 nm laser, emitting 500-600 nm fluorescence. PI was excited with a 555 nm laser, emitting 560-700 nm fluorescence.

Fluorescence imaging of cells interacted with QDs-labeled Virus. QDs-labeled MV was prepared by incubating the N_3-MV with 10 nM PIL-QDs-DBCO. Vero cells were cultured in 24-well plate at 1×10^5 cells/mL density. Then the cells were incubated with as-

prepared QDs-labeled MV for 24 h at 37 ℃ to allow viruses binding, the unbound viruses were removed by washing with PBS. The nucleic acid of the cells was stained with 1 μg/mL DAPI solution for 10 min, after which the cells were imaged by a Carl Zeiss LSM 700 confocal laser scanning microscope imaging system. QDs was excited with a 555 nm laser, emitting 550-650 nm fluorescence. DAPI was excited with 405 nm laser, emitting 420-500 nm fluorescence.

Cell viability assay. Cell viability was determined by using CellTiter-Blue Cell Viability Assay Kit (Promega). Vero cells were incubated with AECho or PIL-QDs-DBCO at certain concentrations for 24 h, followed by addition of 10% CellTiter-Blue Assay reagent and incubation for 2 h. The fluorescence intensity was measured at 560/590 nm (Ex/Em) using Tecan Infinite M200 microplate reader. Cells treated with only medium were considered 100% viable.

4.4 Conclusion

In this chapter, a new group of polymeric imidazole ligands (MA-PIL) have been prepared. These ligands can be effectively conjugated onto core/shell quantum dots, and the exchanged QDs maintain high stability in aqueous solution and decent quantum yield. Moreover, the MA-PIL capped QDs show negligible toxicity and non-specific binding, which makes them as a promising candidate for the bio-labeling applications. Ultimately, PIL-QDs were used to label a model measles virus though a click chemistry reaction, and the QDs-labeled virus maintained its infectious ability against host cells. Our work has provided a model system to prepare QDs-labeled viruses and cells under a mild condition,

using highly repeatable QD preparative methods. For the future work, a better understanding of interaction between the PILs and nanocrystals will be helpful in designing robust biocompatible QD probes against different environment in the biological system.

REFERENCES

1. Hodes, G. Comparison of Dye- and Semiconductor-Sensitized Porous Nanocrystalline Liquid Junction Solar Cells. *J. Phys. Chem. C* **112,** 17778–17787 (2008).
2. Liu, W. *et al.* Compact Biocompatible Quantum Dots via RAFT-Mediated Synthesis of Imidazole-Based Random Copolymer Ligand. *J. Am. Chem. Soc.* **132,** 472–483 (2010).
3. Adam, S. *et al.* The effect of nanocrystal surface structure on the luminescence properties: Photoemission study of HF-etched InP nanocrystals. *J. Chem. Phys.* **123,** 084706 (2005).
4. Wu, X. *et al.* Immunofluorescent labeling of cancer marker Her2 and other cellular targets with semiconductor quantum dots. *Nat. Biotechnol.* **21,** 41–46 (2003).
5. Wood, V. *et al.* Air-Stable Operation of Transparent, Colloidal Quantum Dot Based LEDs with a Unipolar Device Architecture. *Nano Lett.* **10,** 24–29 (2010).
6. Yang, Z. *et al.* All-Quantum-Dot Infrared Light-Emitting Diodes. *ACS Nano* (2015). **ASAP**
7. Carey, G. H. *et al.* Colloidal Quantum Dot Solar Cells. *Chem. Rev.* (2015). **ASAP**
8. Lan, X. *et al.* Passivation Using Molecular Halides Increases Quantum Dot Solar Cell Performance. *Adv. Mater.* (2015) **ASAP**
9. Roy, S. C., Varghese, O. K., Paulose, M. & Grimes, C. A. Toward Solar Fuels: Photocatalytic Conversion of Carbon Dioxide to Hydrocarbons. *ACS Nano* **4,** 1259–1278 (2010).
10. Han, Z., Qiu, F., Eisenberg, R., Holland, P. L. & Krauss, T. D. Robust Photogeneration of H2 in Water Using Semiconductor Nanocrystals and a Nickel Catalyst. *Science* **338,** 1321–1324 (2012).

11. Murray, C. B., Norris, D. J. & Bawendi, M. G. Synthesis and characterization of nearly monodisperse CdE (E = sulfur, selenium, tellurium) semiconductor nanocrystallites. *J. Am. Chem. Soc.* **115,** 8706–8715 (1993).
12. Peng, Z. A. & Peng, X. Formation of High-Quality CdTe, CdSe, and CdS Nanocrystals Using CdO as Precursor. *J. Am. Chem. Soc.* **123,** 183–184 (2001).
13. Chen, O. *et al.* Synthesis of Metal–Selenide Nanocrystals Using Selenium Dioxide as the Selenium Precursor. *Angew. Chem. Int. Ed.* **47,** 8638–8641 (2008).
14. Flamee, S. *et al.* Synthesis of metal selenide colloidal nanocrystals by the hot injection of selenium powder. *Dalton Trans.* **42,** 12654–12661 (2013).
15. Hendricks, M. P., Campos, M. P., Cleveland, G. T., Plante, I. J.-L. & Owen, J. S. A tunable library of substituted thiourea precursors to metal sulfide nanocrystals. *Science* **348,** 1226–1230 (2015).
16. Kudera, S. *et al.* Sequential Growth of Magic-Size CdSe Nanocrystals. *Adv. Mater.* **19,** 548–552 (2007).
17. Cossairt, B. M. & Owen, J. S. CdSe Clusters: At the Interface of Small Molecules and Quantum Dots. *Chem. Mater.* **23,** 3114–3119 (2011).
18. Xie, R., Kolb, U., Li, J., Basché, T. & Mews, A. Synthesis and characterization of highly luminescent CdSe-core CdS/Zn0.5Cd0.5S/ZnS multishell nanocrystals. *J. Am. Chem. Soc.* **127,** 7480–7488 (2005).
19. Greytak, A. B. *et al.* Alternating layer addition approach to CdSe/CdS core/shell quantum dots with near-unity quantum yield and high on-time fractions. *Chem. Sci.* **3,** 2028–2034 (2012).
20. Tan, R., Blom, D. A., Ma, S. & Greytak, A. B. Probing Surface Saturation Conditions in Alternating Layer Growth of CdSe/CdS Core/Shell Quantum Dots. *Chem. Mater.* **25,** 3724–3736 (2013).
21. Liu, W. *et al.* Compact Cysteine-Coated CdSe(ZnCdS) Quantum Dots for in Vivo Applications. *J. Am. Chem. Soc.* **129,** 14530–14531 (2007).
22. Dennis, A. M. *et al.* Suppressed Blinking and Auger Recombination in Near-Infrared Type-II InP/CdS Nanocrystal Quantum Dots. *Nano Lett.* **12,** 5545–5551 (2012).
23. Chen, Y. *et al.* 'Giant' multishell CdSe nanocrystal quantum dots with suppressed blinking. *J. Am. Chem. Soc.* **130,** 5026–5027 (2008).

24. Chen, O. *et al.* Compact high-quality CdSe–CdS core–shell nanocrystals with narrow emission linewidths and suppressed blinking. *Nat. Mater.* **12,** 445–451 (2013).
25. Talapin, D. V. *et al.* Seeded Growth of Highly Luminescent CdSe/CdS Nanoheterostructures with Rod and Tetrapod Morphologies. *Nano Lett.* **7,** 2951–2959 (2007).
26. Carbone, L. *et al.* Synthesis and Micrometer-Scale Assembly of Colloidal CdSe/CdS Nanorods Prepared by a Seeded Growth Approach. *Nano Lett.* **7,** 2942–2950 (2007).
27. Li, J. J. *et al.* Large-Scale Synthesis of Nearly Monodisperse CdSe/CdS Core/Shell Nanocrystals Using Air-Stable Reagents via Successive Ion Layer Adsorption and Reaction. *J. Am. Chem. Soc.* **125,** 12567–12575 (2003).
28. Dibbell, R. S. & Watson, D. F. Distance-Dependent Electron Transfer in Tethered Assemblies of CdS Quantum Dots and TiO2 Nanoparticles. *J. Phys. Chem. C* **113,** 3139–3149 (2009).
29. Guo, S. *et al.* Photoinduced Electron Transfer Between Pyridine Coated Cadmium Selenide Quantum Dots and Single Sheet Graphene. *Adv. Funct. Mater.* **23,** 5199–5211 (2013).
30. Ip, A. H. *et al.* Hybrid passivated colloidal quantum dot solids. *Nat. Nanotechnol.* **7,** 577–582 (2012).
31. Chuang, C.-H. M., Brown, P. R., Bulović, V. & Bawendi, M. G. Improved performance and stability in quantum dot solar cells through band alignment engineering. *Nat. Mater.* **13,** 796–801 (2014).
32. Kovalenko, M. V., Scheele, M. & Talapin, D. V. Colloidal Nanocrystals with Molecular Metal Chalcogenide Surface Ligands. *Science* **324,** 1417–1420 (2009).
33. Anderson, N. C. & Owen, J. S. Soluble, Chloride-Terminated CdSe Nanocrystals: Ligand Exchange Monitored by 1H and 31P NMR Spectroscopy. *Chem. Mater.* **25,** 69–76 (2013).
34. Nag, A. *et al.* Metal-free Inorganic Ligands for Colloidal Nanocrystals: S2–, HS–, Se2–, HSe–, Te2–, HTe–, TeS32–, OH–, and NH2– as Surface Ligands. *J. Am. Chem. Soc.* **133,** 10612–10620 (2011).
35. Wuister, S. F., Swart, I., van Driel, F., Hickey, S. G. & de Mello Donegá, C. Highly Luminescent Water-Soluble CdTe Quantum Dots. *Nano Lett.* **3,** 503–507 (2003).

36. Cao, J. *et al.* In vivo NIR imaging with PbS quantum dots entrapped in biodegradable micelles. *J. Biomed. Mater. Res. A* **100A,** 958–968 (2012).
37. Stroh, M. *et al.* Quantum dots spectrally distinguish multiple species within the tumor milieu in vivo. *Nat. Med.* **11,** 678–682 (2005).
38. Liu, W. *et al.* Compact Biocompatible Quantum Dots Functionalized for Cellular Imaging. *J. Am. Chem. Soc.* **130,** 1274–1284 (2008).
39. Susumu, K. *et al.* Enhancing the Stability and Biological Functionalities of Quantum Dots via Compact Multifunctional Ligands. *J. Am. Chem. Soc.* **129,** 13987–13996 (2007).
40. Aldeek, F., Safi, M., Zhan, N., Palui, G. & Mattoussi, H. Understanding the self-assembly of proteins onto gold nanoparticles and quantum dots driven by metal-histidine coordination. *ACS Nano* **7,** 10197–10210 (2013).
41. Zhang, P. *et al.* Click-functionalized compact quantum dots protected by multidentate-imidazole ligands: conjugation-ready nanotags for living-virus labeling and imaging. *J. Am. Chem. Soc.* **134,** 8388–8391 (2012).
42. Howarth, M., Takao, K., Hayashi, Y. & Ting, A. Y. Targeting quantum dots to surface proteins in living cells with biotin ligase. *Proc. Natl. Acad. Sci. U. S. A.* **102,** 7583–7588 (2005).
43. Jaiswal, J. K., Mattoussi, H., Mauro, J. M. & Simon, S. M. Long-term multiple color imaging of live cells using quantum dot bioconjugates. *Nat. Biotechnol.* **21,** 47–51 (2003).
44. Clark, M. D., Kumar, S. K., Owen, J. S. & Chan, E. M. Focusing Nanocrystal Size Distributions via Production Control. *Nano Lett.* **11,** 1976–1980 (2011).
45. Leatherdale, C. A., Woo, W.-K., Mikulec, F. V. & Bawendi, M. G. On the Absorption Cross Section of CdSe Nanocrystal Quantum Dots. *J. Phys. Chem. B* **106,** 7619–7622 (2002).
46. Liu, H., Owen, J. S. & Alivisatos, A. P. Mechanistic Study of Precursor Evolution in Colloidal Group II−VI Semiconductor Nanocrystal Synthesis. *J. Am. Chem. Soc.* **129,** 305–312 (2007).
47. Hines, M. A. & Guyot-Sionnest, P. Synthesis and Characterization of Strongly Luminescing ZnS-Capped CdSe Nanocrystals. *J. Phys. Chem.* **100,** 468–471 (1996).

48. Snee, P. T., Chan, Y., Nocera, D. G. & Bawendi, M. G. Whispering-Gallery-Mode Lasing from a Semiconductor Nanocrystal/Microsphere Resonator Composite. *Adv. Mater*. **17,** 1131–1136 (2005).
49. Mattoussi, H. *et al.* Self-Assembly of CdSe−ZnS Quantum Dot Bioconjugates Using an Engineered Recombinant Protein. *J. Am. Chem. Soc.* **122,** 12142–12150 (2000).
50. Tagliazucchi, M., Tice, D. B., Sweeney, C. M., Morris-Cohen, A. J. & Weiss, E. A. Ligand-Controlled Rates of Photoinduced Electron Transfer in Hybrid CdSe Nanocrystal/Poly(viologen) Films. *ACS Nano* **5,** 9907–9917 (2011).
51. Sambur, J. B., Riha, S. C., Choi, D. & Parkinson, B. A. Influence of Surface Chemistry on the Binding and Electronic Coupling of CdSe Quantum Dots to Single Crystal TiO2 Surfaces. *Langmuir* **26,** 4839–4847 (2010).
52. King, L. A. & Riley, D. J. Importance of QD Purification Procedure on Surface Adsorbance of QDs and Performance of QD Sensitized Photoanodes. *J. Phys. Chem. C* **116,** 3349–3355 (2012).
53. Morris-Cohen, A. J., Donakowski, M. D., Knowles, K. E. & Weiss, E. A. The Effect of a Common Purification Procedure on the Chemical Composition of the Surfaces of CdSe Quantum Dots Synthesized with Trioctylphosphine Oxide. *J. Phys. Chem. C* **114,** 897–906 (2010).
54. Hassinen, A. *et al.* Short-Chain Alcohols Strip X-Type Ligands and Quench the Luminescence of PbSe and CdSe Quantum Dots, Acetonitrile Does Not. *J. Am. Chem. Soc.* **134,** 20705–20712 (2012).
55. Shen, Y., Tan, R., Gee, M. Y. & Greytak, A. B. Quantum Yield Regeneration: Influence of Neutral Ligand Binding on Photophysical Properties in Colloidal Core/Shell Quantum Dots. *ACS Nano* **9,** 3345–3359 (2015).
56. Kalyuzhny, G. & Murray, R. W. Ligand Effects on Optical Properties of CdSe Nanocrystals. *J. Phys. Chem. B* **109,** 7012–7021 (2005).
57. Kowalczyk, B., Lagzi, I. & Grzybowski, B. A. Nanoseparations: Strategies for size and/or shape-selective purification of nanoparticles. *Curr. Opin. Colloid Interface Sci.* **16,** 135–148 (2011).

58. Liu, J., Liu, R., Yin, Y. & Jiang, G. Triton X-114 based cloud point extraction: a thermoreversible approach for separation/concentration and dispersion of nanomaterials in the aqueous phase. *Chem. Commun.* 1514–1516 (2009).
59. Lees, E. E. *et al.* Experimental Determination of Quantum Dot Size Distributions, Ligand Packing Densities, and Bioconjugation Using Analytical Ultracentrifugation. *Nano Lett.* **8,** 2883–2890 (2008).
60. Bai, L. *et al.* Rapid Separation and Purification of Nanoparticles in Organic Density Gradients. *J. Am. Chem. Soc.* **132,** 2333–2337 (2010).
61. Bass, J. D. *et al.* An Efficient and Low-Cost Method for the Purification of Colloidal Nanoparticles. *Angew. Chem. Int. Ed.* **50,** 6538–6542 (2011).
62. Lhuillier, E., Hease, P., Ithurria, S. & Dubertret, B. Selective Electrophoretic Deposition of CdSe Nanoplatelets. *Chem. Mater.* **26,** 4514–4520 (2014).
63. Krueger, K. M., Al-Somali, A. M., Falkner, J. C. & Colvin, V. L. Characterization of Nanocrystalline CdSe by Size Exclusion Chromatography. *Anal. Chem.* **77,** 3511–3515 (2005).
64. Wang, M. *et al.* Preparative size-exclusion chromatography for purification and characterization of colloidal quantum dots bound by chromophore-labeled polymers and low-molecular-weight chromophores. *J. Chromatogr. A* **1216,** 5011–5019 (2009).
65. Alamo-Nole, L., Bailon-Ruiz, S., Perales-Perez, O. & Roman, F. R. Preparative size-exclusion chromatography for separation and purification of water-stable Cd-based quantum dots. *Anal. Methods* **4,** 3127–3132 (2012).
66. Wang, M. *et al.* Colloidal CdSe Nanocrystals Passivated by a Dye-Labeled Multidentate Polymer: Quantitative Analysis by Size-Exclusion Chromatography. *Angew. Chem. Int. Ed.* **45,** 2221–2224 (2006).
67. Kanelidis, I. *et al.* Inorganic–organic nanocomposites of CdSe nanocrystals surface-modified with oligo- and poly(fluorene) moieties. *J. Mater. Chem.* **21,** 2656–2662 (2011).
68. Soo Choi, H. *et al.* Renal clearance of quantum dots. *Nat. Biotechnol.* **25,** 1165–1170 (2007).

69. Biesta, W. *et al.* Preparation, Characterization, and Surface Modification of Trifluoroethyl Ester-Terminated Silicon Nanoparticles. *Chem. Mater.* **24,** 4311–4318 (2012).
70. Ren, L. *et al.* Preparation of Side-Chain 18-e Cobaltocenium-Containing Acrylate Monomers and Polymers. *Macromolecules* **43,** 9304–9310 (2010).
71. Jasieniak, J. & Mulvaney, P. From Cd-Rich to Se-Rich − the Manipulation of CdSe Nanocrystal Surface Stoichiometry. *J. Am. Chem. Soc.* **129,** 2841–2848 (2007).
72. Fritzinger, B., Capek, R. K., Lambert, K., Martins, J. C. & Hens, Z. Utilizing Self-Exchange To Address the Binding of Carboxylic Acid Ligands to CdSe Quantum Dots. *J. Am. Chem. Soc.* **132,** 10195–10201 (2010).
73. Gomes, R. *et al.* Binding of Phosphonic Acids to CdSe Quantum Dots: A Solution NMR Study. *J. Phys. Chem. Lett.* **2,** 145–152 (2011).
74. Hens, Z. & Martins, J. C. A Solution NMR Toolbox for Characterizing the Surface Chemistry of Colloidal Nanocrystals. *Chem. Mater.* **25,** 1211–1221 (2013).
75. Morris-Cohen, A. J., Frederick, M. T., Lilly, G. D., McArthur, E. A. & Weiss, E. A. Organic Surfactant-Controlled Composition of the Surfaces of CdSe Quantum Dots. *J. Phys. Chem. Lett.* **1,** 1078–1081 (2010).
76. Canzi, G., Mrse, A. A. & Kubiak, C. P. Diffusion-Ordered NMR Spectroscopy as a Reliable Alternative to TEM for Determining the Size of Gold Nanoparticles in Organic Solutions. *J. Phys. Chem. C* **115,** 7972–7978 (2011).
77. Virieux, H. *et al.* InP/ZnS Nanocrystals: Coupling NMR and XPS for Fine Surface and Interface Description. *J. Am. Chem. Soc.* **134,** 19701–19708 (2012).
78. Dyadin, Y. A., Larionov, E. G., Manakov, A. Y. & Zhurko, F. V. Double clathrate hydrate of tetrahydrofuran and xenon at pressures up to 15 kBar. *Mendeleev Commun.* **9,** 80–81 (1999).
79. Yang, Y. *et al.* Characterization of multivalent lactose quantum dots and its application in carbohydrate-protein interactions study and cell imaging. *Bioorg. Med. Chem.* **18,** 5234–5240 (2010).
80. Tan, R. *et al.* Reducing Competition by Coordinating Solvent Promotes Morphological Control in Alternating Layer Growth of CdSe/CdS Core/Shell Quantum Dots. *Chem. Mater.* **27,** 7468–7480 (2015).

81. Palui, G. *et al.* Photoinduced phase transfer of luminescent quantum dots to polar and aqueous media. *J. Am. Chem. Soc.* **134,** 16370–16378 (2012).
82. Ding, T. X., Olshansky, J. H., Leone, S. R. & Alivisatos, A. P. Efficiency of Hole Transfer from Photoexcited Quantum Dots to Covalently Linked Molecular Species. *J. Am. Chem. Soc.* **137,** 2021–2029 (2015).
83. Dubois, F., Mahler, B., Dubertret, B., Doris, E. & Mioskowski, C. A versatile strategy for quantum dot ligand exchange. *J. Am. Chem. Soc.* **129,** 482–483 (2007).
84. Gary, D. C. & Cossairt, B. M. Role of Acid in Precursor Conversion During InP Quantum Dot Synthesis. *Chem. Mater.* **25,** 2463–2469 (2013).
85. Brust, M., Walker, M., Bethell, D., Schiffrin, D. J. & Whyman, R. Synthesis of thiol-derivatised gold nanoparticles in a two-phase Liquid–Liquid system. *J. Chem. Soc. Chem. Commun.* 801–802 (1994).
86. Peng, X., Schlamp, M. C., Kadavanich, A. V. & Alivisatos, A. P. Epitaxial Growth of Highly Luminescent CdSe/CdS Core/Shell Nanocrystals with Photostability and Electronic Accessibility. *J. Am. Chem. Soc.* **119,** 7019–7029 (1997).
87. Zhu, H., Song, N. & Lian, T. Wave function engineering for ultrafast charge separation and slow charge recombination in type II core/shell quantum dots. *J. Am. Chem. Soc.* **133,** 8762–8771 (2011).
88. van Embden, J., Jasieniak, J. & Mulvaney, P. Mapping the optical properties of CdSe/CdS heterostructure nanocrystals: the effects of core size and shell thickness. *J. Am. Chem. Soc.* **131,** 14299–14309 (2009).
89. Owen, J. S., Park, J., Trudeau, P.-E. & Alivisatos, A. P. Reaction chemistry and ligand exchange at cadmium-selenide nanocrystal surfaces. *J. Am. Chem. Soc.* **130,** 12279–12281 (2008).
90. Caldwell, M. A. *et al.* Driving oxygen coordinated ligand exchange at nanocrystal surfaces using trialkylsilylated chalcogenides. *Chem. Commun. Camb. Engl.* **47,** 556–558 (2011).
91. Palui, G., Aldeek, F., Wang, W. & Mattoussi, H. Strategies for interfacing inorganic nanocrystals with biological systems based on polymer-coating. *Chem. Soc. Rev.* **44,** 193–227 (2014).

92. Zhou, J., Yang, Y. & Zhang, C. Toward Biocompatible Semiconductor Quantum Dots: From Biosynthesis and Bioconjugation to Biomedical Application. *Chem. Rev.* **115,** 11669–11717 (2015).
93. Talapin, D. V., Rogach, A. L., Kornowski, A., Haase, M. & Weller, H. Highly Luminescent Monodisperse CdSe and CdSe/ZnS Nanocrystals Synthesized in a Hexadecylamine−Trioctylphosphine Oxide−Trioctylphospine Mixture. *Nano Lett.* **1,** 207–211 (2001).
94. Smith, A. M., Duan, H., Rhyner, M. N., Ruan, G. & Nie, S. A systematic examination of surface coatings on the optical and chemical properties of semiconductor quantum dots. *Phys. Chem. Chem. Phys. PCCP* **8,** 3895–3903 (2006).
95. Anderson, N. C., Hendricks, M. P., Choi, J. J. & Owen, J. S. Ligand exchange and the stoichiometry of metal chalcogenide nanocrystals: spectroscopic observation of facile metal-carboxylate displacement and binding. *J. Am. Chem. Soc.* **135,** 18536–18548 (2013).
96. Zhu, H., Yang, Y. & Lian, T. Multiexciton annihilation and dissociation in quantum confined semiconductor nanocrystals. *Acc. Chem. Res.* **46,** 1270–1279 (2013).
97. Efros, A. L. & Rosen, M. Random Telegraph Signal in the Photoluminescence Intensity of a Single Quantum Dot. *Phys. Rev. Lett.* **78,** 1110–1113 (1997).
98. Frantsuzov, P. A., Volkán-Kacsó, S. & Jankó, B. Model of fluorescence intermittency of single colloidal semiconductor quantum dots using multiple recombination centers. *Phys. Rev. Lett.* **103,** 207402 (2009).
99. Mahler, B. *et al.* Towards non-blinking colloidal quantum dots. *Nat. Mater.* **7,** 659–664 (2008).
100. Spinicelli, P. *et al.* Bright and grey states in CdSe-CdS nanocrystals exhibiting strongly reduced blinking. *Phys. Rev. Lett.* **102,** 136801 (2009).
101. Efros, null *et al.* Band-edge exciton in quantum dots of semiconductors with a degenerate valence band: Dark and bright exciton states. *Phys. Rev. B Condens. Matter* **54,** 4843–4856 (1996).
102. Fisher, B. R., Eisler, H.-J., Stott, N. E. & Bawendi, M. G. Emission Intensity Dependence and Single-Exponential Behavior In Single Colloidal Quantum Dot Fluorescence Lifetimes. *J. Phys. Chem. B* **108,** 143–148 (2004).

103. Schlegel, G., Bohnenberger, J., Potapova, I. & Mews, A. Fluorescence decay time of single semiconductor nanocrystals. *Phys. Rev. Lett.* **88,** 137401 (2002).
104. Kuno, M., Lee, J. K., Dabbousi, B. O., Mikulec, F. V. & Bawendi, M. G. The band edge luminescence of surface modified CdSe nanocrystallites: Probing the luminescing state. *J. Chem. Phys.* **106,** 9869–9882 (1997).
105. Mooney, J., Krause, M. M., Saari, J. I. & Kambhampati, P. A microscopic picture of surface charge trapping in semiconductor nanocrystals. *J. Chem. Phys.* **138,** 204705 (2013).
106. Bullen, C. & Mulvaney, P. The effects of chemisorption on the luminescence of CdSe quantum dots. *Langmuir ACS J. Surf. Colloids* **22,** 3007–3013 (2006).
107. Munro, A. M. & Ginger, D. S. Photoluminescence quenching of single CdSe nanocrystals by ligand adsorption. *Nano Lett.* **8,** 2585–2590 (2008).
108. Peterson, M. D. *et al.* The role of ligands in determining the exciton relaxation dynamics in semiconductor quantum dots. *Annu. Rev. Phys. Chem.* **65,** 317–339 (2014).
109. Qin, H. *et al.* Single-dot spectroscopy of zinc-blende CdSe/CdS core/shell nanocrystals: nonblinking and correlation with ensemble measurements. *J. Am. Chem. Soc.* **136,** 179–187 (2014).
110. Morris-Cohen, A. J., Malicki, M., Peterson, M. D., Slavin, J. W. J. & Weiss, E. A. Chemical, Structural, and Quantitative Analysis of the Ligand Shells of Colloidal Quantum Dots. *Chem. Mater.* **25,** 1155–1165 (2013).
111. Shen, Y., Gee, M. Y., Tan, R., Pellechia, P. J. & Greytak, A. B. Purification of Quantum Dots by Gel Permeation Chromatography and the Effect of Excess Ligands on Shell Growth and Ligand Exchange. *Chem. Mater.* **25,** 2838–2848 (2013).
112. Owen, J. The coordination chemistry of nanocrystal surfaces. *Science* **347,** 615–616 (2015).
113. Guyot-Sionnest, P., Wehrenberg, B. & Yu, D. Intraband relaxation in CdSe nanocrystals and the strong influence of the surface ligands. *J. Chem. Phys.* **123,** 074709 (2005).
114. McArthur, E. A., Morris-Cohen, A. J., Knowles, K. E. & Weiss, E. A. Charge Carrier Resolved Relaxation of the First Excitonic State in CdSe Quantum Dots Probed with

Near-Infrared Transient Absorption Spectroscopy. *J. Phys. Chem. B* **114,** 14514–14520 (2010).

115. Kilina, S., Velizhanin, K. A., Ivanov, S., Prezhdo, O. V. & Tretiak, S. Surface ligands increase photoexcitation relaxation rates in CdSe quantum dots. *ACS Nano* **6,** 6515–6524 (2012).
116. Munro, A. M., Jen-La Plante, I., Ng, M. S. & Ginger, D. S. Quantitative Study of the Effects of Surface Ligand Concentration on CdSe Nanocrystal Photoluminescence. *J. Phys. Chem. C* **111,** 6220–6227 (2007).
117. Knowles, K. E., Tice, D. B., McArthur, E. A., Solomon, G. C. & Weiss, E. A. Chemical Control of the Photoluminescence of CdSe Quantum Dot−Organic Complexes with a Series of Para-Substituted Aniline Ligands. *J. Am. Chem. Soc.* **132,** 1041–1050 (2010).
118. Zhao, H., Chaker, M. & Ma, D. Self-selective recovery of photoluminescence in amphiphilic polymer encapsulated PbS quantum dots. *Phys. Chem. Chem. Phys. PCCP* **12,** 14754–14761 (2010).
119. Lee, J. R. I. *et al.* Ligand-mediated modification of the electronic structure of CdSe quantum dots. *Nano Lett.* **12,** 2763–2767 (2012).
120. Ji, X., Copenhaver, D., Sichmeller, C. & Peng, X. Ligand bonding and dynamics on colloidal nanocrystals at room temperature: the case of alkylamines on CdSe nanocrystals. *J. Am. Chem. Soc.* **130,** 5726–5735 (2008).
121. Williams, E. S. *et al.* Characterizing the Influence of TOPO on Exciton Recombination Dynamics in Colloidal CdSe Quantum Dots. *J. Phys. Chem. C* **117,** 4227–4237 (2013).
122. Yang, J. & Yang, P. Photoluminescent enhancement of CdSe/Cd(1-x) Zn(x)S quantum dots by hexadecylamine at room temperature. *J. Nanosci. Nanotechnol.* **12,** 7322–7328 (2012).
123. Park, C. & Yoon, T. H. L-cysteine-induced photoluminescence enhancement of CdSe/ZnSe quantum dots in aqueous solution. *Colloids Surf. B Biointerfaces* **75,** 472–477 (2010).
124. Chen, C.-J., Chiang, R.-K., Huang, C.-Y., Lien, J.-Y. & Wang, S.-L. Thiol treatment to enhance photoluminescence and electroluminescence of CdSe/CdS core–shell

quantum dots prepared by thermal cycling of single source precursors. *RSC Adv.* **5,** 9819–9827 (2015).

125. Wang, M. *et al.* Enhancing the photoluminescence of polymer-stabilized CdSe/CdS/ZnS core/shell/shell and CdSe/ZnS core/shell quantum dots in water through a chemical-activation approach. *Langmuir ACS J. Surf. Colloids* **25,** 11732–11740 (2009).
126. Oszajca, M. *et al.* Photoluminescence Enhancement of CdSe and CdSe–ZnS Nanocrystals by On-Surface Ligand Modification. *Eur. J. Inorg. Chem.* **2013,** 3550–3556 (2013).
127. Sharma, S. N., Pillai, Z. S. & Kamat, P. V. Photoinduced Charge Transfer between CdSe Quantum Dots and p-Phenylenediamine. *J. Phys. Chem. B* **107,** 10088–10093 (2003).
128. Burda, C., Link, S., Mohamed, M. & El-Sayed, M. The Relaxation Pathways of CdSe Nanoparticles Monitored with Femtosecond Time-Resolution from the Visible to the IR: Assignment of the Transient Features by Carrier Quenching. *J. Phys. Chem. B* **105,** 12286–12292 (2001).
129. Kern, S. J., Sahu, K. & Berg, M. A. Heterogeneity of the electron-trapping kinetics in CdSe nanoparticles. *Nano Lett.* **11,** 3493–3498 (2011).
130. Jones, M., Lo, S. S. & Scholes, G. D. Quantitative modeling of the role of surface traps in CdSe/CdS/ZnS nanocrystal photoluminescence decay dynamics. *Proc. Natl. Acad. Sci. U. S. A.* **106,** 3011–3016 (2009).
131. Zhao, J., Nair, G., Fisher, B. R. & Bawendi, M. G. Challenge to the Charging Model of Semiconductor-Nanocrystal Fluorescence Intermittency from Off-State Quantum Yields and Multiexciton Blinking. *Phys. Rev. Lett.* **104,** 157403 (2010).
132. Freyer, M. W. & Lewis, E. A. Isothermal titration calorimetry: experimental design, data analysis, and probing macromolecule/ligand binding and kinetic interactions. *Methods Cell Biol.* **84,** 79–113 (2008).
133. Grossoehme, N. E., Spuches, A. M. & Wilcox, D. E. Application of isothermal titration calorimetry in bioinorganic chemistry. *JBIC J. Biol. Inorg. Chem.* **15,** 1183–1191 (2010).

134. Ravi, V., Binz, J. M. & Rioux, R. M. Thermodynamic profiles at the solvated inorganic-organic interface: the case of gold-thiolate monolayers. *Nano Lett.* **13,** 4442–4448 (2013).
135. Lindman, S. *et al.* Systematic investigation of the thermodynamics of HSA adsorption to N-iso-propylacrylamide/N-tert-butylacrylamide copolymer nanoparticles. Effects of particle size and hydrophobicity. *Nano Lett.* **7,** 914–920 (2007).
136. Mondal, S., Ghosh, S., Ghosh, D. & Saha, A. Physico-Chemical Aspects of Quantum Dot–Vasodialator Interaction: Implications in Nanodiagnostics. *J. Phys. Chem. C* **116,** 9774–9782 (2012).
137. Kopping, J. T. & Patten, T. E. Identification of acidic phosphorus-containing ligands involved in the surface chemistry of CdSe nanoparticles prepared in tri-N-octylphosphine oxide solvents. *J. Am. Chem. Soc.* **130,** 5689–5698 (2008).
138. Knowles, K. E., Frederick, M. T., Tice, D. B., Morris-Cohen, A. J. & Weiss, E. A. Colloidal Quantum Dots: Think Outside the (Particle-in-a-)Box. *J. Phys. Chem. Lett.* **3,** 18–26 (2012).
139. Ning, Z. *et al.* Role of surface ligands in optical properties of colloidal CdSe/CdS quantum dots. *Phys. Chem. Chem. Phys.* **13,** 5848–5854 (2011).
140. Minotto, A. *et al.* Role of Core–Shell Interfaces on Exciton Recombination in CdSe–CdxZn1–xS Quantum Dots. *J. Phys. Chem. C* **118,** 24117–24126 (2014).
141. in *Principles of Fluorescence Spectroscopy* (ed. Lakowicz, J. R.) 1–26 (Springer US, 2006).
142. Sillen, A. & Engelborghs, Y. The Correct Use of 'Average' Fluorescence Parameters. *Photochem. Photobiol.* **67,** 475–486 (1998).
143. Galland, C. *et al.* Two types of luminescence blinking revealed by spectroelectrochemistry of single quantum dots. *Nature* **479,** 203–207 (2011).
144. Orfield, N. J., McBride, J. R., Keene, J. D., Davis, L. M. & Rosenthal, S. J. Correlation of Atomic Structure and Photoluminescence of the Same Quantum Dot: Pinpointing Surface and Internal Defects That Inhibit Photoluminescence. *ACS Nano* **9,** 831–839 (2015).

145. Tyagi, P. & Kambhampati, P. False multiple exciton recombination and multiple exciton generation signals in semiconductor quantum dots arise from surface charge trapping. *J. Chem. Phys.* **134,** 094706 (2011).
146. Singh, G., Guericke, M. A., Song, Q. & Jones, M. A Multipulse Time-Resolved Fluorescence Method for Probing Second-Order Recombination Dynamics in Colloidal Quantum Dots. *J. Phys. Chem. C* **118,** 14692–14702 (2014).
147. Son, D. H., Hughes, S. M., Yin, Y. & Paul Alivisatos, A. Cation exchange reactions in ionic nanocrystals. *Science* **306,** 1009–1012 (2004).
148. Lambert, K., Geyter, B. D., Moreels, I. & Hens, Z. PbTe|CdTe Core|Shell Particles by Cation Exchange, a HR-TEM study. *Chem. Mater.* **21,** 778–780 (2009).
149. Li, H. *et al.* Sequential cation exchange in nanocrystals: preservation of crystal phase and formation of metastable phases. *Nano Lett.* **11,** 4964–4970 (2011).
150. Hassinen, A., Moreels, I., de Mello Donegá, C., Martins, J. C. & Hens, Z. Nuclear Magnetic Resonance Spectroscopy Demonstrating Dynamic Stabilization of CdSe Quantum Dots by Alkylamines. *J. Phys. Chem. Lett.* **1,** 2577–2581 (2010).
151. Fleischer, C. C. & Payne, C. K. Secondary structure of corona proteins determines the cell surface receptors used by nanoparticles. *J. Phys. Chem. B* **118,** 14017–14026 (2014).
152. Rempel, J. Y., Trout, B. L., Bawendi, M. G. & Jensen, K. F. Density functional theory study of ligand binding on CdSe (0001), (0001), and (1120) single crystal relaxed and reconstructed surfaces: implications for nanocrystalline growth. *J. Phys. Chem. B* **110,** 18007–18016 (2006).
153. Shanavas, K. V. *et al.* First-Principles Study of the Effect of Organic Ligands on the Crystal Structure of CdS Nanoparticles. *J. Phys. Chem. C* **116,** 6507–6511 (2012).
154. Beaumont, P. C., Johnson, D. G. & Parsons, B. J. Photophysical properties of laser dyes: picosecond laser flash photolysis studies of Rhodamine 6G, Rhodamine B and Rhodamine 101. *J. Chem. Soc. Faraday Trans.* **89,** 4185–4191 (1993).
155. Grabolle, M. *et al.* Determination of the Fluorescence Quantum Yield of Quantum Dots: Suitable Procedures and Achievable Uncertainties. *Anal. Chem.* **81,** 6285–6294 (2009).

156. Talapin, D. V. *et al.* Highly Emissive Colloidal CdSe/CdS Heterostructures of Mixed Dimensionality. *Nano Lett.* **3,** 1677–1681 (2003).
157. Garc á-Rodr ǵuez, R. & Liu, H. Mechanistic Insights into the Role of Alkylamine in the Synthesis of CdSe Nanocrystals. *J. Am. Chem. Soc.* **136,** 1968–1975 (2014).
158. Guo, Y. *et al.* Unique Challenges Accompany Thick-Shell CdSe/nCdS (n > 10) Nanocrystal Synthesis. *J. Phys. Chem. C* **116,** 2791–2800 (2012).
159. Foos, E. E. *et al.* Synthesis and Surface Composition Study of CdSe Nanoclusters Prepared Using Solvent Systems Containing Primary, Secondary, and Tertiary Amines. *Chem. Mater.* **18,** 2886–2894 (2006).
160. Jasieniak, J., Smith, L., Embden, J. van, Mulvaney, P. & Califano, M. Re-examination of the Size-Dependent Absorption Properties of CdSe Quantum Dots. *J. Phys. Chem. C* **113,** 19468–19474 (2009).
161. Thessing, J., Qian, J., Chen, H., Pradhan, N. & Peng, X. Interparticle Influence on Size/Size Distribution Evolution of Nanocrystals. *J. Am. Chem. Soc.* **129,** 2736–2737 (2007).
162. Kim, J. I. *et al.* Photoluminescence enhancement in CdS quantum dots by thermal annealing. *Nanoscale Res. Lett.* **7,** 1–7 (2012).
163. Kalasad, M. N., Rabinal, M. K. & Mulimani, B. G. Ambient Synthesis and Characterization of High-Quality CdSe Quantum Dots by an Aqueous Route. *Langmuir* **25,** 12729–12735 (2009).
164. Rogach, A. L. *et al.* Aqueous Synthesis of Thiol-Capped CdTe Nanocrystals: State-of-the-Art. *J. Phys. Chem. C* **111,** 14628–14637 (2007).
165. Yi, D. K. *et al.* Silica-coated nanocomposites of magnetic nanoparticles and quantum dots. *J. Am. Chem. Soc.* **127,** 4990–4991 (2005).
166. Kloust, H. *et al.* Poly(ethylene oxide) and Polystyrene Encapsulated Quantum Dots: Highly Fluorescent, Functionalizable, and Ultrastable in Aqueous Media. *J. Phys. Chem. C* **117,** 23244–23250 (2013).
167. Schieber, C. *et al.* Conjugation of Transferrin to Azide-Modified CdSe/ZnS Core–Shell Quantum Dots using Cyclooctyne Click Chemistry. *Angew. Chem. Int. Ed.* **51,** 10523–10527 (2012).

168. Clapp, A. R., Goldman, E. R. & Mattoussi, H. Capping of CdSe–ZnS quantum dots with DHLA and subsequent conjugation with proteins. *Nat. Protoc.* **1,** 1258–1266 (2006).
169. Wang, W., Ji, X., Kapur, A., Zhang, C. & Mattoussi, H. A Multifunctional Polymer Combining the Imidazole and Zwitterion Motifs as a Biocompatible Compact Coating for Quantum Dots. *J. Am. Chem. Soc.* **137,** 14158–14172 (2015).
170. Algar, W. R. & Krull, U. J. Adsorption and hybridization of oligonucleotides on mercaptoacetic acid-capped CdSe/ZnS quantum dots and quantum dot-oligonucleotide conjugates. *Langmuir ACS J. Surf. Colloids* **22,** 11346–11352 (2006).
171. Petryayeva, E. & Krull, U. J. Quantum dot and gold nanoparticle immobilization for biosensing applications using multidentate imidazole surface ligands. *Langmuir ACS J. Surf. Colloids* **28,** 13943–13951 (2012).
172. Petryayeva, E., Algar, W. R. & Krull, U. J. Adapting fluorescence resonance energy transfer with quantum dot donors for solid-phase hybridization assays in microtiter plate format. *Langmuir ACS J. Surf. Colloids* **29,** 977–987 (2013).
173. Pan, H. *et al.* Noninvasive Visualization of Respiratory Viral Infection Using Bioorthogonal Conjugated Near-Infrared-Emitting Quantum Dots. *ACS Nano* **8,** 5468–5477 (2014).
174. Li, Y., Tao, P., Viswanath, A., Benicewicz, B. C. & Schadler, L. S. Bimodal surface ligand engineering: the key to tunable nanocomposites. *Langmuir ACS J. Surf. Colloids* **29,** 1211–1220 (2013).
175. Tao, P. *et al.* TiO2 nanocomposites with high refractive index and transparency. *J. Mater. Chem.* **21,** 18623–18629 (2011).
176. Tao, P., Viswanath, A., Schadler, L. S., Benicewicz, B. C. & Siegel, R. W. Preparation and optical properties of indium tin oxide/epoxy nanocomposites with polyglycidyl methacrylate grafted nanoparticles. *ACS Appl. Mater. Interfaces* **3,** 3638–3645 (2011).
177. Mulder, W. J. M. *et al.* Quantum Dots with a Paramagnetic Coating as a Bimodal Molecular Imaging Probe. *Nano Lett.* **6,** 1–6 (2006).
178. Yan, M. *et al.* An in vitro study of vascular endothelial toxicity of CdTe quantum dots. *Toxicology* **282,** 94–103 (2011).

179. Soenen, S. J., Demeester, J., De Smedt, S. C. & Braeckmans, K. The cytotoxic effects of polymer-coated quantum dots and restrictions for live cell applications. *Biomaterials* **33,** 4882–4888 (2012).
180. Lutz, J.-F. Polymerization of oligo(ethylene glycol) (meth)acrylates: Toward new generations of smart biocompatible materials. *J. Polym. Sci. Part Polym. Chem.* **46,** 3459–3470 (2008).
181. Viswanath, A. *et al.* Synthesis of random terpolymers bearing multidentate imidazole units and their use in functionalization of cadmium sulfide nanowires. *Polym. Chem.* **6,** 7036–7044 (2015).
182. Hardwick, J. M. & Bussell, R. H. Glycoproteins of measles virus under reducing and nonreducing conditions. *J. Virol.* **25,** 687–692 (1978).
183. Nakamura, T. & Russell, S. J. Oncolytic measles viruses for cancer therapy. *Expert Opin. Biol. Ther.* **4,** 1685–1692 (2004).
184. Hasegawa, K. *et al.* The Use of a Tropism-Modified Measles Virus in Folate Receptor–Targeted Virotherapy of Ovarian Cancer. *Clin. Cancer Res.* **12,** 6170–6178 (2006).
185. Lu, Y. & Low, P. S. Immunotherapy of folate receptor-expressing tumors: review of recent advances and future prospects. *J. Controlled Release* **91,** 17–29 (2003).
186. Hao, J., Huang, L.-L., Zhang, R., Wang, H.-Z. & Xie, H.-Y. A Mild and Reliable Method to Label Enveloped Virus with Quantum Dots by Copper-Free Click Chemistry. *Anal. Chem.* **84,** 8364–8370 (2012).
187. Finke, S., Brzózka, K. & Conzelmann, K.-K. Tracking Fluorescence-Labeled Rabies Virus: Enhanced Green Fluorescent Protein-Tagged Phosphoprotein P Supports Virus Gene Expression and Formation of Infectious Particles. *J. Virol.* **78,** 12333–12343 (2004).
188. Zhao, X. *et al.* Labeling of Enveloped Virus via Metabolic Incorporation of Azido Sugars. *Bioconjug. Chem.* **26,** 1868–1872 (2015).
189. Banerjee, P. S., Ostapchuk, P., Hearing, P. & Carrico, I. Chemoselective Attachment of Small Molecule Effector Functionality to Human Adenoviruses Facilitates Gene Delivery to Cancer Cells. *J. Am. Chem. Soc.* **132,** 13615–13617 (2010).

190. Garoff, H., Hewson, R. & Opstelten, D.-J. E. Virus Maturation by Budding. *Microbiol. Mol. Biol. Rev.* **62,** 1171–1190 (1998).
191. Chen, Y.-H., Wang, C.-H., Chang, C.-W. & Peng, C.-A. In situ formation of viruses tagged with quantum dots. *Integr. Biol.* **2,** 258–264 (2010).
192. Joo, K.-I. *et al.* Site-Specific Labeling of Enveloped Viruses with Quantum Dots for Single Virus Tracking. *ACS Nano* **2,** 1553–1562 (2008).
193. Liu, S.-L. *et al.* Effectively and Efficiently Dissecting the Infection of Influenza Virus by Quantum-Dot-Based Single-Particle Tracking. *ACS Nano* **6,** 141–150 (2012).
194. Liu, S.-L. *et al.* High-efficiency dual labeling of influenza virus for single-virus imaging. *Biomaterials* **33,** 7828–7833 (2012).
195. Huang, L.-L. *et al.* A fast and biocompatible living virus labeling method based on sialic acid-phenylboronic acid recognition system. *Anal. Bioanal. Chem.* **406,** 2687–2693 (2014).
196. Hong, Z.-Y. *et al.* Clicking Hydrazine and Aldehyde: The Way to Labeling of Viruses with Quantum Dots. *ACS Nano* (2015). **ASAP**
197. Johnson, C. M. *et al.* A methacrylate-based polymeric imidazole ligand yields quantum dots with low cytotoxicity and low nonspecific binding. *J. Colloid Interface Sci.* **458,** 310–314 (2015).
198. Viswanath, A. *et al.* Copolymerization and Synthesis of Multiply Binding Histamine Ligands for the Robust Functionalization of Quantum Dots. *Macromolecules* **47,** 8137–8144 (2014).
199. Bellini, W. J., Trudgett, A. & McFarlin, D. E. Purification of Measles Virus with Preservation of Infectivity and Antigenicity. *J. Gen. Virol.* **43,** 633–639 (1979).
200. Kopp, M., Klupp, B. G., Granzow, H., Fuchs, W. & Mettenleiter, T. C. Identification and Characterization of the Pseudorabies Virus Tegument Proteins UL46 and UL47: Role for UL47 in Virion Morphogenesis in the Cytoplasm. *J. Virol.* **76,** 8820–8833 (2002).

APPENDIX A – COPYRIGHT PERMISSION

Copyright for Chapter 2.2 to 2.5

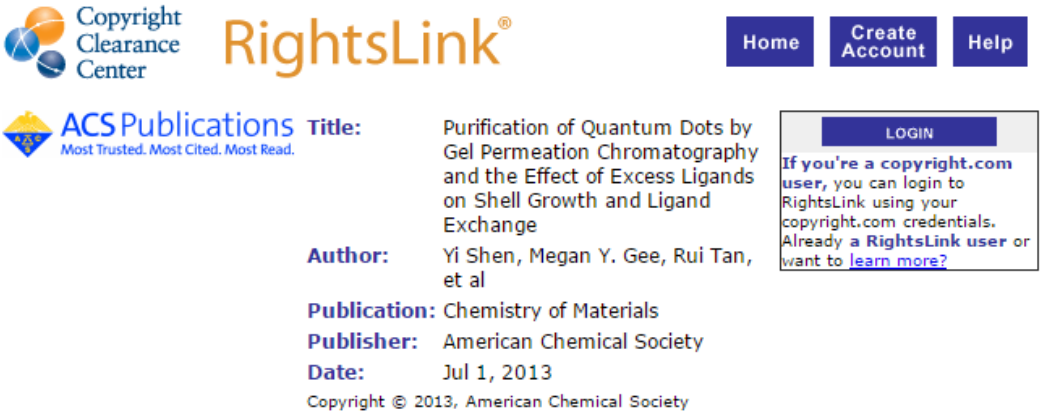

Copyright Clearance Center RightsLink®

Home | Create Account | Help

ACS Publications
Most Trusted. Most Cited. Most Read.

Title: Purification of Quantum Dots by Gel Permeation Chromatography and the Effect of Excess Ligands on Shell Growth and Ligand Exchange

Author: Yi Shen, Megan Y. Gee, Rui Tan, et al

Publication: Chemistry of Materials

Publisher: American Chemical Society

Date: Jul 1, 2013

Copyright © 2013, American Chemical Society

LOGIN

If you're a copyright.com user, you can login to RightsLink using your copyright.com credentials. Already a RightsLink user or want to learn more?

PERMISSION/LICENSE IS GRANTED FOR YOUR ORDER AT NO CHARGE

This type of permission/license, instead of the standard Terms & Conditions, is sent to you because no fee is being charged for your order. Please note the following:

- Permission is granted for your request in both print and electronic formats, and translations.
- If figures and/or tables were requested, they may be adapted or used in part.
- Please print this page for your records and send a copy of it to your publisher/graduate school.
- Appropriate credit for the requested material should be given as follows: "Reprinted (adapted) with permission from (COMPLETE REFERENCE CITATION). Copyright (YEAR) American Chemical Society." Insert appropriate information in place of the capitalized words.
- One-time permission is granted only for the use specified in your request. No additional uses are granted (such as derivative works or other editions). For any other uses, please submit a new request.

BACK | CLOSE WINDOW

Copyright © 2015 Copyright Clearance Center, Inc. All Rights Reserved. Privacy statement. Terms and Conditions.
Comments? We would like to hear from you. E-mail us at customercare@copyright.com

Copyright for Chapter 3.2

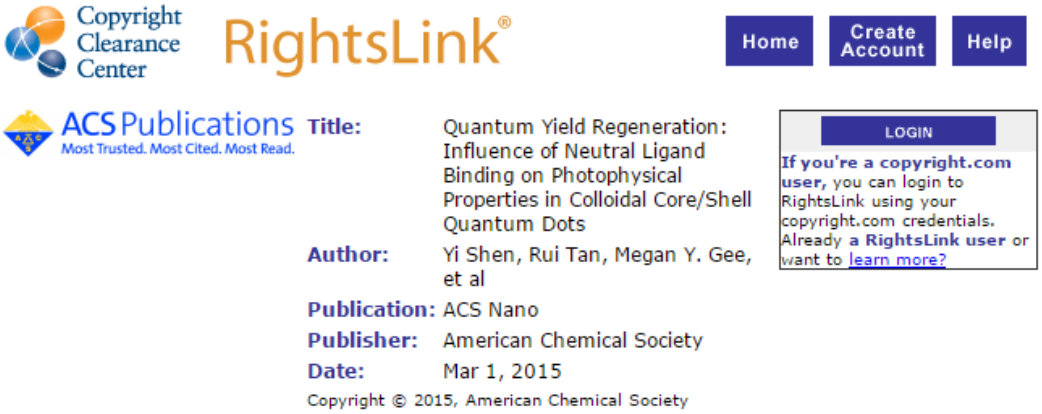

Copyright Clearance Center RightsLink®

Home | Create Account | Help

ACS Publications
Most Trusted. Most Cited. Most Read.

Title: Quantum Yield Regeneration: Influence of Neutral Ligand Binding on Photophysical Properties in Colloidal Core/Shell Quantum Dots

Author: Yi Shen, Rui Tan, Megan Y. Gee, et al

Publication: ACS Nano

Publisher: American Chemical Society

Date: Mar 1, 2015

Copyright © 2015, American Chemical Society

LOGIN

If you're a copyright.com user, you can login to RightsLink using your copyright.com credentials. Already a RightsLink user or want to learn more?

PERMISSION/LICENSE IS GRANTED FOR YOUR ORDER AT NO CHARGE

This type of permission/license, instead of the standard Terms & Conditions, is sent to you because no fee is being charged for your order. Please note the following:

- Permission is granted for your request in both print and electronic formats, and translations.
- If figures and/or tables were requested, they may be adapted or used in part.
- Please print this page for your records and send a copy of it to your publisher/graduate school.
- Appropriate credit for the requested material should be given as follows: "Reprinted (adapted) with permission from (COMPLETE REFERENCE CITATION). Copyright (YEAR) American Chemical Society." Insert appropriate information in place of the capitalized words.
- One-time permission is granted only for the use specified in your request. No additional uses are granted (such as derivative works or other editions). For any other uses, please submit a new request.

BACK | CLOSE WINDOW

Copyright for Chapter 3.3

Copyright Clearance Center RightsLink®

Home | Create Account | Help

ACS Publications
Most Trusted. Most Cited. Most Read.

Title: Reducing Competition by Coordinating Solvent Promotes Morphological Control in Alternating Layer Growth of CdSe/CdS Core/Shell Quantum Dots

Author: Rui Tan, Yi Shen, Stephen K. Roberts, et al

Publication: Chemistry of Materials

Publisher: American Chemical Society

Date: Nov 1, 2015

Copyright © 2015, American Chemical Society

LOGIN

If you're a copyright.com user, you can login to RightsLink using your copyright.com credentials. Already **a RightsLink user** or want to learn more?

PERMISSION/LICENSE IS GRANTED FOR YOUR ORDER AT NO CHARGE

This type of permission/license, instead of the standard Terms & Conditions, is sent to you because no fee is being charged for your order. Please note the following:

- Permission is granted for your request in both print and electronic formats, and translations.
- If figures and/or tables were requested, they may be adapted or used in part.
- Please print this page for your records and send a copy of it to your publisher/graduate school.
- Appropriate credit for the requested material should be given as follows: "Reprinted (adapted) with permission from (COMPLETE REFERENCE CITATION). Copyright (YEAR) American Chemical Society." Insert appropriate information in place of the capitalized words.
- One-time permission is granted only for the use specified in your request. No additional uses are granted (such as derivative works or other editions). For any other uses, please submit a new request.

BACK | CLOSE WINDOW

Copyright for Chapter 4.2.2 to 4.2.3

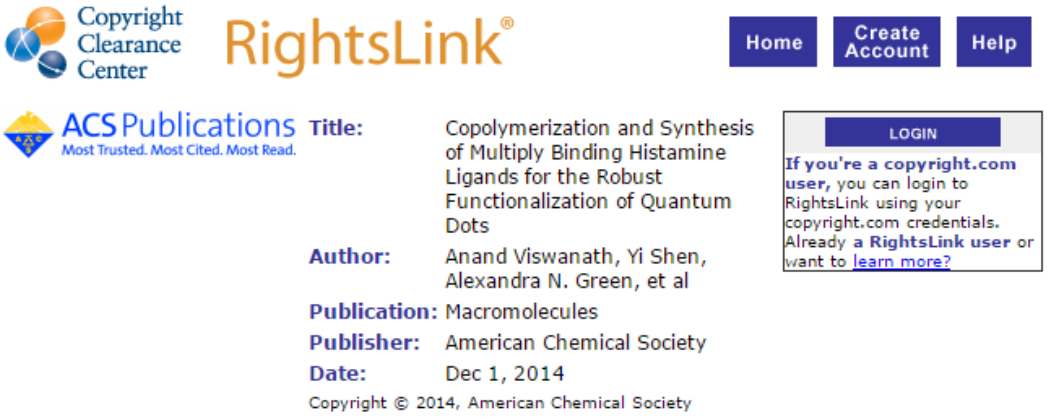

PERMISSION/LICENSE IS GRANTED FOR YOUR ORDER AT NO CHARGE

This type of permission/license, instead of the standard Terms & Conditions, is sent to you because no fee is being charged for your order. Please note the following:

- Permission is granted for your request in both print and electronic formats, and translations.
- If figures and/or tables were requested, they may be adapted or used in part.
- Please print this page for your records and send a copy of it to your publisher/graduate school.
- Appropriate credit for the requested material should be given as follows: "Reprinted (adapted) with permission from (COMPLETE REFERENCE CITATION). Copyright (YEAR) American Chemical Society." Insert appropriate information in place of the capitalized words.
- One-time permission is granted only for the use specified in your request. No additional uses are granted (such as derivative works or other editions). For any other uses, please submit a new request.

BACK CLOSE WINDOW

Copyright for Chapter 4.2.4

ELSEVIER LICENSE
TERMS AND CONDITIONS

Dec 09, 2015

This is a License Agreement between YI SHEN ("You") and Elsevier ("Elsevier") provided by Copyright Clearance Center ("CCC"). The license consists of your order details, the terms and conditions provided by Elsevier, and the payment terms and conditions.

All payments must be made in full to CCC. For payment instructions, please see information listed at the bottom of this form.

Supplier	Elsevier Limited The Boulevard,Langford Lane Kidlington,Oxford,OX5 1GB,UK
Registered Company Number	1982084
Customer name	YI SHEN
Customer address	631 SUMTER STREET COLUMBIA, SC 29208
License number	3764800120743
License date	Dec 09, 2015
Licensed content publisher	Elsevier
Licensed content publication	Journal of Colloid and Interface Science
Licensed content title	A methacrylate-based polymeric imidazole ligand yields quantum dots with low cytotoxicity and low nonspecific binding
Licensed content author	Colin M. Johnson,Kayla M. Pate,Yi Shen,Anand Viswanath,Rui Tan,Brian C. Benicewicz,Melissa A. Moss,Andrew B. Greytak
Licensed content date	15 November 2015
Licensed content volume number	458
Licensed content issue number	n/a
Number of pages	5
Start Page	310
End Page	314
Type of Use	reuse in a thesis/dissertation
Portion	figures/tables/illustrations